Universidade do Minho
Escola de Ciências

Miguel António Faria Ribeiro

Modeling the Effects of Eye Shape in Peripheral Refraction and Myopia Progression

March 2016

Modeling the Effects of Eye Shape in Peripheral Refraction and Myopia Progression
Miguel António Faria Ribeiro
UMinho | 2016

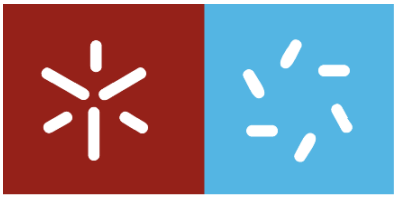

Universidade do Minho
School of Sciences

Miguel António Faria Ribeiro

Modeling the Effects of Eye Shape in Peripheral Refraction and Myopia Progression

PhD Thesis in Sciences

Specialty in Physics

Developed Under Supervision of:

José Manuel González – Méijome, PhD
Professor Associado, School of Sciences
Universidade do Minho (Portugal)

Jorge Manuel Martins Jorge, PhD
Professor Auxiliar, School of Sciences
Universidade do Minho (Portugal)

Norberto López-Gil, PhD
Profesor Titular, Facultad de Óptica y Optometria
Universidad de Múrcia (Spain)

March 2016

STATEMENT OF INTEGRITY

I hereby declare having conducted my thesis with integrity. I confirm that I have not used plagiarism or any form of falsification of results in the process of the thesis elaboration. I further declare that I have fully acknowledged the Code of Ethical Conduct of the University of Minho.

University of Minho, 8/3/2016

Full name: Miguel António Faria Ribeiro

Signature:_____

Acknowledgments

All the work developed would not have been possible without the help and inspiration of some the great minds of our times in vision sciences. I sincerely like to express my gratitude to Norberto López-Gil and Rafael Navarro for their support and contribution during these years. A special thank you to my main supervisor and friend José Manuel González-Méijome for always inspired me to become better and provided me with the opportunity, technical support and wisdom to do so.

The history of science shows that theories are perishable. With every new truth that is revealed we get a better understanding of Nature and our conceptions and views are modified.

Nikola Tesla

Abstract

Myopia affects approximately 25% of the World population, being a public health concern due to the socioeconomic impact and to the risk of vision loss related to other co-morbidities. If current trends continue, half the world's population (almost 5 billion) will be short-sighted in just over three decades, with one-fifth of those expected to have a significantly increased risk of blindness.

Clinical evidence from animal models and human clinical trials seems to indicate that the peripheral refraction pattern plays an important role in the regulation of eye growth. Lower progression rates have been reported over the last years in myopic children wearing orthokeratology (ortho-k) or special design contact lenses, when compared with those wearing traditional ophthalmic lenses. To date, the only justification for this effect seems to lie in the significant myopization effect induced by these alternative forms of correction beyond the foveal area, but despite the moderate results obtained researcher's still lack knowledge of the exact mechanism behind this effect and why does it work better in some subjects than others. In this thesis a frame work was developed to model the possible impact of the eye's posterior shape and the optical changes produced by ortho-k in myopia progression.

Optical modeling and biometric eye length measures were used to calculate the retinal contour in 55 myopic subjects, with an accuracy of tenths of a micron. The results show that there is large inter-subject variability in the shape of the posterior pole, even among subjects with similar refractive errors. An exhaustive characterization of the ortho-k cornea was also conducted to analyze the main morphological, topographical and optical changes induced by these treatments and their possible implications in the peripheral refractive error and accommodative response. The results suggest that the reported effects in the retention of eye growth, supposedly due to the peripheral myopization produced by ortho-k treatments, might be dependent on pupil size. Optical quality analysis revealed that although the increase in positive spherical aberration is the main cause of the loss of retinal image quality in the unaccommodated eye after ortho-k, it also seems to have a positive effect, as it extends the depth of field of the eye and may contribute to a better image quality in subjects with accommodative lag during high contrast near vision tasks.

Resumo

A actual prevalência mundial da Miopia (25%) é já considerada um problema de saúde pública devido ao impacto sócio-económico e ao risco de perda de visão relacionada com outras co-morbidades. Se as tendências actuais se mantiverem, metade da população mundial (quase 5 mil milhões) será míope daqui a pouco mais de três décadas, e cerca de um quinto deverá ter um aumento significativo do risco de cegueira. Evidências clínicas baseadas em modelos animais e ensaios clínicos com pacientes humanos parecem indicar que o padrão da refracção periférica desempenha um papel importante na regulação do crescimento axial do olho. Níveis mais baixos de progressão têm sido reportados ao longo dos últimos anos em grupos de crianças míopes corrigidas com ortoqueratologia (orto-k) ou lentes de contacto com geometrias especiais, em comparação grupos de controle compensados com lentes oftálmicas tradicionais. Até à data, a única justificação plausível para estes resultados parece residir no efeito miopização periférica induzido por essas formas alternativas de correção para além da área foveal, mas apesar dos resultados moderados obtidos ainda falta conhecimento do exacto mecanismo por trás deste efeito e porque o efeito é maior em alguns indivíduos que em outros. Nesta tese foi desenvolvido um quadro de trabalho com o objectivo de modelizar o possível impacto da forma do polo posterior do olho e a das alterações estruturais induzidas pela ortoqueratologia na progressão da miopia.

O contorno da retina de 55 indivíduos míopes foi calculado com recurso a modelização óptica e medidas biométricas do comprimento do olho, com uma precisão de décimos de micras. Os resultados demonstram que existe uma grande variabilidade inter-individual na forma do pólo posterior do olho, mesmo entre indivíduos com erros refractivos semelhantes. Foi também realizada uma caracterização exaustiva da córnea pós orto-k, com o objectivo de analisar as principais alterações morfológicas, topográficas e ópticas induzidas por estes tratamentos e as suas possíveis implicações no erro refractivo periférico, assim na resposta acomodativa. Os resultados sugerem que os relatos de uma menor taxa de progressão da miopia em olhos tratados com orto-k, supostamente devido à miopização periférica produzida por estes tratamentos, pode ser dependente do tamanho da pupila. A análise da qualidade óptica revelou que, embora o aumento da aberração esférica positiva após orto-k seja a principal causa da

diminuição da qualidade da imagem retiniana no olho desacomodado, também aparenta ter um efeito positivo na extensão da profundidade de campo, o que poderá contribui para um aumento da qualidade da imagem retiniana em indivíduos com atraso acomodativo durante tarefas de alto contraste em visão próxima.

Abbreviations

SA	Spherical Aberration
AL	Axial length
D	Diopter
SD	Standard Deviation
F_S	Sagittal Focal
F_T	Tangential Focal
J_O	Astigmatic vector component with axis at 180º/90º
J_{45}	Astigmatic vector component with axis at 45º/135º
M	Spherical Equivalent
Rx	Refraction
N	Nasal Hemifield of the Retina
T	Temporal Hemifield of the Retina
T-test	T Student Test
MTF	Modulation Transfer Function
OTF	Optical Transfer Function
PTF	Phase Transfer Function
PSF	Point Spread Function
FT	Fourier Transform
FT^{-1}	Inverse Fourier Transform
CSF	Contrast Sensitivity Function
VS	Visual Strehl Ratio
RMS	Root Mean Square Error
logMAR	The logarithm of minimum resolvable angle in arc minutes (visual acuity)
HS	Hartmann-Shack (wavefront sensor)
PCIB	Partial Coherence Interferometry Biometry
OPL	Optical Path Length
OPD	Optical Path Difference
WFE	Wavefront Error

List of Figures

List of Tables

List of Publications

Included in this Thesis:

Faria-Ribeiro, M., Lopes-Ferreira, D., López-Gil, N., Jorge, J., & González-Méijome, J. M. (2014). Errors associated with IOLMaster biometry as a function of internal ocular dimensions. *Journal of optometry*, *7(2),* 75-78.

Faria-Ribeiro, M., López-Gil, N., Navarro, R., Lopes-Ferreira, D., Jorge, J., & González-Méijome, J. M. (2014). Computing retinal contour from optical biometry. *Optometry & Vision Science, 91(4),* 430-436.

Faria-Ribeiro, M., Navarro, R., González-Méijome, J.M. Effect of pupil size on wavefront refraction during orthokeratology. Accepted for publication in Optometry and Vision Science, at 8 June 2016.

Faria-Ribeiro, M., López-Gil, N., Navarro, R., González-Méijome, J.M. Morphology, topography and optics of the ortho-k cornea. Accepted for publication in Journal of Biomedical Optics (SPIE), at 31 May 2016.

Faria-Ribeiro, M., López-Gil, N., Navarro, R., González-Méijome, J.M. Depth-of-Field after Orthokeratology: A theoretical study. Submission in process.

Not included but related to this Thesis:

Faria-Ribeiro, M., Queirós, A., Lopes-Ferreira, D., Jorge, J., & González-Méijome, J. M. (2013). Peripheral refraction and retinal contour in stable and progressive myopia. *Optometry & Vision Science*, *90*(1), 9-15.

Lopes-Ferreira, D., Ribeiro, C., Neves, H., Faria-Ribeiro, M., Queirós, A., Villa-Collar, C, & González-Méijome, J. M. (2013). Peripheral refraction with dominant design multifocal contact lenses in young myopes. *Journal of optometry*, *6*(2), 85-94.

González-Méijome, J. M., Peixoto-de-Matos, S. C., Faria-Ribeiro, M., Lopes-Ferreira, D. P., Jorge, J., Legerton, J., & Queiros, A. (2016). Strategies to regulate myopia progression with contact lenses: a review. *Eye & contact lens*, *42*(1), 24-34.

Lopes-Ferreira, D. P., Neves, H. I., Faria-Ribeiro, M., Queirós, A., Fernandes, P. R., & González-Méijome, J. M. (2015). Peripheral refraction with eye and head rotation with contact lenses. *Contact Lens and Anterior Eye*, *38*(2), 104-109.

González-Méijome, J. M., Faria-Ribeiro, M. A., Lopes-Ferreira, D. P., Fernandes, P., Carracedo, G., & Queiros, A. (2015). Changes in peripheral refractive profile after orthokeratology for different degrees of myopia. *Current eye research*, 1-9.

González-Méijome, J. M., Carracedo, G., Lopes-Ferreira, D., Faria-Ribeiro, M. A., Peixoto-de-Matos, S. C., & Queirós, A. (2016). Stabilization in early adult-onset myopia with corneal refractive therapy. *Contact Lens and Anterior Eye*, *39*(1), 72-77.

Pauné, J., Morales, H., Armengol, J., Quevedo, L., Faria-Ribeiro, M., & González-Méijome, J. M. (2015). Myopia Control with a Novel Peripheral Gradient Soft Lens and Orthokeratology: A 2-Year Clinical Trial. *BioMed research international*, *2015*.

Pauné, J., Thivent, S., Armengol, J., Quevedo, L., Faria-Ribeiro, M., & González-Méijome, J. M. (2016). Changes in Peripheral Refraction, Higher-Order Aberrations, and Accommodative Lag with a Radial Refractive Gradient Contact Lens in Young Myopes. *Eye & contact lens*.

Queirós, A., Faria-Ribeiro, M., Lopes-Ferreira, D., Fernandes, P., & González-Méijome, J. M. (2013). Astigmatic peripheral refraction patterns in orthokeratology for different myopic treatments. Contact Lens and Anterior Eye, 36, e33.

Contents

Chapter 1: Introduction

1.1. Peripheral Refraction and Myopia Progression

Myopia progression is a serious public health concern. Beyond the limitations caused by refractive error, moderate to high myopia is associated with an increased risk of serious ophthalmic diseases like primary open angle glaucoma, retinal detachment, sub-capsular posterior cataract or macular degeneration.[1,2]

Clinical evidence indicates that the peripheral refraction pattern plays an important role in the regulation of the growth of the human eye, as first reported by Hoogerheide *et al*.[3] who found that, in a group of 214 young pilots entering the Danish Army, those who showed greater myopic progression over time also developed more hyperopic peripheral defocus. Another example is the lower progression rates in children wearing orthokeratology (ortho-k)[4-8] lenses, when compared with those wearing spectacle or contact lenses. One possible justification for this behavior lies in the significant myopization effect induced by the ortho-k treatments beyond the foveal area.[9,10] This has led to the development of soft contact lenses attempting to reproduce similar refractive patterns of peripheral myopic defocus, which have already proved effective in slowing myopia progression.[11,12] Furthermore, animal studies have confirmed that locally induced hyperopic defocus causes a local increase in the axial length in chicks[13-15] and that central vision is not essential for guiding the emmetropization mechanism,[16] while the peripheral retina seems to be more relevant in this respect. This was also demonstrated in the studies by Smith *et al*.[17-19], who reported that myopia could be induced even after laser photoablation of the fovea, in rhesus monkeys. This peripheral hyperopic refraction is believed to be responsible for

myopia development, as the eye's visually-guided growth mechanism tries to compensate with further elongation for the imposed peripheral defocus even in the presence of an optimal central correction and a perfectly focused central image.

An obvious problem is how this supposed visually guided growth mechanism is able to perceive the defocus signal. Like all optical systems, the eye suffers from oblique astigmatism. Thus, rather than there being a unique image surface at each point in the periphery, there are two surfaces, corresponding to the radial (sagittal) and tangential focal line images of each object point. The tangential focal lies anterior to the sagittal focal. There is great evidence that the peripheral retina has neurons tuned for different orientations[20-22] and that it makes use of the two astigmatic foci to recognize the defocus signal.[23] Bearing this in mind, the peripheral retinal neuron circuits might have distinct levels of sensitivity for the tangential and sagittal foci inputs. A similar process is used in some optical devices such as compact disc players which use an astigmatic lens to optimize the focusing mechanism. When one axis is better focused than the other, dot-like features on the disc are projected into elliptical shapes. The orientation of the major and minor elliptical axes indicates which axis is better focused, and hence in which direction the lens needs to move to compensate for it. In a similar fashion, it could be hypothesized that the ocular growth mechanism in the peripheral retina might also use similar orientation cues to assess the two astigmatic image shell "positions" and thus compensate for peripheral hyperopic defocus when the relative peripheral sagittal focal line "stands behind" the retina, as previously suggested by Howland.[24] This hypothesis is also consistent with the experiments described in US patent 7,025,460 by Smith *et al.*[25] who reported a trend for the eye, in the presence of mixed astigmatism, to grow in order to reposition the retina with the most "posteriorly positioned" astigmatic focal

line. This process may then start over when new lenses are prescribed to compensate for the increase in central myopia; furthermore, as the eyeball elongates, the retina becomes steeper, thus increasing the hyperopic trend in the periphery.

In fact, by comparing two groups of progressive (P) versus non-progressing (NP) myopes, Faria-Ribeiro et al.[26] demonstrated that the myopic patients in the P group had a more hyperopic relative astigmatic defocus than the NP group. Even when mean refractive error (M) assumes values close to zero or slightly myopic, it still seems that the hyperopic stimulus provided by the sagittal foci can be sufficient to induce axial growth in the P group. The authors also found a strong correlation between eye shape and peripheral refraction along with high differences in shape and refraction between both groups in the nasal retina that may be indicative of a distinct sensitivity ‘‘weight’’ between the two retina hemifields. Although not include in this thesis the cited paper was the starting point for the work developed in the next chapters, were the influence of eye shape in peripheral refraction and myopia progression is investigated using optical modeling.

1.2. Optic Biometry: The IOLMaster

The IOLMaster (Carl Zeiss Jena GmbH) is a commercially available device which uses partial coherent interferometry (PCI) to measure axial length. Accurate measurement of the axial length (AL) of the eye is critical in several research and clinical applications. PCI is the actual election method for total or partial measurement of intra-ocular dimensions as a main variable for intra-ocular lens calculation.[27] Figure 1.1 is a schematic representation of the IOLMaster operating principle.

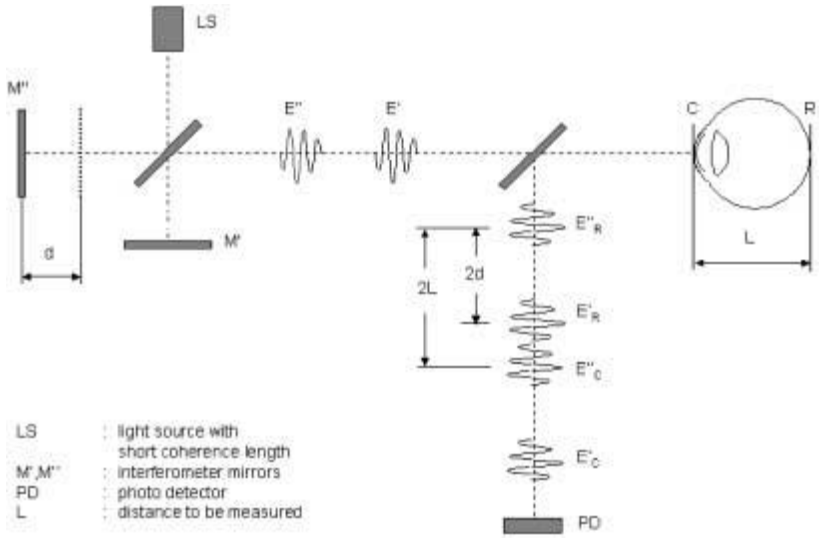

Figure 1.1. IOLMaster setup. Reproduced from Haigis et al.[28]

The instrument uses infrared light (peak λ=780 nm; bandwidth 3-4 nm) of short coherence length (~160 µm).[29] In physics, coherence length is the propagation distance over which an electromagnetic wave maintains a specified degree of coherence. The light emitted by a laser diode (LS) is split in a Michelson interferometer setup into two separate coaxial beams E' and E'', with E'' being delayed by twice the displacement d of the measuring mirror M'' (Figure 1.1). Both partial beams illuminate the eye to be measured and are reflected at the cornea (C) and the retina (R), more specifically at the pigmentary epithelium. This introduces an additional path difference of twice the optical length (L) of the eye between the two beams reflected at the cornea and the two beams reflected at the retina, respectively. After passing through a beam splitter, all beam components are detected by a photodetector (PD). Interference is stronger when the paths taken by the two interfering waves differ by less than the coherence length.

Eye length L is defined in this technique as the path integral of the group refractive index n_g of the eye media along the geometric path from the anterior surface to the retina $\int n_g . ds$, with the group index defined by the following equation:

$$n_g(\lambda) = n_p(\lambda) - \lambda \frac{dn_p}{d\lambda} \qquad Eq.(1.1)$$

where $n_g(\lambda)$ and $n_p(\lambda)$ are group and phase refractive indices at wavelength λ, and $\frac{dn_p}{d\lambda}$ is the derivative of n_p with respect to λ.

The IOLMaster determines optical path lengths (OPL) and converts them into geometric/anatomical lengths by assuming estimate values for the eye internal refractive indices. It uses a unique average index (1.3549) based the average group refractive index of a Gullstrand's 24 mm model eye for an envelope of waves at the instrument's infrared radiation wavelength peak. The obtained results are then calibrated to match the geometric length values to the ones measured using ultrasonography by using the equation 2 wired in the instrument's firmware.[28]

$$\frac{OPL}{1.3549} = AL_{ultrasound} \times 0.9571 - 1.3033 \qquad (Eq\ 1.2)$$

Table 1.1. Group refractive indices n_g of the eye media for λ = 780 nm.[29]

Cornea	Aqueous	Lens (mean)	Vitreous	Mean *n*
1.3856	1.3459	1.4070	1.3445	1.3549

Atchison et al.[30] calculated the errors that this assumption might induce in axial length measurement during accommodation, and more recently in retinal shape estimation.[31] However, no correction factor was suggested within the normal range of AL and crystalline lens thickness (LT) which might have an impact in the final estimations.

This potential source of error was addressed in chapter 2 and a correction factor was proposed.

As previously demonstrated by Faria-Ribeiro et. al, peripheral refraction is highly correlated with retinal contour, as eyes with more curved retinas tend to have more peripheral hyperopic defocus.[26] Personalized eye models based on the patient's real data are a primary tool to help understand these relations between optics and eye anatomy. PCI measure techniques are fundamental for the estimation of the eye internal dimensions and shape, but eye length measured by PCI does not represent the real distance from the cornea to the retina intercept, as the IOLMaster off-axis measurements fails to account for refraction within the eye and ignores differences in refractive indices along the optical path, particularly along oblique directions inside the crystalline lens. The methodology in chapter 3 proposes a solution to overcome this problem.

1.3. Optical Models of the Human Eye: Predicting Function from Structure

Optical models of the human eye are an important tool to study the optical performance of devices such as ophthalmic, contact or intraocular lenses.[32-38] Their application in vision sciences can be used to predict the average optical/image quality performance of a population,[32,39-45] or in a personalized approach to "tailor" custom optical solutions, such as myopia control contact lenses. In the statistical eye model approach, average population optical quality features, such as spherical aberration, mean biometric internal dimensions, oblique astigmatism, etc. are used to calculate the eye model surfaces curvatures and asphericities that closely match average population data.[46-48] Throughout the last 150 years several models have appeared with different

levels of sophistication, from anatomically closely accurate models capable of predicting on- and off-axis optical function—often called finite or wide angle models—to less sophisticated and simple models such as the Indiana two surfaces eye model that despite the unrealistic anatomy still preserves good functionality when predicting off-axis astigmatism and chromatic aberrations.[40,49]

Despite the degree of sophistication of some of those eye models, they are still generic models with average features and can only be used as approximation when studying the optical function of a subgroup of individuals such as myopes. Although some authors have closely studied the anatomy and optics of myopic eyes, with the purpose of designing a refraction dependent myopic eye model, the variations among individuals are large[50] thus, individual optical performance cannot be accurately inferred from the structure of such models.

Peripheral optics are an important aspect concerning the study of myopia progression and development of personalized optical solutions. Retinal shape is closely related to peripheral refraction and can be predictive of myopia development.[51] Knowledge of the posterior retinal contour is potentially useful to understand the mechanisms of emmetropization and myopia progression. Furthermore, the current knowledge in this field suggests that it might be possible to interfere with myopia progression by customizing the relative position of the peripheral image focusing regarding the retinal surface.[52,53] To achieve a true customization of these treatments it will be essential to know the actual position and shape of the retinal surface in order to design an optical device able to change the refraction in the desired way. Theoretical results suggest that partial coherence interferometric instruments can be used for estimating retinal shape with good accuracy, if improvements are made to correct for distortion by using optical modeling.[31]

To achieve customization through modeling several biometric data are needed, such as corneal topography, lens topography/geometry, refractive indices and internal ocular dimensions. However, designing a realistic customized eye model can be very complex due to lack of detailed measurements of the front and back surface of the lens and its gradient index. Conversely, there are a number of commercial systems available to obtain highly precise measurements of the corneal topography of the eye. Taking into

account that PCI measures cornea-to-retina optical path length (OPL),[27-29] and that the cornea sagittal heights at the points of intercept can vary significantly between subjects, it can be presumed that corneal topography will be an essential part of the eye model that should be used to obtain reliable data of the retinal contour from PCI measures. On the other hand, considering the relatively small changes in refractive indices within the eye it might not be critical to know in detail the internal optics to compute the contour of the retina with an acceptable error margin.

A modeling customization approach has been used in chapter 3 based on the Navarro eye model[54] to compute the individual retinal contour based of PCI measures and ray tracing. This generic eye model possesses interesting features such as aspheric surfaces and dispersive media, adjusted to fit the experimentally observed chromatic aberration of the eye and is also accommodation-dependent.

Table 1.2. Unaccommodated Navarro Eye Model parameters. Radius of curvature (R) and thickness (t) are expressed in millimeters. *Q* and *n* refer to the conic constant and refractive index, respectively. Total paraxial refractive power equals 60.42 diopters.

Medium	***n***	***R***	***Q***	***t***
Air	1.000			
Cornea	1.376	7.72	-0.26	0.55
		6.50	0	3.05
Aqueous	1.337			
Lens	1.420	10.20	-3.132	4.0
		-6.00	-1.00	16.404
Vitreous	1.336			
Retina		-12.00		

All modeling was performed in Zemax-EE ray trace software.[55] Zemax is an optical design software that is used to design and analyze imaging systems such as the

human eye. It works by modeling the propagation of rays through an optical system. It can model the effect of optical elements such as aspheric lenses, gradient index lenses, mirrors, and diffractive optical elements. To model the different elements of the eye several surfaces can used that allow to account for the difference in sagitta along a radius r. The simplest one—the Standard surface—is defined by the equation of a conic surface plus an expansion of higher order aspheric terms. A Standard surface can be a plane, spherical, or conic aspheric surface, which is followed by a homogeneous material such as air, corneal tissue, vitreous, etc. The only parameters required are a radius (which may be infinity to yield a plane), a thickness (distance from one element to the other), a conic constant (the default zero value indicates a sphere), and the name of the glass type. The name of the glass should be specified in Zemax's glass catalog, along with its dispersion data.

Although this surface can be used to model the best conic that fits each subject's topography, in practice the topographies of real corneas do not match exactly any of these ideal models, but, rather, they exhibit different irregularities and departures from that basic geometry. The difference, or residual, between the actual topography and the ideal basis surface model is often adjusted to some sort of orthogonal polynomial expansion, or interpolating functions such as splines. The Zernike polynomial expansion is the most commonly used method. Accurate representations of real corneal shape can be achieved in Zemax's environment by using a Zernike Standard Sag surface. Zernike Standard Sag surface is defined by the same polynomial as the Standard surface (regular conic basis) plus additional aspheric terms defined by the Zernike coefficients. The surface sagitta *z* is of the form:

$$z = \frac{cr^2}{1+\sqrt{1-(1+Q)c^2r^2}} + \sum_{i=1}^{N} A_i Z_i(\rho, \varphi) \qquad (Eq\ 1.3)$$

Where *N* is the number of Zernike coefficients in the series, A_i is the coefficient on the i^{th} Zernike Standard polynomial, is *r* the radial ray coordinate in lens units, *c* is the conic surface inverse radius (curvature), *Q* is the conic constant (-eccentricity^2), ρ is the normalized radial ray coordinate, and φ is the angular ray coordinate. Zernike Standard polynomials are expressed in millimeters. Zemax supports the first 231 Zernike terms. Note that the Zernike Standard Sag surface describes surface deformations, not

wavefront error directly. Each polynomial represents a surface deformation mode, and its correspondent coefficient the magnitude of the deformation.

These models are much more general and realistic and, in fact, they are able to fit real corneal topographies with very low Root Mean Square errors (RMSe < 0.5 microns for a normal anterior cornea fitted with a 6^{th} order Zernike expansion). In the semi-customized eye model approach, the front corneal surface of the Navarro eye model was replaced with a Zernike Standard Sag surface computed from the topographic data of the subject. The Medmont E300 (Medmont, Australia) topographer allows to export elevation data given in a polar coordinates grid (300 spokes going counter clockwise with the first at the horizontal 3 o'clock position, and 32 rings). Individual data obtained from anterior elevation topography were fitted to the Zernike Standard Surface equation by a least-squares method implemented in Matlab (The MathWorks, Natick MA).

1.4. Wavefront Refraction

Clinical assessment of refractive sate is a common task in Optometry and Ophthalmology practices. The gold standard technique—subjective refraction—consists in a sequential strategy to search the best sphere and cylindrical lens combination that yields the best image quality, according to the patients subjective criteria and the spatial visual task performed during this process.[56] Over the last years there has been a great interest in developing objective metrics that can replicate the patient's subjective criteria in an autonomous way.[57-61] Those would be quite useful in clinical practice such as for refracting eyes with irregular corneas, children, patients with especial disabilities, and also in myopia progression for objective assessment of peripheral refraction and visual quality.

Peripheral refraction can be obtained using an open field autorefractor as described in previous works,[10,26,62] but the working principle of this equipment—uses a near infrared 2.3 mm ring-like target to illuminate the test eye and calculates second order refraction based on the size and shape of the rings' reflected image[63]—makes the

equipment insensitive to the increased aberration contribution from larger pupil diameters as well to irregularities in the wavefront that lie inside the rings' area.[64] This is particularly relevant when measuring refraction over anti-myopia contact lenses or in eyes treated with orthokeratology, due to the increase in high order aberrations.

Modern wavefront aberrometers like the Shack–Hartmann wavefront aberrometer, for example, can yield a comprehensive description of the eye's optical aberrations and display the result in the form of an aberration map that describes the variation in optical path length (OPL) from source to retinal image through each point in the pupil. From this information, retinal image can be computed using the theories of physical optics to determine the refractive state of the eye. Although this can be straight forward for foveal vision, in the periphery things became complicated due to some inherent problems:[65]

- When seen from off-axis eccentricities circular pupils become elliptical.
- For larger eccentricities the scattered light from the retina does not fill the entire pupil, so it is easy to make a mistake by assuming the oval array of spots is due to viewing a circle obliquely.
- When measuring the aberration map over bifocal contact lenses some spots in the Shack–Hartmann array may become double which can produce an incorrect estimation of the wavefront.

Another effective way of measuring peripheral refraction and optical quality is through the combination of real anatomical/structural measures of the eye combined with optical modeling (customization). Real optical changes can be calculated using a computational model, thus avoiding the challenging task of actually measuring peripheral refraction.

In the past a variety of methods for quantifying the optical quality of an eye based on analysis of wavefront aberrations using pupil plane metrics and analysis of retinal image quality using image plane metrics has been proposed that can be somehow divided in (i) pupil and (ii) image plane metrics.[57-59,61,66-68] Image plane metrics compute retinal image quality based either on the point spread function (PSF) or from its Fourier

transform, the optical transfer function (OTF). Passing from the wavefront W to the PSF (or OTF) involves two nonlinear stages. The generalized pupil function, *P*, is first calculated as:[69]

$$P = Ae^{i\frac{2\pi W}{\lambda}} \qquad (Eq.1.4)$$

Where *A* can either denote a circular pupil aperture with a unit amplitude function, or in alternative the Stiles-Crawford effect can be incorporated into the pupil function by using an amplitude Gaussian model in *A*. The incoherent PSF is calculated as the squared modulus of the Fourier transform (FT) of the generalized pupil function *P*:

$$PSF = |FT(P)|^2 \qquad (Eq.1.5)$$

As a result, in order to find the prescription (best correction) from image plane metrics one has to solve a nonlinear optimization problem. This nonlinear search is not trivial and can become time consuming since it involves a 3-dimensional search of the three unknown variables: sphere, cylinder and axis of the correcting lens that yields the maximum value according to a certain pre-defined criterion (visual quality metric). Computationally this can be achieved by adding to the wavefront a series of defocused spherical and cylindrical wavefronts that simulate the trial lenses employed during a subjective refraction examination. It is well known that nonlinear optimization methods in a multidimensional space can stagnate in local minima and usually require departing from an initial guess not too far from the solution (global minimum). Marsack et al.,[59] has suggested that in the presence of spherical aberration Paraxial and Zernike refraction appear to locate each of the limits of the depth of field of the eye, consequently the optimum focus should lie somewhere between these limits. Thus, one possible strategy to minimize computation time is to confine the 3-dimensional search to the interval of vergences between these two points. Alternatively, it is always possible to adopt a sequential strategy similar as the one used in clinical refraction, by searching first for the best sphere, and then for axis and magnitude of cylinder; later adding the spherical equivalent, etc. This approach has revealed itself more difficult and less accurate, since it implies to retrieve the astigmatism axis from the PSF orientation—in an analogy to the subjective clock dial—which in off-axis locations, where the wavefront can suffer from high amounts of coma, can become quiet challenging.

Nevertheless, an even more challenging issue is which criteria to use to define the best possible correction since that different image quality metrics may eventually give different results. The next paragraphs resume some of those metrics that were used or considered in chapter 5 of this thesis.

Pupil Plane Metrics

Zernike and Paraxial refraction

One obvious strategy for objective refraction used by most commercial aberrometers is to prescribe correcting lenses based on a Zernike polynomial expansion of the aberration map. Modern Aberrometers normally use the coefficients of these expansions to estimate refraction from wavefront data with two different criteria. The first, named Zernike refraction, specifies the vergence of a point source that focuses a ‘‘disk of least confusion’’ into the image plane, defined by the retinal layer where the aberrometer’s probe beam reflects. The vergence concept is based on the geometrical concept of longitudinal ray aberrations that is illustrated in Figure 1.2.

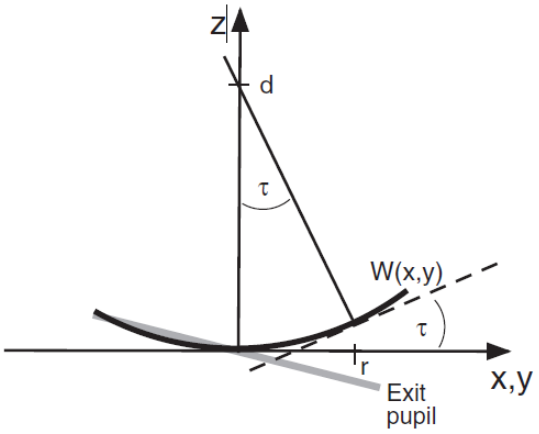

Figure 1.2. Geometry of the wavefront vergence definition. The z axis indicates the direction of the chief ray, which is not necessarily perpendicular to the exit pupil (reproduced from Nam et al.[70])

Differentiating W(x,y) with respect to radius(r) generates the radial slope of wavefront, which when divided by r, produces the radial vergence of the wavefront. Zernike refraction calculates the corrective lens prescription based on the assumption that the second order Zernike polynomial coefficients c_2^0 corresponds to defocus *M* and

c_2^2 and c_2^{-2} to a Jackson crossed-cylinder of power J_0 with axes at 90º and 180º, and a Jackson crossed-cylinder of power J_{45} with axes at 45º and at 135º,[71] respectively. Consequently, one can estimate the considered power vectors as:

$$M = \frac{-c_2^0 4\sqrt{3}}{r^2}$$
$$J_0 = \frac{-c_2^2 2\sqrt{6}}{r^2} \qquad (Eq. 1.6)$$
$$J_{45} = \frac{-c_2^{-2} 2\sqrt{6}}{r^2}$$

Where the Zernike polynomials coefficients and r in are express in meters. The power vector notation is a cross-cylinder convention that is easily transposed into conventional minus-cylinder formats used by clinicians, using the equations previously described by Thibos.[71]

Eliminating second-order Zernike aberrations is somehow equivalent to calculate the corrective lens vergence that minimizes the Root Mean Square error (RMSe) of the wavefront, but this minimization does not necessarily optimize the quality of the retinal image.[72] This correction is optimal only when high order aberrations (HOAs) are small, which under the Marèchal criterion occurs when the RMS wavefront error is below 1/14 λ. However, this is not the case for human eyes, which usually show higher values of HOA.[73-75]

In a second approach named Paraxial refraction, the Zernike coefficients used in the previous metric are expanded to higher orders (truncated at 6th order in the example below):[61]

$$M = \frac{-c_2^0 4\sqrt{3} + c_4^0 12\sqrt{5} - c_6^0 24\sqrt{7}}{r^2} \ldots$$
$$J_0 = \frac{-c_2^2 2\sqrt{6} + c_4^2 6\sqrt{10} - c_6^2 12\sqrt{14}}{r^2} \ldots \qquad (Eq. 1.7)$$
$$J_{45} = \frac{-c_2^{-2} 2\sqrt{6} + c_4^{-2} 6\sqrt{10} - c_6^{-2} 12\sqrt{14}}{r^2} \ldots$$

This metric criterion is somehow equivalent to calculate the vergence of a point source that focuses paraxial rays into the plane of reflection of the aberrometer's probe beam. In the absence of HOAs, Zernike and Paraxial refractions are identical, but in eyes

highly aberrated these criteria may become biased in different ways. For instance, in the presence of positive spherical aberration Zernike defocus will tend to yield more myopic refractions as the pupil becomes larger, whereas Paraxial refraction, by definition, will not be affected by the wavefront error of the non-paraxial regions of the pupil, such as in the case of spherical aberration. Therefore, the main difference between these two metrics is that the Zernike refraction can be highly influenced by the effects of HOAs, whereas Paraxial method is insensitive to HOAs. Thus, none of this methods may be robust enough to obtain an unbiased estimation of refraction,[76] especially for aberrated wavefronts such as the ones measured off-axis, in eyes treated with orthokeratology or fitted with anti-myopia contact lenses.

Refractive Error Sensing

As it can be perceived from Figure 1.2, standard refraction is directly linked to longitudinal aberration. The main difference between early and modern aberrometry is that modern Shack-Hartman aberrometers measure transverse displacements of light spots (transverse aberration) instead of longitudinal shifts and then compute the wavefront error by numerical integration.[77-80] Thus, as Navarro suggested,[68] refractive error can be obtained from the lateral displacements of spots measured by the aberrometer, and that wave aberration (optical path differences) might be less relevant to this subject. This metric is based on the principle that for each small sampled point in the pupil the local refractive error can be calculated from the mean principle curvatures of an infinitesimal wavefront at that point, obtained directly from differentiation of the raw aberrometry data. The formulism, based on differential geometry concepts, directly relates the principal local curvatures of the wavefront to the prescription sphere, cylinder and axis:

$$S = -\frac{1}{2}(W''_{XX}(x,y) + W''_{YY}(x,y))$$
$$C_0 = -\frac{1}{2}\left(W''_{XX}(x,y) - W''_{YY}(x,y)\right) \qquad (Eq.\,1.8)$$
$$C_{45} = -W''_{XY}(x,y)$$

Where $W''_{XX}(x,y)$ and $W''_{YY}(x,y)$, are the second derivatives of the wavefront error—or the first derivatives of the wavefront slopes—along the horizontal and vertical directions

at point (x, y), and $W''_{XY}(x, y)$, is the crossed second derivative. Thus, S, C_0 and C_{45} in equation 1.8 describes the local refractive error in a similar fashion as Thibos el al. power vectors, but here C is positive. The clinical sphere is S_C = S - C/2. These elements are not constant over the pupil but are functions of the coordinates S(x, y), C_0(x, y), and C_{45}(x, y). In presence of HOA, refractive errors are different for each infinitesimal portion of the pupil.[81] Therefore, a complete correction is not possible with standard ophthalmic lenses. The best correction must then be calculated with one of different possible strategies, to obtain a global refractive error from each local infinitesimal wavefront. An efficient strategy is to choose a value for the correction that minimizes the resulting set of refractive errors. Although the mean seems like a good strategy, as it maximizes the number of sampled points corrected, it can be highly sensitive to outliers (i.e., a few samples with high values may strongly bias the mean) and needs a high number of samples to have an accurate estimation. Another possible approach adopted by Navarro[68] is to subtract the mode from all points. In this case the mode seems to be a better candidate to estimate the best global refractive correction, as it is equivalent to maximizing the number of points (or pupil area) corrected, which is expected to produce a higher impact retinal image quality.

Image Plane Metrics

Visual Strehl Ratio

Although it is unknown which criteria the human eye actually uses for focusing and the ideal optimization method is yet to be determined, Cheng and co-workers[58] found that when HOAs are significant, image plane quality metrics such as the Visual Strehl ratio computed in frequency domain (MTF method) (VSMTF) are less biased by the high levels of spherical aberration (SA). This metric takes into account that different frequencies respond differently to defocus and neural sensitivity varies with frequency in accordance to visual channel theory, which establishes that the visual pathway decomposes the input signal into frequency bands.

The theoretical estimation of the retinal image quality can be calculated according to the VSMTF expression:

$$VSMTF = \frac{\int_{-\infty}^{\infty}\int_{-\infty}^{\infty} \mathrm{CSF}_N(\mathrm{fx,fy})\cdot\mathrm{MTF}(\mathrm{fx,fy})\,\mathrm{dfxdfy}}{\int_{-\infty}^{\infty}\int_{-\infty}^{\infty} \mathrm{CSF}_N(\mathrm{fx,fy})\cdot\mathrm{MTF}_{\mathrm{DL}}(\mathrm{fx,fy})\,\mathrm{dfxdfy}} \qquad (Eq.\,1.9)$$

VSMTF is a normalized measure of image quality defined as the volume under the visually-weighted modulation transfer function (MTF) for an aberrated eye divided by the corresponding volume for an optically perfect eye (diffraction limited). CSF_N is the nominal neural Contrast Sensitivity Function and the MTF is the one computed in the eye model. MTF_{DL} is the diffraction limited MTF corresponding to the pupil diameter used. This image quality metric provides a single value normalized between 0 and 1.

For objective refraction without considering any particular visual task, the VSMTF ratio seems an especially interesting metric. It has a twofold meaning as the peak intensity of the PSF and as the volume under the MTF. Roughly speaking, volume is proportional both to the covered area of spatial frequency plane (resolution) and to the mean height (contrast), so that the VSMTF seems a good compromise of the two main image quality criteria of contrast and resolution, heighted for the spatial frequencies that matter most to the eye. This choice of metric is further supported by evidence that visual Strehl ratio is monotonically related to visual acuity over a large range of aberration magnitude in normal[58,82] and abnormal eyes.[83,84] According to those studies, a 0.22 change in log visual Strehl ratio corresponds on average to a clinically significant change of 0.1 logMAR (1 line on a letter chart) in visual acuity.

1.5. Orthokeratology

Orthokeratology (ortho-k) changes the ocular refraction by the programmed application of reverse geometry rigid gas permeable contact lenses (CLs). To correct myopia, the central cornea is flattened to induce a reversible change on the epithelial thickness profile. The central epithelial layer thins and the front surface corneal power decreases over the central 4 to 5 mm central zone.[85] The paracentral zone of 1.5 to 2.0 mm surrounding the treatment zone increases in curvature, in a direct relationship with the amount of central flattening needed to correct the myopic refractive error. This has the effect of changing the shape of a normal cornea from an average prolate ellipsoid to a less prolate/more oblate average ellipsoid.

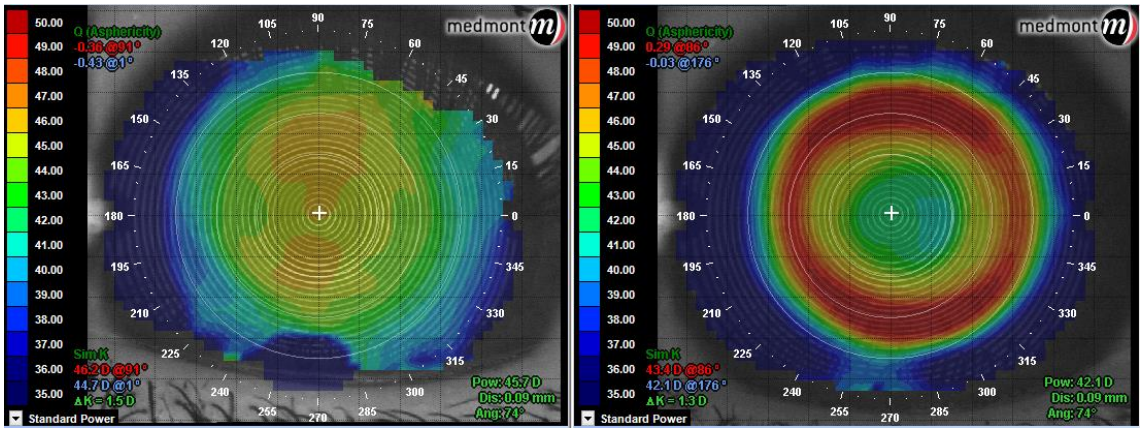

Figure 1.3. Topographical tangential power maps from a subject before ortho-k (left) and after (right).

For myopic correction the ortho-k CLs are fitted with a base curve flatter than central corneal curvature to apply pressure to the central area of the cornea. Reverse geometry ortho-k CLs have three main different fitting parameters: optic zone, reserve zone depth and landing zone angle or equivalent in other lens designs/brands. The optic zone is fitted taking into account the myopic refraction of the patient and the flatter corneal curvature. The other two parameters are modified to obtain a well centered fit of the CLs. The difference in thickness of the tear film between the posterior surface of the CL and the anterior corneal profile creates a positive relative pressure in the center of the cornea and a negative pressure in the middle-periphery. It is believed that this difference of pressures helps to reshape the cornea[86] (Figure 1.4).

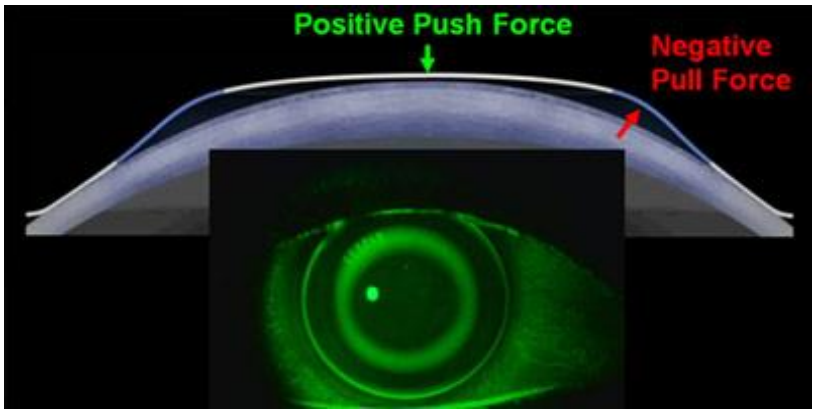

Figure 1.4. Diagram of the forces that act during the myopic ortho-k treatment. Courtesy of Paragon Vision Sciences (Mesa, Arizona, USA).

These anatomical changes have huge optical consequences. Besides the correction of central myopia, as the pupil dilates the quality of vision deteriorates due to the significant increase in optical aberrations—especially spherical aberration (SA)—[87-89]as well as fluctuations in vision over the course of the day due to the temporary and reversible nature of the treatment. To maintain the ortho-k effect, retainer CLs must be worn every night, or in the case of slow regressions every second or third night. Once the correct corneal shape is well-established the visual performance of ortho-k patients will then rely on the centration, area and power distribution of the central flattened zone (treatment zone or optical zone) and the surrounding steepening zone (transition zone).

Ortho-k in myopia control

Over the last decade, systematic research reports, including randomized and controlled clinical trials, confirmed that ortho-k reduces the rate of axial length increase by 40% to 60% when compared with single vision spectacles or contact lenses.[90] The mechanism behind these results seems to be related with the change in peripheral optics after ortho-k. There is evidence that the posterior retinal contour of myopic eyes is relatively more prolate—or relatively less oblate—than that of emmetropic and hyperopic eyes. This difference in shape seems to produce a difference in the field curvature of the myopic eyes, making them relatively more hyperopic in the periphery compared to emmetropic or hyperopic eyes. This relative hyperopic peripheral refractive error might be a risk factor for the onset and progression of myopia in children, and traditional spectacle lens designs do nothing to reduce or eliminate peripheral hyperopic defocus. Furthermore, there is evidence that myopia correction with single vision spectacle lenses induces absolute hyperopic defocus on the retinal periphery of low and moderate myopic eyes.[91]

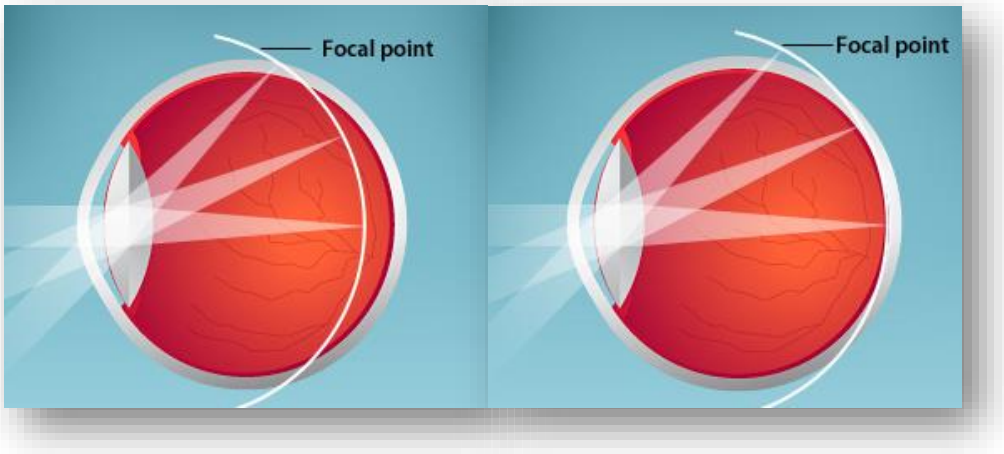

Figure 1.5. Diagram of the field curvature of the uncorrected myopic eye (left) and corrected with traditional strategies such as ophthalmic lenses (right).

On the other hand, ortho-k seems to increase the eye's field curvature, hypothetically due to the more curved transition zone. According to Queirós et al., at 30° and 35° of field eccentricity, the amount of myopia induced in terms of spherical equivalent has an almost 1:1 relationship with the amount of baseline spherical equivalent refraction to be corrected, mostly due to the high increase in peripheral astigmatism.[89]

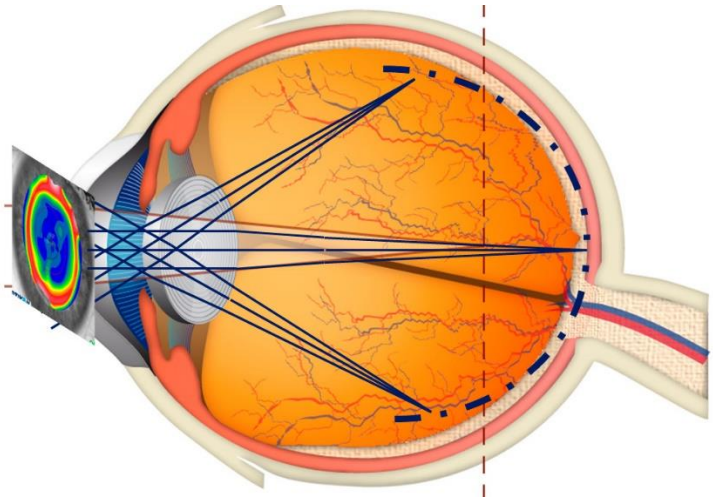

Figure 1.6. Diagram of the field curvature of the myopic eye corrected with ortho-k (Adapted from Pauné Vision).

Despite the good results obtained with ortho-k in myopia control, researcher's still lack knowledge of the exact mechanism behind this effect and why it is not observed in all subjects. It seems that until now results rely only on an observed side effect. To attain better outcomes in myopia control, treatments need to be directed for myopia retention instead of just its correction. Understanding the exact mechanism behind myopia control is therefore a priority in vision sciences. An exhaustive analysis of the morphology, topography and optics of the ortho-k cornea was conducted in chapter 4 of this thesis.

When considering the peripheral myopization theory, one obvious variable that comes to mind is the pupil diameter. The effect of peripheral myopization has to be somehow pupil dependent, since smaller pupils will tend to block light refracted from more peripheral locations of the cornea. In fact, Chen et al.[92] found that larger pupil diameters were associated with a higher control effect, hypothetically as a result of a larger retinal area being exposed to the peripheral myopic defocus. This supposed pupil dependence was investigated in chapter 5. Peripheral refraction was calculated by ray-trace for different pupil sizes using eye models semi-customized with the anterior corneal topography each ortho-k patient.

An alternative theory to the peripheral myopization focus its attention on foveal vision during near tasks. Hypothetically, a subject with accommodative lag might experience a decrease in retinal image quality (RIQ) when performing near vision activities. This decreased in RIQ is due to the presence of central hyperopic defocus and it might act as a trigger effect for more eye growth, in a similar fashion as the peripheral refraction hypothesis. [93]

Based on this theory, the increase in positive SA is seen as possible explanation for the myopia control effect, not only after ortho-k but also with different treatments targeted to alter the eye's SA, due to a hypothetical change in behavior of the accommodative system. This hypothetical effect was investigated in chapter 6.

1.6. References

1 Saw SM, Gazzard G, Shih-Yen EC, Chua WH. Myopia and associated pathological complications. *Ophthalmic Physiol Opt* 2005; 25: 381-391.

2 Verkicharla PK, Ohno-Matsui K, Saw SM. Current and predicted demographics of high myopia and an update of its associated pathological changes. *Ophthalmic Physiol Opt* 2015; 35: 465-475.

3 Hoogerheide J, Rempt F, Hoogenboom WP. Acquired myopia in young pilots. *Ophthalmologica* 1971; 163: 209-215.

4 Ziff SL. Orthokeratology. 1. *J Am Optom Assoc* 1968; 39: 143-147 contd.

5 Santodomingo-Rubido J, Villa-Collar C, Gilmartin B, Gutiérrez-Ortega R. Myopia control with orthokeratology contact lenses in Spain: refractive and biometric changes. *Invest Ophthalmol Vis Sci* 2012; 53: 5060-5065.

6 Sun Y, Xu F, Zhang T, Liu M, Wang D, Chen Y, Liu Q. Orthokeratology to control myopia progression: a meta-analysis. *PLoS One* 2015; 10: e0124535.

7 Walline JJ. Myopia Control: A Review. *Eye Contact Lens* 2015.

8 González-Méijome JM, Peixoto-de-Matos SC, Faria-Ribeiro M, Lopes-Ferreira DP, Jorge J, Legerton J, Queiros A. Strategies to Regulate Myopia Progression With Contact Lenses: A Review. *Eye Contact Lens* 2016; 42: 24-34.

9 Charman WN, Mountford J, Atchison DA, Markwell EL. Peripheral refraction in orthokeratology patients. *Optom Vis Sci* 2006; 83: 641-648.

10 Queirós A, González-Méijome JM, Jorge J, Villa-Collar C, Gutiérrez AR. Peripheral refraction in myopic patients after orthokeratology. *Optom Vis Sci* 2010; 87: 323-329.

11 Sankaridurg P, Holden B, Smith E, Naduvilath T, Chen X, de la Jara PL, Martinez A, Kwan J, Ho A, Frick K, Ge J. Decrease in rate of myopia progression with a contact lens

designed to reduce relative peripheral hyperopia: one-year results. *Invest Ophthalmol Vis Sci* 2011; 52: 9362-9367.

12 Pauné J, Morales H, Armengol J, Quevedo L, Faria-Ribeiro M, González-Méijome JM. Myopia Control with a Novel Peripheral Gradient Soft Lens and Orthokeratology: A 2-Year Clinical Trial. *Biomed Res Int* 2015; 2015: 507572.

13 Irving EL, Callender MG, Sivak JG. Inducing myopia, hyperopia, and astigmatism in chicks. *Optom Vis Sci* 1991; 68: 364-368.

14 Wallman J, Adams JI. Developmental aspects of experimental myopia in chicks: susceptibility, recovery and relation to emmetropization. *Vision Res* 1987; 27: 1139-1163.

15 Wallman J, Gottlieb MD, Rajaram V, Fugate-Wentzek LA. Local retinal regions control local eye growth and myopia. *Science* 1987; 237: 73-77.

16 Troilo D, Gottlieb MD, Wallman J. Visual deprivation causes myopia in chicks with optic nerve section. *Curr Eye Res* 1987; 6: 993-999.

17 Smith EL, Ramamirtham R, Qiao-Grider Y, Hung LF, Huang J, Kee CS, Coats D, Paysse E. Effects of foveal ablation on emmetropization and form-deprivation myopia. *Invest Ophthalmol Vis Sci* 2007; 48: 3914-3922.

18 Smith EL, Huang J, Hung LF, Blasdel TL, Humbird TL, Bockhorst KH. Hemiretinal form deprivation: evidence for local control of eye growth and refractive development in infant monkeys. *Invest Ophthalmol Vis Sci* 2009; 50: 5057-5069.

19 Smith EL, Hung LF, Huang J. Relative peripheral hyperopic defocus alters central refractive development in infant monkeys. *Vision Res* 2009; 49: 2386-2392.

20 Leventhal AG, Schall JD, Wallace W. Relationship between preferred orientation and receptive field position of neurons in extrastriate cortex (area 19) in the cat. *J Comp Neurol* 1984; 222: 445-451.

21 Schall JD, Vitek DJ, Leventhal AG. Retinal constraints on orientation specificity in cat visual cortex. *J Neurosci* 1986; 6: 823-836.

22 Shou TD, Leventhal AG. Organized arrangement of orientation-sensitive relay cells in the cat's dorsal lateral geniculate nucleus. *J Neurosci* 1989; 9: 4287-4302.

23 Kee CS, Hung LF, Qiao-Grider Y, Roorda A, Smith EL. Effects of optically imposed astigmatism on emmetropization in infant monkeys. *Invest Ophthalmol Vis Sci* 2004; 45: 1647-1659.

24 Howland H. A possible role for peripheral astigmatism in the emmetropization of the eye. In. International myopia Conference. Tubingen. Germany. July 26-29, 2010, 2010.

25 Smith III E, Greeman N, Ho A, Holden B. US Patent 7,025,460 B2 - Methods an Apparatuses for Altering Relative Curvature of Field and off-axis Focal Positions. In, 2006.

26 Faria-Ribeiro M, Queirós A, Lopes-Ferreira D, Jorge J, González-Méijome JM. Peripheral refraction and retinal contour in stable and progressive myopia. *Optom Vis Sci* 2013; 90: 9-15.

27 Santodomingo-Rubido J, Mallen EA, Gilmartin B, Wolffsohn JS. A new non-contact optical device for ocular biometry. *Br J Ophthalmol* 2002; 86: 458-462.

28 Haigis W, Lege B, Miller N, Schneider B. Comparison of immersion ultrasound biometry and partial coherence interferometry for intraocular lens calculation according to Haigis. *Graefes Arch Clin Exp Ophthalmol* 2000; 238: 765-773.

29 Hitzenberger CK. Optical measurement of the axial eye length by laser Doppler interferometry. *Invest Ophthalmol Vis Sci* 1991; 32: 616-624.

30 Atchison DA, Smith G. Possible errors in determining axial length changes during accommodation with the IOLMaster. *Optom Vis Sci* 2004; 81: 283-286.

31 Atchison DA, Charman WN. Can partial coherence interferometry be used to determine retinal shape? *Optom Vis Sci* 2011; 88: E601-607.

32 Levick WR, Thibos LN, Cohn TE, Catanzaro D, Barlow HB. Performance of cat retinal ganglion cells at low light levels. *J Gen Physiol* 1983; 82: 405-426.

33 Atchison DA. Optical design of intraocular lenses. I. On-axis performance. *Optom Vis Sci* 1989; 66: 492-506.

34 Atchison DA. Optical design of intraocular lenses. II. Off-axis performance. *Optom Vis Sci* 1989; 66: 579-590.

35 Atchison DA. Optical design of intraocular lenses. III. On-axis performance in the presence of lens displacement. *Optom Vis Sci* 1989; 66: 671-681.

36 López-Gil N, Montés-Micó R. New intraocular lens for achromatizing the human eye. *J Cataract Refract Surg* 2007; 33: 1296-1302.

37 Kingston AC, Cox IG. Predicting through-focus visual acuity with the eye's natural aberrations. *Optom Vis Sci* 2013; 90: 1111-1118.

38 Ribeiro FJ, Castanheira-Dinis A, Dias JM. Personalized pseudophakic model for refractive assessment. *PLoS One* 2012; 7: e46780.

39 Thibos LN, Ye M, Zhang X, Bradley A. The chromatic eye: a new reduced-eye model of ocular chromatic aberration in humans. *Appl Opt* 1992; 31: 3594-3600.

40 Thibos LN, Ye M, Zhang X, Bradley A. Spherical aberration of the reduced schematic eye with elliptical refracting surface. *Optom Vis Sci* 1997; 74: 548-556.

41 Strang NC, Atchison DA, Woods RL. Effects of defocus and pupil size on human contrast sensitivity. *Ophthalmic Physiol Opt* 1999; 19: 415-426.

42 Charman WN, Atchison DA, Scott DH. Theoretical analysis of peripheral imaging after excimer laser corneal refractive surgery for myopia. *J Cataract Refract Surg* 2002; 28: 2017-2025.

43 Thibos LN. Retinal image quality for virtual eyes generated by a statistical model of ocular wavefront aberrations. *Ophthalmic Physiol Opt* 2009; 29: 288-291.

44 Nam J, Rubinstein J, Thibos L. Wavelength adjustment using an eye model from aberrometry data. *J Opt Soc Am A Opt Image Sci Vis* 2010; 27: 1561-1574.

45 Legras R, Benard Y, Lopez-Gil N. Effect of coma and spherical aberration on depth-of-focus measured using adaptive optics and computationally blurred images. *J Cataract Refract Surg* 2012; 38: 458-469.

46 Cagigal MP, Canales VF, Castejón-Mochón JF, Prieto PM, López-Gil N, Artal P. Statistical description of wave-front aberration in the human eye. *Opt Lett* 2002; 27: 37-39.

47 Thibos LN, Bradley A, Hong X. A statistical model of the aberration structure of normal, well-corrected eyes. *Ophthalmic Physiol Opt* 2002; 22: 427-433.

48 Rozema JJ, Atchison DA, Tassignon MJ. Statistical eye model for normal eyes. *Invest Ophthalmol Vis Sci* 2011; 52: 4525-4533.

49 Wang YZ, Thibos LN. Oblique (off-axis) astigmatism of the reduced schematic eye with elliptical refracting surface. *Optom Vis Sci* 1997; 74: 557-562.

50 Atchison DA. Optical models for human myopic eyes. *Vision Res* 2006; 46: 2236-2250.

51 Schmid GF. Association between retinal steepness and central myopic shift in children. *Optom Vis Sci* 2011; 88: 684-690.

52 Smith G, Atchison DA, Avudainayagam C, Avudainayagam K. Designing lenses to correct peripheral refractive errors of the eye. *J Opt Soc Am A Opt Image Sci Vis* 2002; 19: 10-18.

53 Smith EL. Optical treatment strategies to slow myopia progression: effects of the visual extent of the optical treatment zone. *Exp Eye Res* 2013; 114: 77-88.

54 Navarro R, Santamaría J, Bescós J. Accommodation-dependent model of the human eye with aspherics. *J Opt Soc Am A* 1985; 2: 1273-1281.

55 Zemax. *User's Guide*. In, 2005.

56 Liang J, Williams DR. Aberrations and retinal image quality of the normal human eye. *J Opt Soc Am A Opt Image Sci Vis* 1997; 14: 2873-2883.

57 Guirao A, Williams DR. A method to predict refractive errors from wave aberration data. *Optom Vis Sci* 2003; 80: 36-42.

58 Cheng X, Bradley A, Thibos LN. Predicting subjective judgment of best focus with objective image quality metrics. *J Vis* 2004; 4: 310-321.

59 Marsack JD, Thibos LN, Applegate RA. Metrics of optical quality derived from wave aberrations predict visual performance. *J Vis* 2004; 4: 322-328.

60 Thibos LN. Unresolved issues in the prediction of subjective refraction from wavefront aberration maps. *J Refract Surg* 2004; 20: S533-536.

61 Thibos LN, Hong X, Bradley A, Applegate RA. Accuracy and precision of objective refraction from wavefront aberrations. *J Vis* 2004; 4: 329-351.

62 Queirós A, Villa-Collar C, Jorge J, Gutiérrez AR, González-Méijome JM. Peripheral refraction in myopic eyes after LASIK surgery. *Optom Vis Sci* 2012; 89: 977-983.

63 Davies LN, Mallen EA, Wolffsohn JS, Gilmartin B. Clinical evaluation of the Shin-Nippon NVision-K 5001/Grand Seiko WR-5100K autorefractor. *Optom Vis Sci* 2003; 80: 320-324.

64 Bakaraju RC, Fedtke C, Ehrmann K, Ho A. Comparing the relative peripheral refraction effect of single vision and multifocal contact lenses measured using an autorefractor and an aberrometer: A pilot study. *J Optom* 2015; 8: 206-218.

65 Shen J, Thibos LN. Measuring ocular aberrations and image quality in peripheral vision with a clinical wavefront aberrometer. *Clin Exp Optom* 2009; 92: 212-222.

66 Chen L, Singer B, Guirao A, Porter J, Williams DR. Image metrics for predicting subjective image quality. *Optom Vis Sci* 2005; 82: 358-369.

67 Navarro R. Objective refraction from aberrometry: theory. *J Biomed Opt* 2009; 14: 024021.

68 Navarro R. Refractive error sensing from wavefront slopes. *J Vis* 2010; 10: 3.

69 Goodman J. Introduction to Fourier Optics. New York: McGraw-Hill Book Co, 1968.

70 Nam J, Thibos LN, Iskander DR. Describing ocular aberrations with wavefront vergence maps. *Clin Exp Optom* 2009; 92: 194-205.

71 Thibos LN, Wheeler W, Horner D. Power vectors: an application of Fourier analysis to the description and statistical analysis of refractive error. *Optom Vis Sci* 1997; 74: 367-375.

72 Xu R, Bradley A, Thibos LN. Impact of primary spherical aberration, spatial frequency and Stiles Crawford apodization on wavefront determined refractive error: a computational study. *Ophthalmic Physiol Opt* 2013; 33: 444-455.

73 Williams D, Yoon GY, Porter J, Guirao A, Hofer H, Cox I. Visual benefit of correcting higher order aberrations of the eye. *J Refract Surg* 2000; 16: S554-559.

74 Porter J, Guirao A, Cox IG, Williams DR. Monochromatic aberrations of the human eye in a large population. *J Opt Soc Am A Opt Image Sci Vis* 2001; 18: 1793-1803.

75 Guirao A, Porter J, Williams DR, Cox IG. Calculated impact of higher-order monochromatic aberrations on retinal image quality in a population of human eyes. *J Opt Soc Am A Opt Image Sci Vis* 2002; 19: 620-628.

76 Martin J, Vasudevan B, Himebaugh N, Bradley A, Thibos L. Unbiased estimation of refractive state of aberrated eyes. *Vision Res* 2011; 51: 1932-1940.

77 Thibos LN. Principles of Hartmann-Shack aberrometry. *J Refract Surg* 2000; 16: S563-565.

78 Navarro R, Losada MA. Shape of stars and optical quality of the human eye. *J Opt Soc Am A Opt Image Sci Vis* 1997; 14: 353-359.

79 Walsh G, Charman WN, Howland HC. Objective technique for the determination of monochromatic aberrations of the human eye. *J Opt Soc Am A* 1984; 1: 987-992.

80 Howland HC, Howland B. A subjective method for the measurement of monochromatic aberrations of the eye. *J Opt Soc Am* 1977; 67: 1508-1518.

81 Charman WN, Walsh G. Variations in the local refractive correction of the eye across its entrance pupil. *Optom Vis Sci* 1989; 66: 34-40.

82 Ravikumar A, Marsack JD, Bedell HE, Shi Y, Applegate RA. Change in visual acuity is well correlated with change in image-quality metrics for both normal and keratoconic wavefront errors. *J Vis* 2013; 13: 28.

83 Fernández-Sánchez V, Ponce ME, Lara F, Montés-Micó R, Castejón-Mochón JF, López-Gil N. Effect of 3rd-order aberrations on human vision. *J Cataract Refract Surg* 2008; 34: 1339-1344.

84 Pesudovs K, Coster DJ. Penetrating keratoplasty for keratoconus: the nexus between corneal wavefront aberrations and visual performance. *J Refract Surg* 2006; 22: 926-931.

85 Lu F, Simpson T, Sorbara L, Fonn D. The relationship between the treatment zone diameter and visual, optical and subjective performance in Corneal Refractive Therapy lens wearers. *Ophthalmic Physiol Opt* 2007; 27: 568-578.

86 Choo J, Caroline P, Harlin D. How does the cornea change under corneal reshaping contact lenses? *Eye Contact Lens* 2004; 30: 211-213; discussion 218.

87 Hiraoka T, Okamoto F, Kaji Y, Oshika T. Optical quality of the cornea after overnight orthokeratology. *Cornea* 2006; 25: S59-63.

88 Hiraoka T, Okamoto C, Ishii Y, Kakita T, Oshika T. Contrast sensitivity function and ocular higher-order aberrations following overnight orthokeratology. *Invest Ophthalmol Vis Sci* 2007; 48: 550-556.

89 Queirós A, Villa-Collar C, González-Méijome JM, Jorge J, Gutiérrez AR. Effect of pupil size on corneal aberrations before and after standard laser in situ keratomileusis, custom laser in situ keratomileusis, and corneal refractive therapy. *Am J Ophthalmol* 2010; 150: 97-109.e101.

90 González-Méijome JM, Peixoto-de-Matos SC, Faria-Ribeiro M, Lopes-Ferreira DP, Jorge J, Legerton J, Queiros A. Strategies to Regulate Myopia Progression With Contact Lenses: A Review. *Eye Contact Lens* 2015.

91 Lin Z, Martinez A, Chen X, Li L, Sankaridurg P, Holden BA, Ge J. Peripheral defocus with single-vision spectacle lenses in myopic children. *Optom Vis Sci* 2010; 87: 4-9.

92 Chen Z, Niu L, Xue F, Qu X, Zhou Z, Zhou X, Chu R. Impact of pupil diameter on axial growth in orthokeratology. *Optom Vis Sci* 2012; 89: 1636-1640.

93 Gwiazda JE, Hyman L, Norton TT, Hussein ME, Marsh-Tootle W, Manny R, Wang Y, Everett D, Grouup C. Accommodation and related risk factors associated with myopia progression and their interaction with treatment in COMET children. *Invest Ophthalmol Vis Sci* 2004; 45: 2143-2151.

Chapter 2: Errors Associated with IOLMaster Biometry as Function of Internal Ocular Dimensions

2.1. Abstract

PURPOSE: To evaluate the error in the estimation of axial length (AL) with the IOLMaster partial coherence interferometry (PCI) biometer and obtain a correction factor that varies as function of AL and crystalline lens thickness (LT).

METHODS: Optical simulations were produced for theoretical eyes using Zemax-EE software. Thirty-three combinations including eleven different AL (from 20 to 30 mm in 1 mm steps) and three different LT (3.6; 4.2 and 4.8 mm) were used. Errors were obtained comparing the AL measured for a constant equivalent refractive index of 1.3549 and for the actual combinations of indices and intra-ocular dimensions of LT and AL in each model eye.

RESULTS: In the range from 20 to 30 mm AL and 3.6 to 4.8 mm LT, the instrument measurements yielded an error between -0.043 and +0.089 mm. Regression analyses for the three LT condition were combined in order to derive a correction factor as a function of the instrument measured AL for each combination of AL and LT in the theoretical eye.

CONCLUSIONS: The assumption of a single “average” refractive index in the estimation of AL by the IOLMaster PCI biometer only induces very small errors in a wide range of combinations of ocular dimensions. Even so, the accurate estimation of those errors may help to improve accuracy of intra-ocular lens calculations trough exact ray tracing, particularly in longer eyes and eyes with thicker of thinner crystalline lenses.

KEYWORDS: intra-ocular lens calculation; IOL calculation; axial length measurement.

2.2. Introduction

Accurate measurement of the axial length (AL) of the eye is critical in several research and clinical applications. Partial coherence interferometry (PCI) is a non-invasive objective method to measure axial length (AL) and is the election method for total or partial measurement of intra-ocular dimensions[1;2] as a main variable for intra-ocular lens calculation. It is also used in clinical trials involving emmetropization and myopia progression[3] and, recently, to evaluate the actual shape of the posterior segment of the eye.[4;5] However, such biometers determine optical path lengths (OPL) and convert them into geometric/anatomical lengths by assuming estimate values for the eye internal refractive indices. In the case of the IOLMaster (Carl Zeiss Meditec, Jena, Germany), it uses a unique average index (1.3549) based the average group refractive index of a Gullstrand's 24 mm model eye for an envelope of waves at the instrument's infrared radiation wavelength λ=780 nm.[6]

Atchison et al.[7] calculated the errors that this assumption might induce in axial length measurement during accommodation, and more recently in retinal shape estimation.[8] However, no correction factor was suggested within the normal range of AL and crystalline lens thickness (LT) which might have an impact in the final estimations, as the authors acknowledge.

Beyond solely measuring AL and other biometric parameters, current intra-ocular refractive surgical procedures require a high level of accuracy in the estimation of the power of the intra-ocular lenses (IOL) to be implanted. This is particularly relevant in patients with very good preoperative visual acuity as in the case of presbyopic patients undergoing clear lens exchange (CLE) with implantation of multifocal IOL's.[9] IOL power calculation has evolved from the initial empirical methods to the newest generation formulas.[10] The potential errors involved in AL measurement within the normal range seem to be assumed by correction factors in the IOL formulas, but for eyes with out-of-the-normal-range internal dimensions significant errors might be involved.[11;12]

In the search for more accurate estimations several authors have made significant efforts to develop new customized methods to estimate the IOL power

trough optical modelization[13] based on the patient´s own data, obtained with the most recent methods of ocular imaging.[14] As the axial length of the patient's eye is paramount in these efforts for higher accuracy, better estimations of the AL should be useful to improve the accuracy of these models.

The goal of this paper was to evaluate the impact of different combinations of AL and LT in the measurement obtained with the IOLMaster through optical ray tracing simulation, and to derive a correction method for such measurements.

2.3. Methods

Optical design programs are used to model and analyze different kinds of imaging systems including the human eye. They use Snell's law to trace the propagation of light through the surfaces of an optical system. Using ray-tracing software Zemax-EE (Zemax Development Corporation, Washington, USA) a set of unaccommodated eyes were designed based on the Navarro Eye Model.[15] Three different LT values (3.6, 4.2 and 4.8 mm) were combined with eleven eye lengths (from 20 to 30 mm in 1.0 mm steps), resulting in thirty-three combinations. The LT values were based on the age related changes obtained by Atchison et al.[16] who pointed an average LT shift from of 3.6 mm to 4.8 from 20 to 70 years of age. An additional 4.2 mm intermediate value was included as a value representative of a middle-aged population from 39 to 51 years.[17]

Corneal thickness, curvatures and asphericities were kept constant. Anterior chamber depth (ACD) was set to vary as a function of the change in LT such that 50% of the change in LT resulted in a change in the same magnitude in the ACD. Vitreous chamber depth (VCD) was set to vary as a function of ACD and eye length as most of the axial elongation of the eye is attributed to VCD elongation.[18] This was assumed for simplicity after previous simulation demonstrated no implication in the error calculations presented. As ACD and VCD have similar refractive indices, the sum of their optical path lengths (OPL) will be the approximately the same regardless of their physical length distribution. The individual group refractive indices were derived by Hitzenberger,[6] starting from the known phase refractive indices at λ=550 nm and assuming the dispersion of water for the ocular media.

Unlike ultrasound biometry that measures AL along the optical axis of the eye, PCI – as a fixation-bound method – measures AL along the eye's visual axis. Because of the temporal displacement of the fovea in the human eye, the horizontal field angle was adjusted so that the chief ray would maintain a 5-degree angle at the 2nd nodal point (Figure 2.1). Normal incidence with the first corneal surface was maintained in all theoretical simulations.

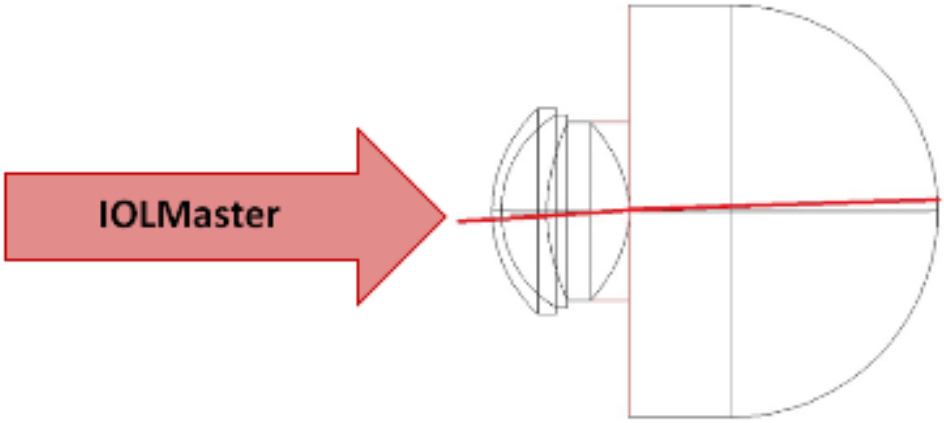

Figure 2.1. Ray-trace simulation of the IOLMaster infrared beam**,** in the Navarro Eye Model, along the visual axis. Due to the temporal decentration of the fovea the beam will be slightly deviated after refraction in the internal surfaces of the eye.

For the cornea-to-fovea physical distance to be the same between the eye model and the instrument estimated AL, the average group refractive index of the eye model must equal the one assumed by the instrument for the same wavelength. Whenever these values are different, depending mainly on varying distribution of AL and LT values, the optical measurement will result in an estimation error. The error was obtained using equation 2.1.

$$ERROR = \ Instrument\ AL - Eye\ Model\ AL \qquad Eq(2.1)$$

Here the instrument measured AL is the result of dividing the calculated OPL by the estimated group refractive index "wired in" the instrument (1.3549), and the Eye Model

AL is the result of ray tracing simulation by adding each individual surface physical path length.

Linear regression was used to evaluate the error as a function of LT and AL and then combined into a single correction equation. In each step the residual error was calculated.

2.4. Results

The errors for each one of the eye models under evaluation have been calculated and plotted as a function of the axial length, for each crystalline lens thickness. Figure 2.2 shows the error variations in the instrument measurements for all the thirty-three eye model combinations. From 20 to 30 mm axial lengths and 3.6 to 4.8 mm lens thickness, the instrument measurements will yield an estimated error between -0.043 and +0.089 mm.

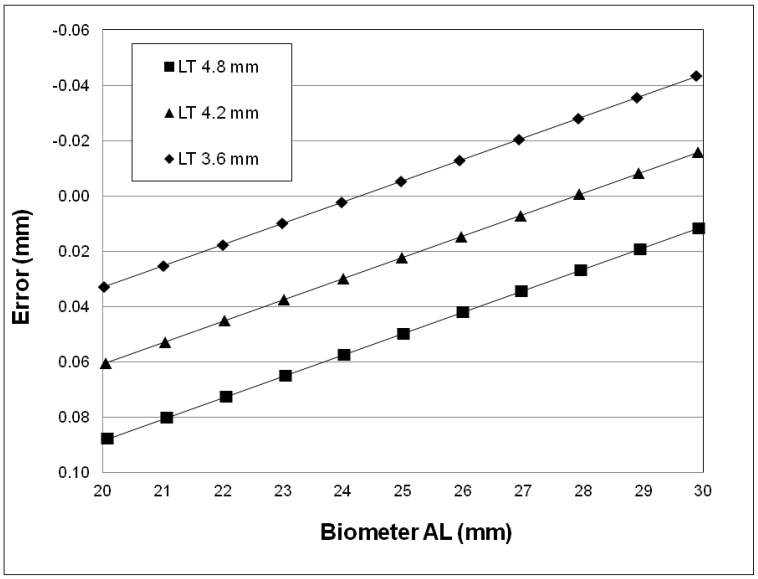

Figure 2.2. Error from the instrument measure as a linear function actual AL and LT combinations.

The slope obtained in the three linear regression equations was the same (-0.007735), with the equation constant values corresponding to the thinner and the thicker LT configuration presenting a difference of approximately ±0.028 mm with respect to the middle thickness equation constant value (LT= 4.2 mm). The coefficient

of determination (r^2) was 1.00 for the three equations as expected due to the linear relation between the optical path length and the real distance.

Using the parameters in table 2.1, a new regression equation was derived in order to predict the variation from the constant terms in each equation for each LT. This allowed us to create a combined regression equation that will be able to estimate the amount of error as a function of AL and LT within the range of values considered in this work (equation 2.2).

Table 2.1. Equations coefficients from the regressions in Figure 2.1.

LT (mm)	Slope R1	Constant R1
3.6	-0.007735	0.18791
4.2	-0.007735	0.2156
4.8	-0.007735	0.2433

$$ERROR = -0.007735 \times Instrument\ AL + 0.046140 \times LT + 0.021806 \qquad Eq(2.2)$$

2.5. Discussion

Nowadays, accurate determinations of AL are of paramount importance in several research and clinical applications. From the results of the present study we can observe that the equivalent refractive index of 1.3549 used by the instrument is optimized for an AL value near 24 mm with a LT around 3.6 mm. This does not seem to be consistent with the normal LT value found in the general elderly population,[16] especially when considering that these instruments are primarily used in pre-surgical evaluation of cataract patients. Although the errors found are quite small, usually lower than 0.1 mm, which corresponds to error in the power of the IOL around 0.25 D, these errors are expected to be higher for AL values out the range than the ones plotted in Figure 2.2 due to the linear relation between the error and the AL. Even so, we stress that the correction of the AL measured by the IOLMaster might not be clinical relevant

when the calculation of the IOL is done using one of the traditional formulas, due to the lack of precision that they offer. On the other hand, personalized eye models can help to improve the accuracy of IOL power choice through numerical ray-tracing software like Zemax,[13] but the biometric data used in the customization of the eye models must be corrected for the errors here reported, and the parameters of the IOL geometry other than the lens constant must be known. Also better estimates of group refractive indices in the infrared are needed; there is not enough information in the literature on dispersion in the various ocular media to make better estimates than the ones reported by Hitzenberger.[6]

Another important area that might benefit from these corrections is the clear lens exchange (CLE) surgery. In CLE, patients expect high precision results. Improving the estimation of the actual axial length will certainly improve the prediction of the most accurate post-surgical refraction.

In summary the present results demonstrate minor deviations between the AL obtained with an optical biometer and the actual value predicted using optical modelization. However, correction of AL accounting for distortions induced by refraction within the ocular media and variations in the average refractive index of the eye might help to progress further towards the desirable error-free biometric calculations in cataract surgery and CLE, particularly in longer eyes.

2.6. References

1. Chan B, Cho P, Cheung SW. Repeatability and agreement of two A-scan ultrasonic biometers and IOLMaster in non-orthokeratology subjects and post-orthokeratology children. Clin Exp Optom 2006;89:160-8.

2. Santodomingo-Rubido J, Mallen EA, Gilmartin B, Wolffsohn JS. A new non-contact optical device for ocular biometry. Br J Ophthalmol 2002;86:458-62.

3. Fledelius HC, Goldschmidt E. Oculometry findings in high myopia at adult age: considerations based on oculometric follow-up data over 28 years in a cohort-based Danish high-myopia series. Acta Ophthalmol 2010;88:472-8.

4. Mallen EA, Kashyap P. Technical note: measurement of retinal contour and supine axial length using the Zeiss IOLMaster. Ophthalmic Physiol Opt 2007;27:404-11.

5. Faria-Ribeiro M, Queiros A, Lopes-Ferreira D, et al. Peripheral refraction and retinal contour in stable and progressive myopia. Optom Vis Sci 2013;90:9-15.

6. Hitzenberger CK. Optical measurement of the axial eye length by laser Doppler interferometry. Invest Ophthalmol Vis Sci 1991;32:616-24.

7. Atchison DA, Smith G. Possible errors in determining axial length changes during accommodation with the IOLMaster. Optom Vis Sci 2004;81:283-6.

8. Atchison DA, Charman WN. Can partial coherence interferometry be used to determine retinal shape? Optom Vis Sci 2011;88:E601-E607.

9. de Vries NE, Webers CA, Touwslager WR, et al. Dissatisfaction after implantation of multifocal intraocular lenses. J Cataract Refract Surg 2011;37:859-65.

10. Narvaez J, Zimmerman G, Stulting RD, Chang DH. Accuracy of intraocular lens power prediction using the Hoffer Q, Holladay 1, Holladay 2, and SRK/T formulas. J Cataract Refract Surg 2006;32:2050-3.

11. Tsang CS, Chong GS, Yiu EP, Ho CK. Intraocular lens power calculation formulas in Chinese eyes with high axial myopia. J Cataract Refract Surg 2003;29:1358-64.

12. Aristodemou P, Knox Cartwright NE, Sparrow JM, Johnston RL. Intraocular lens formula constant optimization and partial coherence interferometry biometry: Refractive outcomes in 8108 eyes after cataract surgery. J Cataract Refract Surg 2011;37:50-62.

13. Ribeiro FJ, Castanheira-Dinis A, Dias JM. Personalized pseudophakic model for refractive assessment. PLoS One 2012;7:e46780.

14. Tang M, Li Y, Huang D. An intraocular lens power calculation formula based on optical coherence tomography: a pilot study. J Refract Surg 2010;26:430-7.

15. Navarro R, Santamaria J, Bescos J. Accommodation-dependent model of the human eye with aspherics. J Opt Soc Am A 1985;2:1273-81.

16. Atchison DA, Markwell EL, Kasthurirangan S, et al. Age-related changes in optical and biometric characteristics of emmetropic eyes. J Vis 2008;8:29-0.

17. Richdale K, Bullimore MA, Zadnik K. Lens thickness with age and accommodation by optical coherence tomography. Ophthalmic Physiol Opt 2008;28:441-7.

18. Shih YF, Chiang TH, Lin LL. Lens thickness changes among schoolchildren in Taiwan. Invest Ophthalmol Vis Sci 2009;50:2637-44.

Chapter 3: Computing Retinal Contour from Optical Biometry

3.1. Abstract

PURPOSE: To describe a new methodology that derives horizontal posterior retinal contours from partial coherence interference biometry (PCIB) and ray tracing using the corneal topography (CT).

METHODS: CT and PCIB for seven horizontal visual field eccentricities correspondent to the central sixty degrees of the posterior pole were obtained in 55 myopic eyes. A semi-customized eye model based on subject's CT and Navarro's eye model was generated using Zemax-EE software. The model was used to compute the optical path length (OPL) in the seven directions where PCIB measurements were obtained. Vitreous chamber depth was computed using the PCIB values obtained at each of those directions. Matlab software was developed to fit the best conic curve to the set of points previous obtained. We tested the limit in the accuracy of the methodology when it is not used the actual corneal of the subject and for two different lens geometry.

RESULTS: A standard eye model can induce an error in the retinal sagittas estimation of the order of hundreds of microns in comparison to the semi-customized eye model. However, the use of a different lens models leaves to an error of the order of tens of microns. The apical radius and conic constant of the average fit was -11.91 mm and -0.15, respectively. In general, a nasal-temporal asymmetry in the retina contour was found showing mean larger values of vitreous chamber depth in the nasal side of the eye.

CONCLUSIONS: The use of a semi-customized eye model together with OPL measured by PCIB for different angles can be used to predict the retinal contour within tenths of microns. This methodology can be useful in studies trying to understand the effect of peripheral retinal location on myopia progression as well as modelization of the optics of the human eye for a wide field.

KEYWORDS: coherence optical biometry; IOL Master; retinal contour; myopia; model eye for a wide field.

3.2. Introduction

Knowledge of the posterior retinal contour is potentially useful to understand the mechanisms of emmetropization and myopia progression.[1-3] Furthermore, the current knowledge in this field suggests that it might be possible to interfere with myopia progression by customizing the relative position of the peripheral focalization regarding the retinal surface.[4] To achieve a true customization of these treatments it will be essential to know the position and shape of the retinal surface in order to design an optical device able to change the refraction in the desired way.[5]

Retinal contour can be derived by a number of techniques, including indirect estimation from peripheral refraction measurements,[6] Optical Coherent Tomography (OCT),[7] and advanced imaging techniques such as magnetic resonance imaging (MRI).[8] While these techniques are not usually available in the context of a personalized optical prescription, they also lack the resolution needed to achieve a detailed knowledge of the retinal contour beyond 30º to 50º away from the fovea, where some of the currently available optical treatments aim to have a significant optical effect.[9-11]

Mallen and Kashyap used partial coherence interferometry (PCI) to perform peripheral biometry using the IOLMaster,[12] but their work has not dealt with optical distortion in peripheral measures, especially when the IOLMaster infrared beam passes through the lens in an oblique direction, pointed by Atchison and Charman as a potentially significant source of error.[13] Previous work also fails to consider the different refractive indices in the eye's media, as the IOLMaster measures the optical path length (OPL) between the corneal surface and the retina (RPE) and uses a single average refractive index in order to derive the physical eye length (EL) from the optical path length.[14]

Atchison and Charman,[13] have shown recently that PCIB technology might be suitable to measure the retinal contour if the OPL within each component of the eye is known. Then authors performed an interesting study theoretical study using a Gullstrand eye model to identify the potential errors when using PCIB obtained in two different axes. These authors already indicated in their article an eye model together with ray tracing and experimental measurements of PCI can be used to find the position of the retina as a function of the angle of the incident beam. Authors also mentioned

that accurate description of the retinal contour depends on the eye model used. PCIB values for different angles are relatively easy to obtain using commercial apparatus such as IOL master or the Lenstar. However, to perform a realistic customize eye model can be very complex due to lack of detailed measurements of the front and back surface of the lens and its gradient index. Conversely, there are a number of commercial systems available to obtain highly precise measurements of the corneal topography of the eye. Taking in to account that OPL is very sensitive to the corneal topography since it can differ very much from a sphere, as is the case of the front surface of the cornea of the Gullstrand eye model, we can presume that corneal topography will be an essential part of the eye model that should be used to obtain reliable data of the retinal contour. However, knowing the relatively small changes in refractive indices within the eye it might not be totally necessary to know the internal optics to compute the contour of its retina with an acceptable error margin.

Under this context, the goal of this work was to study the possibilities of using a semi-customized eye model to derive the horizontal posterior retinal contours using measures of eye length obtained with PCI biometry. The methodology will be use to find retinal contour of a group of subjects.

3.3. Methods

Measurements and subjects.

Eye length (EL) was measured in a group of 55 non-pathological young (22.05±1.78 years) myopes (-2.59 ± 1.29 D) by means of the IOLMaster (Carl Zeiss Meditec, Jena, Germany). For each subject, EL measures were obtained in 7 horizontal meridians (θ: from 30º nasal to 30º temporal, with respect to the visual axis, in 10º steps. Negative and positive values of θ represent nasal and temporal positions in the retina plane respectively. The procedure used was similar to the one previously described by Mallen et al.[12] The axis of the IOLMaster was maintained perpendicular to the corneal curvature at each position of measurement. A narrow beam of coherent light coming from the IOL Master entrances the eye along the apparatus axis it is captured a narrow beam coming out along the same axis and after diffused reflection in the retina. Thus,

following Fermat's principle, the optical paths traveled by the ray going-in and that going-out the eye are the same.

Corneal topography was also measured using a commercial topographer (Medmont E-300, Vermont, Australia). For each subject, all measurements were performed in the same eye (right eye).

Finding retinal single locations from IOL master measurements.

Direct measurements of the eye length by IOL master should not be used to obtain the position of the retina in the direction of measurement, as has been indicated previously.[13] However, knowing that IOL master uses an equivalent refractive index, n_{eq}=1.3549 ,[14] we can retrieve the OPL of the rays passing thought the eye at a certain angle (θ,multiplying EL by n_{eq}θ Then, assuming homogenous refractive index within the eye, measurements of EL made by the IOL Master at each θ direction can be related to vitreous path length $Vitreous_{PL}$(θ) in the same direction using the following expression:

$$IOLMaster_{EL}(\theta)*\mathbf{1.3549}=\boldsymbol{Cornea}_{PL}(\theta)*\mathbf{1.3856}+\boldsymbol{Aqueous}_{PL}(\theta)*\mathbf{1.3459}+$$
$$+\boldsymbol{Lens}_{PL}(\theta)*\mathbf{1.4070}+\boldsymbol{Vitreous}_{PL}(\theta)*\mathbf{1.3445} \quad \text{(Eq. 3.1)}$$

Where 1.3856, 1.3459, 1.4070 and 1.3445 have been proposed to be the group refractive indices of the eye for the wavelength used by the IOL master (780 nm) .[14] Using a model eye and a ray tracing software Zemax-EE (Zemax Development Corporation, Washington, USA), a ray was traced entering the eye perpendicular to the anterior cornea surface at each angle θ. From ray tracing, it can be known the direction and the physical distance traveled by the chief ray through the different media within the eye model: $Cornea_{PL}$(θ), $Aqueous_{PL}$(θ) and $Lens_{PL}$(θ).Those distances can be used in Eq.3.1 to compute the physical length of the vitreous chamber of the eye model, $Vitreous_{PL}$(θ) Seven points (x – semi-chord, z – sag), correspondent to the IOLMaster point of reflection in the retinal pigment epithelium (RPE), along the horizontal field of view, were obtained according to Zemax ray-trace referential, where the point (x=0, z=0) corresponds to the intersection of the visual axis with the retina plane.

Semi-customized eye-model.

For each subject a semi-customized eye model was built using the Navarro eye model,[15] with the front corneal surface replaced with a Zernike Standard Sag surface[16;17] computed from the topography of the subject. This surface includes a regular revolution conic surface plus a Zernike polynomial expansion, which accounts for departures of the real surface from the regular basis. Individual data obtained from anterior elevation topography were fitted to the Zernike Standard Surface equation by a least-squares method implemented in MATLAB (Mathworks, MA).[18]

Zemax-EE was then used to compute the ray tracing for each angle θ. As refractive index of the eye we have used the same mentioned in Eq. 3.1. In all cases, and especially for large negative or positive values of θ the beam from the instrument does not travel in a straight line inside the eye and the point where the ray reaches the retina does not lie in the direction of measurement as already described.

Estimating retinal contour from retinal single locations.

Traditionally ocular surfaces are described in terms of conic sections. A software was developed in Matlab (matrix laboratory, MathWorks) based in a minimum square method to compute the best fit of a conic surface to the seven retinal location points obtained using the methodology described above. The software was programmed to allow a free orientation of the fitted conic sections in order to express possible asymmetry aspects from the retina contour that would be lost if the conic sections were fitted in their canonical form. Thus, the program was able to estimate the apical radius, conic constant, orientation and apex location of the best conic fit. Once the software was applied to all the subjects we computed the mean and SD of the fitting errors to the conic curves (RMS) and removed fittings with errors above the mean ±3 SDs.

Testing the validity of the semi-customized eye model.

Finally, we studied the validity of using a semi-customized eye by did the calculations in two different ways. In the first one we computed the retinal contour using the anterior cornea from the Navarro eye model, consisting of a rotationally symmetric aspheric surface with apical radius of 7.72 mm and a conic constant of -0.26.[15] After this, the contour was estimated by incorporating the actual corneal topography from the

subject (semi-customized approach). Comparing the retinal contour results of the full Navarro eye model with those obtained in the semi-customized eyes, will let us know the importance of using corneal topography in our methodology.

In the second study we studied the need for a highly customized eye including the internal partial dimensions of the ocular media. We know that the thickness and shape of the crystalline lens changes with age becoming larger and thicker.[19;20] The use of an age-independent lens with a constant shape and thickness in our semi-customized model could then result in an important lack of accuracy in determining the retinal contour. We have checked this potential source of error by analyzing the change in the retinal contour using a full Navarro model eye, and them changing its lens for a 20 and 70 years lens as proposed by Atchison and collaborators.[19] In the procedure we first used the full Navarro eye model with a spherical retina of -12 mm radius to obtain the readings that the IOL master would produce for the seven angle θ values analyzed. Then we computed the changes in retinal contour obtained by modifying the lens geometry.

3.4. Results

Figure 3.1 presents the mean retinal contour obtained in the 55 right eyes by using the semi-customized eye model. Error bars showed ±2 times the intersubject standard deviation accounting for about 95% of the values. The large value of the error bars at ±8 mm from the fovea (corresponding to approximate θ=±30º) indicates the large variability of retinal contour between subjects. It can also be noted that there is an asymmetry between the nasal and temporal hemifields. An unpaired T-test comparing the average sagitta values obtained for both retina hemifields confirmed the asymmetry ($p<0.001$).

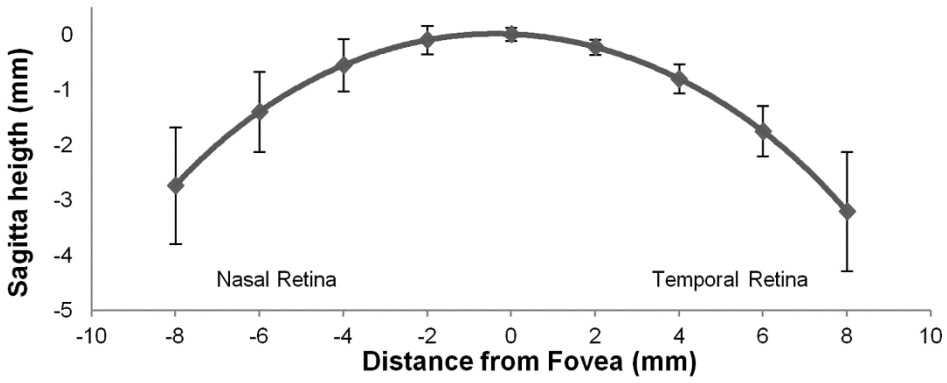

Figure 3.1. Average retina contour of the 55 subjects. Error bars represent ±2SDs.

Figure 3.2 also shows the mean retinal contour as a function of the angle of incidence of the ray, . We included two particular cases corresponding to those eyes that showed the largest, positive or negative, difference between hemifields (nasal-temporal).

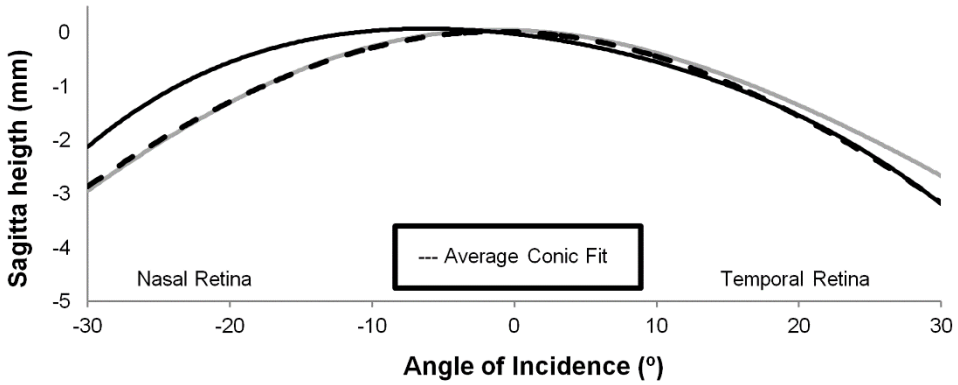

Figure3. 2. Average conic fit as a function of angle in object space (dotted line) and Nasal-Temporal retinal asymmetry of two individuals (squares and triangles).

Table 3.1, shows the statistics of the fitted conics regarding the apical curvature radius (R), conic constant (Q) angle of axis rotation (Theta), apex (x_0,z_0) coordinates and RMS as well as the fitted curve to the seven data points.

Table 3.1.

Range of the values obtained for the 55 fitted conics regarding orientation, tilt, apex decentrations, RMS of the residual and the resulting conic fit of the average sagitta values.

	Range			Conic Fit
RMS (mm)	0.007	to	0.104	0.002
Radius (mm)	-19.06	to	-7.26	-11.91
Q	-2.37	to	3.38	-0.15
Theta (º)	-43.47	to	44.51	11.56
Apex x_0 (mm)	-1.91	to	1.72	-0.36
Apex z_0 (mm)	-0.28	to	0.21	0.02

Figure 3.3 plots the average differences in the retina sagittas when using the generic cornea of the Navarro eye model instead of the individual corneal topographic data. Negative values represent steeper retinas across the posterior 16 mm of the horizontal posterior pole when using the generic cornea.

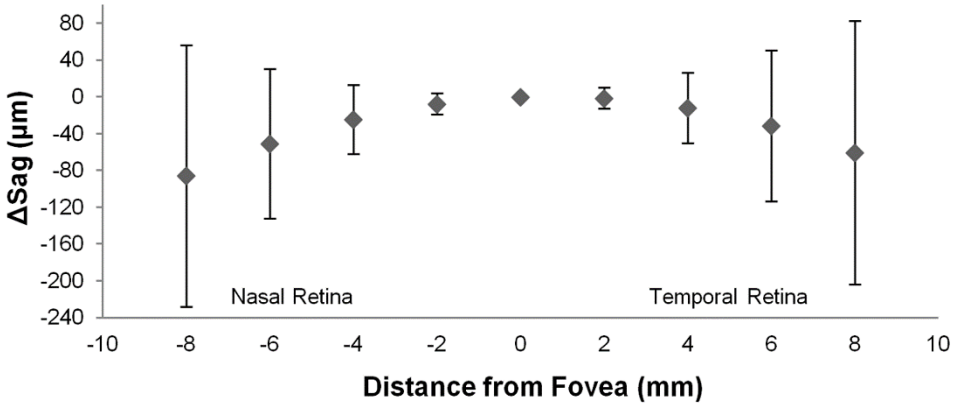

Figure 3.3. Average differences in the retina sagitta values when using a generic anterior cornea. Error bars represent ±2SD.

Figure 3.4 shows the differences in the retinal sagittas obtained when the lens of the Navarro eye model is changed to match that thickness and curvatures of a 20 and a 70 year old eye.[19] Negative values represent steeper retinas across the posterior 16 mm of the horizontal posterior pole when using an alternative lens model.

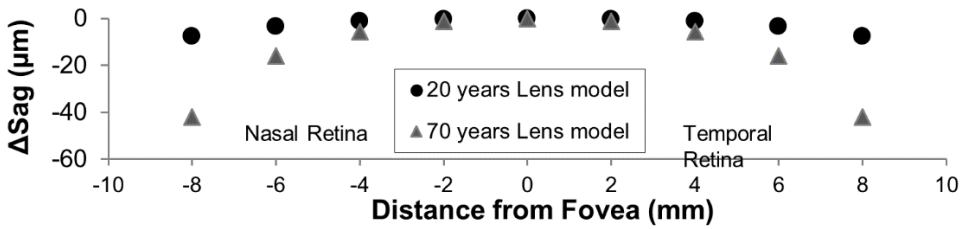

Figure 3.4. Differences in retinal sagitta height obtained, through the same method, for the 20 and 70 years old lens models.

3.5. Discussion

The present work describes a new method to derive a two-dimensional retinal contour within the central 16 mm of the horizontal posterior pole using clinically available technology to measure intra-ocular dimensions and numerical ray tracing.

As IOLMaster measures the OPL between the cornea and the retina, it can be expected that differences in the anterior elevation of the cornea (initial point of the OPL) as well as the length of the vitreous chamber (locating the final point of the OPL) and thickness of the crystalline lens should be critical when retrieving the retinal shape. Our results in 55 eyes agree with this rationale showing that the difference between assuming a standard cornea, for instance that proposed in Navarro eye model, and a customized cornea can lead to an error in the measurements of the retinal contour up to 244 microns (see Figure 3.3), which represents an error in the refraction of about 0.75D. Although not tested, we can assume that in eyes with pathological corneas, such as keratoconus or corneal penetrating keratoplastia, where deviations from a regular shape are much larger than in the population study in our study, the retinal contour estimates will be much more affected.

However, the cornea and lens change in thickness with respect the one presented in the Navarro eye model are usually lower than 150 and 500 microns, respectively. Thus, taking into account that the change in refractive index between those two refractive elements and the humors are about 0.04 and 0.06 for the cornea-aqueous humor and lens-aqueous or vitreous humor (see Eq. 3.1), we can expect that changes in OPL with the lens will differ about 36 microns between different eyes, except for phaquic or pseudophaquic eyes. Moreover, our previous simulation work has also shown that errors in estimating the actual axial length of the eye with PCI might be biased only by 56 µm in eyes with different lens thickness within a range of axial length from 20 to 30 mm.[21]

Our simulations in the present work have also confirmed this finding. Figure 3.4 shows that the difference in the retinal contour for the two lens configurations used in the simulations are within the range of tenths of microns. This value is typically in the order of magnitude of error in of repetitive measurements of the axial length given by the IOL Master,[22] and represents changes in the equivalent refractive sphere of the order of 0.1 D, which also are in the order of the repeatability of the open field autorefractometers usually used in the peripheral refractive measurements.[23]

Besides the small difference in the OPL for different optics inside the eye, there is also a change in the direction of the ray exiting the lens. This will also modify the retinal contour estimate. The actual deviation will depend on the particular model eye used,

but taking into account that the distances traveled by the rays within the eye are relatively small, it can be expected that a deviation of a few degrees will be traduced in a relatively small traverse deviation at the retinal plane. Our results of Fig. 4 also suggest that the errors given by this fact should be small for a ±8 mm horizontal semi-chord. Moreover, although we have presented the results of the retinal contour in terms of the physical distance in millimeters from the fovea (see Figure 3.1), they can be also presented as a function of angle θ (Fig.3. 2), which is the most common way of presenting the data in the literature.[24;25]

It would be complicated to precise the accuracy of our methodology since we would need to compare our results with another established methodology that give accurate results, to perform the measurements in a real eye with a known retinal contour or use an artificial eye that really mimics the human eye. Instead, to limit the accuracy of our methodology we used two studies. In one it is showed that using a standard eye model as have been indicated[13] let us to error in the retinal contour of the order of hundreds of microns. The second study indicates that using a standard lens model the error in the sagitta of the retinal contour will be of the order of tens microns (usually lower than 40 microns).

According to our data the study performed in 55 eyes highlights the inter-subject differences in the contour of the posterior pole of the eye in mild and moderate myopes using a new method that combines actual PCI measures with correction mechanisms based on ray tracing (see Figure 3.1 and 3.2). These differences can be as much as 2.3 mm at the 8 mm semi-chord of the nasal retina.

Retina sagitta height values as well as asymmetry between nasal and temporal hemifields were not correlated to a significant level with axial length or spherical equivalent refractive error. The majority of the subjects (48 out of 55) presented a positive asymmetry (Nasal Sag – Temporal Sag), i.e. longest vitreous chamber in the nasal hemifield (see fig. 1), which is in agreement with other reported results.[2;24;26] Thus our results indicates that retinal shape can vary considerably for different eyes, particularly beyond 4 mm from the fovea, as has been previously reported as a result of the stretching and elongation forces during emmetropization and ametropia development.[27] However, previous studies have also shown that the posterior shape of the eye might be related with the level of axial elongation, such that longer eyes will

tend to be steeper in the posterior pole. In this study we have not found a correlation between the changes in retinal shape and the central refraction. This is not surprising considering that all eyes included in our study were low to mild myopes and might have not suffered enough stretching or elongation forces that would be reflected in the contour of the posterior pole shape. Rather, our sample might be a good example of how random the posterior ocular surface might be in myopic eyes within a normal range of axial elongation.

Assuming that peripheral imagery has an influence on the emmetropization process and in the development of refractive errors, differences as large as 2 mm in the estimation of the retinal location at an angle of thirty degrees and beyond might help to explain why eyes with similar refractive error react differently to the same treatment as it has been observed in interventional studies that attempt to halt myopia progression using orthokeratology or peripheral gradient ophthalmic and contact lenses.[28-32] The results from the present study strength the need for semi-customized eye models incorporating actual corneal topography and actual retinal contour when it comes to design optical treatments for wide angles.[33]

In a future approach other meridians can be accessed using the same methodology to obtain a two-dimensional retinal surface. In that case, more complex surfaces than conics will be probably needed.

3.6. References

1. Dunne MC. A computing scheme for determination of retinal contour from peripheral refraction, keratometry and A-scan ultrasonography. Ophthalmic Physiol Opt 1995;15:133-43.

2. Logan NS, Gilmartin B, Wildsoet CF, Dunne MC. Posterior retinal contour in adult human anisomyopia. Invest Ophthalmol Vis Sci 2004;45:2152-62.

3. Atchison DA, Pritchard N, Schmid KL, et al. Shape of the retinal surface in emmetropia and myopia. Invest Ophthalmol Vis Sci 2005;46:2698-707.

4. Smith EL, III. Optical treatment strategies to slow myopia progression: Effects of the visual extent of the optical treatment zone. Exp Eye Res 2013.

5. Flitcroft DI. The complex interactions of retinal, optical and environmental factors in myopia aetiology. Prog Retin Eye Res 2012;31:622-60.

6. Logan NS, Gilmartin B, Dunne MC. Computation of retinal contour in anisomyopia. Ophthalmic Physiol Opt 1995;15:363-6.

7. Clark C, Konynenbelt B, Elsner A, et al. Retinal changes and peripheral refraction using optical coherence tomography. AAO . 2012.

8. Singh KD, Logan NS, Gilmartin B. Three-dimensional modeling of the human eye based on magnetic resonance imaging. Invest Ophthalmol Vis Sci 2006;47:2272-9.

9. Rosen R, Jaeken B, Lindskoog PA, et al. Evaluating the peripheral optical effect of multifocal contact lenses. Ophthalmic Physiol Opt 2012;32:527-34.

10. Lopes-Ferreira D, Ribeiro C, Maia R, et al. Peripheral myopization using a dominant design multifocal contact lens. J Optom 2011;4:14-21.

11. Queiros A, Gonzalez-Meijome JM, Jorge J, et al. Peripheral refraction in myopic patients after orthokeratology. Optom Vis Sci 2010;87:323-9.

12. Mallen EA, Kashyap P. Technical note: measurement of retinal contour and supine axial length using the Zeiss IOLMaster. Ophthalmic Physiol Opt 2007;27:404-11.

13. Atchison DA, Charman WN. Can partial coherence interferometry be used to determine retinal shape? Optom Vis Sci 2011;88:E601-E607.

14. Hitzenberger CK. Optical measurement of the axial eye length by laser Doppler interferometry. Invest Ophthalmol Vis Sci 1991;32:616-24.

15. Navarro R, Santamaria J, Bescos J. Accommodation-dependent model of the human eye with aspherics. J Opt Soc Am A 1985;2:1273-81.

16. Navarro R, Gonzalez L, Hernandez-Matamoros JL. On the prediction of optical aberrations by personalized eye models. Optom Vis Sci 2006;83:371-81.

17. Navarro R. The Optical Design of the Human Eye: a Critical Review. Journal of Optometry 2009;2:3-18.

18. Navarro R, Gonzalez L, Hernandez JL. Optics of the average normal cornea from general and canonical representations of its surface topography. J Opt Soc Am A Opt Image Sci Vis 2006;23:219-32.

19. Atchison DA, Markwell EL, Kasthurirangan S, et al. Age-related changes in optical and biometric characteristics of emmetropic eyes. J Vis 2008;8:29-0.

20. Dubbelman M, Van der Heijde GL. The shape of the aging human lens: curvature, equivalent refractive index and the lens paradox. Vision Res 2001;41:1867-77.

21. Faria-Ribeiro M, Lopes-Ferreira D, Lopez-Gil N, Gonzalez-Jeijome JM. Effects of Actual Axial Length and Central Crystalline Lens Thickness on Optical Biometry. 2013. Submitted for publication.

22. Santodomingo-Rubido J, Mallen EA, Gilmartin B, Wolffsohn JS. A new non-contact optical device for ocular biometry. Br J Ophthalmol 2002;86:458-62.

23. Davies LN, Mallen EA, Wolffsohn JS, Gilmartin B. Clinical evaluation of the Shin-Nippon NVision-K 5001/Grand Seiko WR-5100K autorefractor. Optom Vis Sci 2003;80:320-4.

24. Ehsaei A, Chisholm CM, Pacey IE, Mallen EA. Off-axis partial coherence interferometry in myopes and emmetropes. Ophthalmic Physiol Opt 2013;33:26-34.

25. Schmid GF. Association between retinal steepness and central myopic shift in children. Optom Vis Sci 2011;88:684-90.

26. Faria-Ribeiro M, Queiros A, Lopes-Ferreira D, et al. Peripheral refraction and retinal contour in stable and progressive myopia. Optom Vis Sci 2013;90:9-15.

27. Atchison DA, Jones CE, Schmid KL, et al. Eye shape in emmetropia and myopia. Invest Ophthalmol Vis Sci 2004;45:3380-6.

28. Kang P, Swarbrick H. Peripheral refraction in myopic children wearing orthokeratology and gas-permeable lenses. Optom Vis Sci 2011;88:476-82.

29. Cho P, Cheung SW. Retardation of myopia in Orthokeratology (ROMIO) study: a 2-year randomized clinical trial. Invest Ophthalmol Vis Sci 2012;53:7077-85.

30. Sankaridurg P, Donovan L, Varnas S, et al. Spectacle lenses designed to reduce progression of myopia: 12-month results. Optom Vis Sci 2010;87:631-41.

31. Sankaridurg P, Holden B, Smith E, III, et al. Decrease in rate of myopia progression with a contact lens designed to reduce relative peripheral hyperopia: one-year results. Invest Ophthalmol Vis Sci 2011.

32. Anstice NS, Phillips JR. Effect of dual-focus soft contact lens wear on axial myopia progression in children. Ophthalmology 2011;118:1152-61.

33. Wei X, Thibos L. Designing contact lenses for a wide field of view via ocular wavefront tomography. J Optom 2010;3:125-33.

Chapter 4: Morphology, Topography and Optics of the Orthokeratology Cornea

4.1. Abstract

PURPOSE: The goal of this work was to conduct an objective characterization of the external morphology, topography and optics of the cornea after orthokeratology.

METHODS: 24 patients (age 24±5 years) were fitted with Corneal Refractive Therapy® contact lenses to correct myopia between -2.00 and -5.00 D (-3.71±0.94 D). A classification algorithm was applied to conduct an automatic segmentation based on the mean local curvature. As a result, three zones (optical OZ, transition TZ and peripheral PZ) were delimited. Global and zonal fit to a general ellipsoid provided the topographical analysis. Ray trace on partially customized eye models provided wave aberrations and retinal image quality.

RESULTS: Monozone topographic description of the ortho-k cornea loses accuracy when compared with zonal description. Primary (C40) and secondary (C60) spherical aberration (SA) coefficients for a 5 mm pupil increased 3.68 and 19 times, respectively, after the treatments. OZ area showed a strong correlation with C40 ($r = -0.49$, $p<0.05$) and a very strong correlation with C60 ($r = 0.78$, $p<0.01$). OZ, as well as TZ, areas did not correlate with baseline refraction.

CONCLUSIONS: The increase in the eye's positive SA after ortho-k is the major responsible of the decreased retinal optical quality of the unaccommodated eye.

KEYWORDS: orthokeratology, corneal refractive therapy, spherical aberration, ocular aberrations, accommodation, myopia, myopia control, contrast sensitivity function, accommodative lag

4.2. Introduction

Orthokeratology (ortho-k), also known as corneal refractive therapy (CRT), is a safe and effective modality to correct low-to-moderate myopia,[1] by flattening the central cornea with the overnight application of reverse geometry rigid gas permeable contact lenses.[2] The corneal epithelium is reshaped by thinning in the central cornea and thickening in the mid-periphery.[2] These anatomical changes have huge optical consequences. Besides the correction of central myopia and a small reduction in with-the-rule astigmatism,[3] as the pupil dilates the quality of vision deteriorates due to the significant increase in optical aberrations,[4,5] leading to complaints of photic phenomena,[6,7] as well as fluctuations in vision over the course of the day due to the temporary and reversible nature of the treatment.[8] Once the correct corneal shape is well-established, the visual performance of ortho-k patients will then rely on the centration, area and power distribution of the central flattened zone (treatment zone or optical zone —OZ) and the surrounding steepening zone (transition zone –TZ). Other authors have attempted to estimate the dimensions of the optical and transition zones by visual inspection of the differential topographic maps[9] or by using an arbitrary criterion for segmentation of the different new formed zones.[10]

Quantitative methods to estimate the optical characteristics of the post ortho-k corneal surface will potentially be useful in determining the impact of lens design changes on the topographical and visual outcomes.[11] Furthermore, the objective characterization of the front corneal surface of the orthokeratology cornea may allow better understand the impact of t ortho-k corneal optics on visual performance and may eventually allow the optimization of lens designs. Optimal designs could then be used to achieve corrections such as regulation of myopia progression, by acting on the peripheral defocus,[12] or presbyopia correction, by improving the depth of field and/or the accommodative response of the eye.[13]

Thus, the first goal of the present work was to conduct an objective morphological topographical and optical characterization of the ortho-k cornea using an algorithm of classification that analyzes the Mean curvature from the post-treatment topographic map raw data. Subsequently, the influences of those changes in the optical quality were also investigated. Due to the interest in these three types of analysis, three complementary

methods were implemented: (1) Automatic determination and morphological analysis of the optical, transition and peripheral zones; (2) global and zonal topographical analysis by fitting a general ellipsoid topographic model; and (3) ray tracing in partially customized eye models of the patients to study their optical performance.

Throughout this paper the term morphology refers to structure and size changes of the limited zones of the anterior post ortho-k cornea, i.e., external morphology.

4.3. Material and methods

Ortho-K patients and measurements

Twenty-four patients (aged 24 ± 5 years) were fitted with Corneal Refractive Therapy® (Paflucon D, Paragon CRT®) contact lenses (CL) nine months (Mean 277±84 days) prior to data collection, to correct myopia between -2.00 and -5.00 D (Mean -3.71± 0.94 Diopters) with refractive astigmatism below 2.00 D. Paragon CRT® Dual Axis was used in subjects with limbus-to-limbus corneal astigmatism to improve centration of the treatment. Trial lenses were derived from sliding table nomograms provided by the manufacturer, which have shown high levels of predictability in terms of first trial success.[14] If needed, during the first two follow-ups, some CL parameters were changed to obtain a full correction of the myopic refraction with a well centered treatment. Fitting was evaluated according to the recommendations of the manufacturer regarding fluorescein pattern, topographical evaluation, and refractive and visual outcomes. All the enrolled subjects were able to achieve logMAR 0.0 visual acuity without any further compensation. All procedures were performed according to the Declaration of Helsinki. Approval for the study was obtained from the ethics committee of Minho University School of Sciences.

Local Mean Curvature maps

Left eye anterior elevation topography maps were obtained from all patients using Medmont E300 corneal topographer (Medmont, Victoria, Australia), with pupil center determined by the topographer as reference. Considering the high repeatability of the Medmont topographer only one topography per patient was used to extract the anterior elevation data, provided that it scored higher than 99 out of 100. All patients

attending the measurement visit were wearing the lenses overnight for at least three consecutive days. The raw elevation data of each patient was exported to Matlab and used to calculate the Mean curvature (H) which is the average of the principal curvatures k_1 and k_2, defined as the maximum and minimum curvatures of each sampled point among all orientations. Mathematically, the Mean curvature was computed for each corneal point according to its expression for functions with the form Z = Z(x, y) so called Monge Patch:[15]

$$H = \frac{\left(1+Z_y'^{\,2}\right) Z_{xx}'' - 2Z_x' Z_y' Z_{xy}'' + \left(1+Z_x'^{\,2}\right) Z_{yy}''}{2\left(\sqrt{1+Z_x'^{\,2}+ Z_y'^{\,2}}\right)^3} \qquad \text{(Eq.4.1)}$$

Where Z_x', Z_y', Z_{xx}'' and Z_{yy}'', are the first and second derivatives along the horizontal and vertical directions, and Z_{xy}'', is the crossed second derivative.

The Mean curvature can be expressed in keratometric diopters $H_D = 1000 \times (1 - 1.3375) \times H$, by assuming 1.3375 for the refractive index of the cornea. Optically H_D is the local spherical equivalent which is especially appropriated for our purposes.[16,17]

Zonal segmentation

To correct myopia, the central cornea is flattened to induce a reversible change on the epithelial thickness profile and the paracentral annular zone, of about 1.5 to 2.0 mm in width, surrounding the treatment zone, steepens in a direct relationship with the amount of central flattening needed to correct the myopic refractive error.[9] It is then expected that a successful treatment will produce a smooth central area with an almost constant power, followed by a surrounding zone with an abrupt increment in curvature. However, this will depend on the amount of correction and the curvature distribution of the anterior corneal surface before treatment. A third zone, corresponding to the most peripheral area of the cornea, will then be automatically defined by the limits of the steeper zone. The aim of the segmentation algorithm is to identify each of these three new formed zones. To achieve this, a cluster segmentation algorithm was implemented in Matlab based on the its native k-means function similar to the one described by González et al.[18] for LASIK treated corneas. This algorithm was programed to conduct an automatic segmentation based on the mean local curvature at each point. The algorithm assumes that each of the three sets of points of the different zones have

a normal distribution of curvatures. Hence, the global histogram will show a mixture of three Gaussians. The k-means algorithm splits these Gaussians, assigning every point of histogram to one of the three, according to the normalized Euclidean distance between the point and the Gaussian center. The result of the segmentation is that each point in the topography is assigned to one of the three zones, each represented by a binary mask. The main problem that arises from this approach is that some points from the peripheral zone (PZ)—normally more flat—will be assigned to the optical zone (OZ), due to their resemblance in curvature after the treatment. This can be easily solved by reassigning the OZ points that lay beyond the transition zone (TZ) to the PZ. The OZ and TZ diameter and center coordinates (x_0, y_0) can be obtained by least squares fitting the perimeter of the correspondent binary mask to a free orientated ellipse. Thus, coordinates x_0, y_0 of the center of the OZ represent decentrations of the ortho-k treatments with respect to the entrance pupil center.

In order to compute the Mean curvature maps, the original Medmont topography elevation data given in polar coordinates grid (300 spokes going counter clockwise with the first at the horizontal 3 o'clock position, and 32 rings) were interpolated and resampled to a square Cartesian coordinate grid. A fourth "no data" zone was included in the segmentation algorithm to allocate the points that fall out of the measurement area. This process provides a direct analysis of the morphological changes induced by the ortho-k treatments and allowed for an independent topographic fit of each zone.

General ellipsoid model fit

It is clear that topographies of real corneas do not match any ideal models such as spheres, ellipsoids, biconics, etc., but rather they exhibit different irregularities and departures from these simple geometries.[19] In the case of ortho-k corneas it is expected that this difference will be higher than in non-treated corneas. One of the problems that may arise from the fitting approaches used by most corneal topographers is that the entire shape of the ortho-k treated cornea may not be well described by the conic model coefficients, leading to biased estimates especially of the conic constants (asphericities).

In our approach, topographic data was described in terms of principal apical radius R_x, R_y and conic constants Q_x, Q_y, as well as its position (x_0, y_0, z_0) and orientation (Euler

angles α, β, γ) in the 3-dimensional space. This was accomplished by fitting the elevation data correspondent to each of the new formed zones, plus a global fit (monozone), to a general ellipsoid with three orthogonal axes and free position and orientation. A detailed description of the model and least-squares fit can be found elsewhere.[19] This model as well as all subsequent computations were implemented using Matlab (The MathWorks Inc., Natick, MA).

Wavefront error

Optical modeling was used to calculate aberrations of our subjects based on their anterior cornea topographic data. We assumed the same internal optics for all subjects, which enabled us to estimate the contributions of the ortho-k treatments in the optical performance. Two series of twenty four semi-customized eyes models were created in Zemax-EE numerical ray tracing software, based on the Navarro accommodative eye model,[20] with the front surface of the cornea replaced by the individual anterior elevation data of each patient (pre and post ortho-k), obtained from Medmont raw data. Detailed methodology can be found elsewhere.[21] The vitreous length (VL) was adjusted to produce emmetropia, through maximization of the Visual Strehl Modulation Transfer Function (VSMTF) metric[22] (see Retinal image quality section), in the ortho-k eye models. The same VL value was used to model the corresponding pre ortho-k eyes. Into-the-eye ray trace was performed to calculate on-axis aberrations of the eye models for a 5 mm entrance pupil. The wavefronts, sampled in 512 by 512 matrices, were exported to Matlab for additional processing. Results were calculated for 555 nm wavelength. The ANSI Z80.28 standard was used to represent Zernike aberrations of the eye models.[23]

Retinal image quality

Although it is unknown which criterion the human eye actually uses for focusing, and the ideal optimization method is yet to be determined, several metrics have been used to estimate refraction from wavefront data.[22,24,25] When higher-order aberrations are significant Cheng and co-workers[22] found that image plane quality metrics such as the Visual Strehl ratio computed in frequency domain (MTF method) (VSMTF) are less biased by the high levels of spherical aberration (SA). This metric takes into account that different frequencies respond differently to defocus and neural sensitivity varies with

frequency[26] in accordance to visual channel theory, which establishes that the visual pathway decomposes the input signal into frequency bands.[27]

The theoretical estimation of the retinal image quality (RIQ) in our model eyes was calculated according to the VSMTF expression:

$$VSMTF = \frac{\int_{-\infty}^{\infty}\int_{-\infty}^{\infty} \mathrm{CSF}_N(\mathrm{fx,fy})\cdot\mathrm{MTF}(\mathrm{fx,fy})\,\mathrm{dfxdfy}}{\int_{-\infty}^{\infty}\int_{-\infty}^{\infty} \mathrm{CSF}_N(\mathrm{fx,fy})\cdot\mathrm{MTF}_{\mathrm{DL}}(\mathrm{fx,fy})\,\mathrm{dfxdfy}} \quad \text{(Eq. 4.2)}$$

VSMTF is a normalized measure of image quality defined as the volume under the visually-weighted modulation transfer function (MTF) for an aberrated eye divided by the corresponding volume for an optically perfect eye (diffraction limited). CSF_N is the nominal neural Contrast Sensitivity Function and the MTF is the one computed in the eye model. MTF_{DL} is the diffraction limited MTF corresponding to the 5 mm pupil used here. This image quality metric provides a single value normalized between 0 and 1. This criterion was also used for the determination of the refractive state of pre and post ortho-K eye models (VSMTF Rx), using a method previously described.[28] All eye models where assumed to be well corrected for a 5 mm pupil diameter. This was accomplished subtracting the VSMTF Rx from the wavefronts before all calculations.

Statistical Analysis

In what follows all data are reported as means and standard deviations unless otherwise stated. Statistically significant correlations were marked with * and ** for $p < 0.05$ and $p < 0.01$, respectively.

4.4. Results

The upper panels in Figure 4.1 illustrates local spherical equivalent (mean curvature) and the lower panels show the results of the segmentation algorithm, for three different patients (a, b and c). From these examples it is clear that three independent and well delimited zones are formed after the ortho-k treatment is established, although with different power distributions.

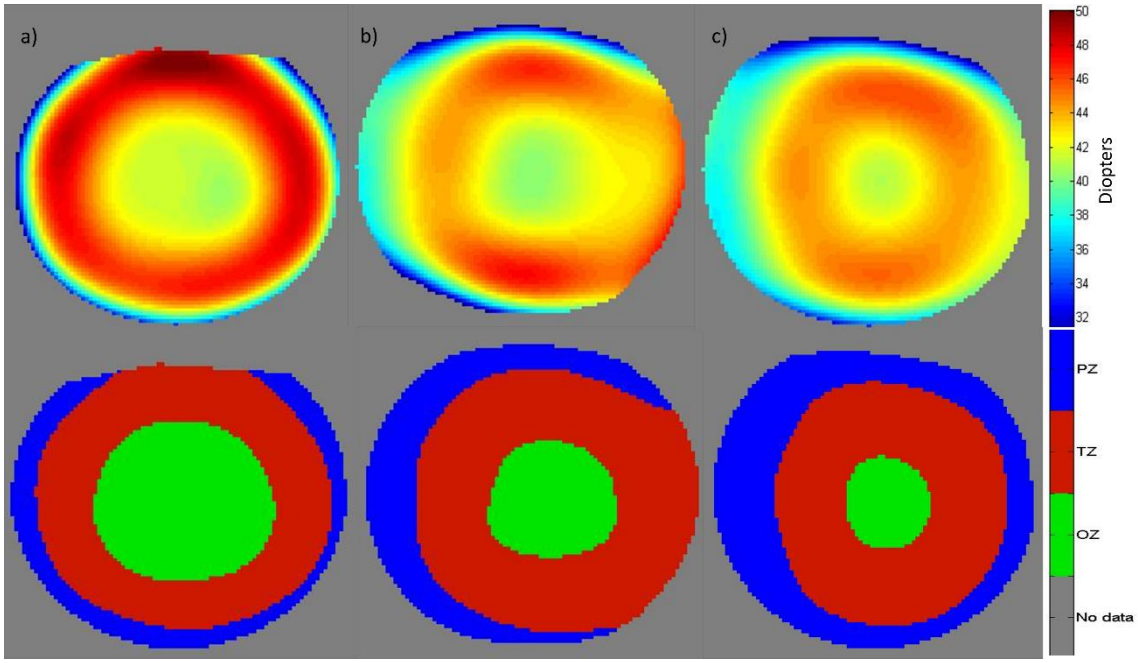

Figure 4.1. Mean curvature maps of three distinct patients (a, b and c) (top). Example of the resulting zonal segmentation obtained with the described algorithm (bottom).

The average results are summarized in Tables 4.1 to 4.4.

Table 4.1. Main topographical and morphological results (mean ± standard deviation) of the analysis of the ortho-k corneal topographies for the 24 subjects. RMSe represents the Root Mean Square error that results from the least squares fit of the anterior cornea elevation data to an ellipsoid with three orthogonal axes. Length units are in millimeters, Root Mean Square errors (RMSe) are in micrometers.

	Monozone		**Optical Zone (OZ)**		**Transition Zone (TZ)**	
	PRE	**POST**	**PRE**	**POST**	**PRE**	**POST**
			Morphologic data			
Diameter (mm)				3.53 ±0.56		6.94 ±0.25
Center (mm) x_0				0.13 ±0.25		0.08 ±1.21
y_0				-0.10 ±0.20		0.00 ±0.00
H_D (Diopters)	42.38 ±0.74	42.20 ±0.72	43.93 ±0.80	41.66 ±0.73	42.98 ±0.24	45.06 ±0.24
			Topographic data			
R_X (mm)	7.68 ±0.16	8.14 ±0.19	7.71 ±0.17	8.44 ±0.21	7.69 ±0.16	8.23 ±0.18
R_Y (mm)	7.50 ±0.15	7.91 ±0.16	7.54 ±0.15	8.26 ±0.16	7.51 ±0.15	8.03 ±0.14
Q_X	-0.27 ±0.06	0.40 ±0.20	-0.16 ±0.13	1.29 ±0.70	-0.23 ±0.08	0.71 ±0.23
Q_Y	-0.29 ±0.06	0.36 ±0.19	-0.17 ±0.13	1.24 ±0.67	-0.25 ±0.08	0.67 ±0.22
RMSe (µm)	1.48 ±0.47	3.48 ±1.03	0.13 ±0.08	0.22 ±0.11	0.96 ±0.38	1.36 ±0.49

The morphological data show that the average optical zone diameter is 3.53 mm. OZ is slightly decentered by an average of about a tenth of mm in the temporal and inferior

directions, but the high standard deviation values suggest a marked intersubject variability. When considered as a single zone, the mean curvature of the cornea did not change significantly following ortho-k treatment (diff=- 0.18D; p>0.05). This was due to the flattening of the central cornea corresponding to the optical zone (-2.27 D) being counterbalanced by a significant steepening of the cornea corresponding to the transition zone (+2.08 D). The RMS ellipsoid fit error increases from 1.48 micrometers in the pre ortho-k cornea up to more than double of that value (3.48 micrometers) for the post ortho-k cornea, which suggests that after the treatment the cornea can hardly be approximated by the ellipsoid model. This is the reason why the multizone model was implemented. The fitting errors improve quite dramatically when separate zones are considered instead of the monozone approach. In fact, the change in spherical equivalent refraction (calculate using the VSMTF criterion) due to the ortho-k treatments seems to agree rather well with the mean apical radius change within the OZ, but not when these changes were calculated from the monozone model fit (see Table 2). An opposite trend is observed when comparing OZ versus TZ. The decreased in Mean curvature inside the OZ is followed by an increase in the TZ by a similar amount. Although the apical radii that describe the post ortho-k corneal TZ are flatter, their correspondent Q values are much more positive which indicates a greater steeping of the corneal curvature away from the apex.

Table 4.2. Refractive changes (spherical equivalent) induced by the ortho-k treatments (mean ± standard deviation), calculated from different corneal descriptors. To convert from apical radius to diopters a refractive index of 1.3375 was considered for the cornea.

Mean Refractive Changes (Diopters)		
Baseline Sph. Eq.	**-3.71**	**±0.94**
ΔRadius OZ	-3.83	±0.89
ΔRadius Monozone	-2.40	±0.72

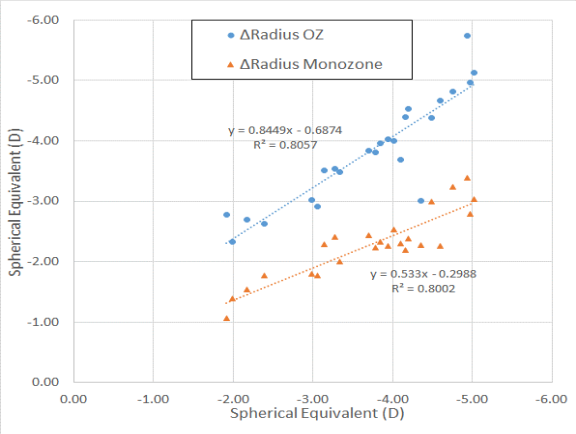

Figure 4.2. Linear regressions of the results listed in Table 2. The slope of the linear regressions is an indicative of the direct relation between refractive descriptors.

Table 4.3. Main results (0mean ± standard deviation) of the optical/image analysis of the ortho-k corneal topographies for the 24 subjects.

		PRE	POST
Optical and Image Quality (5 mm pupil)			
C_4^0	(μm)	0.126 ±0.03	0.464 ±0.12
C_6^0		0.001 ±0.01	0.019 ±0.03
C_3^1		0.041 ±0.11	-0.041 ±0.29
C_3^{-1}		0.029 ±0.15	0.069 ±0.22
RIQ		0.32 ±0.06	0.18 ±0.06

Table 4.3 contains data of the optical and image quality parameters. Primary (C_4^0) and secondary (C_6^0) SA coefficients (5 mm pupil) increased by 3.68 and 19 times, respectively, after the treatments. This seems to be in agreement with the changes also seen in the ellipsoids conic constants passing from negative to positive values (see Table 1). In addition, the small OZ average diameter means that peripheral rays pass through the more curved transition zone, and hence these rays exhibit large amounts of positive SA. Horizontal third order coma retains the same mean value but with opposite sign, while the vertical component more than doubles, although still maintaining reasonable low values. Consequently, due to the high increase in SA, RIQ worsens—almost half VSMTF—in the ortho-k eye models compared to the pre-treatment eyes. Although this seems not to affect high contrast visual acuity (all subjects achieved LogMAR 0.0), it is expected to deteriorate acuity during low contrast tasks.

It is expected that the changes in anterior corneal shape after ortho-k produce changes in the optical performance of these eyes. To test this hypothesis, correlations between topographic, morphologic and image quality descriptors were calculated and listed in Table 4.4.

Table 4.4. Pearson correlations between morphological, topographical and retinal image quality descriptors for the post ortho-k eye models. Only significant correlations are listed.

	Area		H_D	Q_{XY}		OZ		C_4^0	C_6^0
	OZ	TZ	TZ - OZ	OZ	TZ	x_0	y_0		
C_3^{-1}							-0.858**		
C_3^1						-0.936**			
C_4^0	-0.488*		0.588**	0.718**					-0.443*
C_6^0	0.780**	-0.464*	0.407*	-0.695**	0.456*			-0.443*	
RIQ	0.604**			-0.697**				-0.827**	0.576**
Pre SE[+]			-0.764**	-0.590**	-0.529**		-0.414*	-0.836**	

[+] Pre ortho-k spherical equivalent error.

It can be seen that both horizontal and vertical coma correlate strongly with the OZ decentering (coordinates x_0 and y_0, respectively). OZ area, as well as the difference between the OZ and TZ mean curvatures, showed a strong correlation with primary SA C_4^0 and a very strong correlation with secondary SA C_6^0. It seems that higher C_6^0 is associated with larger OZ's. As a consequence, RIQ showed a very strong negative correlation with C_4^0 and a strong but positive correlation with C_6^0. The low correlation found between C_4^0 and TZ area can be attributed to the use of a 5 mm entrance pupil, which will restrain part of the contribution of this zone to the image formation. OZ, as well as TZ, areas did not correlate with baseline spherical equivalent (PRE SE). As expected from the results in Table 4.1 the difference between TZ and OZ mean curvatures (TZ – OZ) is strongly correlated with PRE SE, since the change in power tends to be redistributed between these two zones.

4.5. Discussion

The present study combines three complimentary methods of analysis of the morphology, topography and optical/image quality of the post ortho-k cornea. The first method and algorithm permits the objective quantification of the areas and power distribution across the different new formed zones—optical, transition and peripheral zone. A similar methodology has been previously applied to the particular case of post-LASIK corneas by González el al.[18] The ortho-k treated cornea is a challenging condition as it usually includes significant asymmetries and irregularities. Lu et al.[9] delimitated the different zones using the difference curvature tangential map and used the size of the treatment zone as a metric to correlate with the visual outcomes during the treatment

onset. While this approach could be sufficient for well-defined optic zones, it might become difficult and arbitrary in cases with narrow localized areas of flattening surrounded by a zone with abruptly increasing curvature. Here the Mean curvature H was used instead, which has two crucial advantages. On the one hand H is a physical invariant, which means that it is an intrinsic property of the corneal surface regardless of the measuring conditions. On the other hand, when multiplied by the increment of refractive index, it provides, in a first approximation, the local spherical equivalent.

For the topographical analysis a general ellipsoid model[19] was implemented. It is worth mentioning that while the ellipsoid model provides reasonably good fits of normal corneas, the model fit gets poor in post ortho-k corneas, similarly to what happens in post-LASIK corneas.[18] Thus, elevation data fitted to an ellipsoid by a monozone approach will not reflect the true shape of the ortho-k cornea. Instead, better fits are obtained when individual zones are fitted (see Table 1 RMS values monozone fit vs. zonal fit), which implies that the increase in asphericity after ortho-k—especially in the OZ—would be largely underestimated by the monozone approach.

For the optical and image quality analysis the pre and post ortho-k wavefronts, computed by ray tracing on partially customized eye models, were compared. The strong negative correlation between OZ area and primary SA for a 5 mm pupil diameter seem to indicate that larger OZ's contribute to the decrease in positive C_4^0, but increase—with a more significant correlation—the contribution of positive C_6^0. Contrary to what one might expect, wide and well defined OZ's were not correlated with lower baseline refractions. The lack of correlation between zonal areas and baseline refraction suggests that other factors rather than the degree of corneal remodeling—such as lid tonus and corneal biomechanics—play a more important role in the formation of those zones. It is worth to remark that these resulting zones, OZ, TZ, and PZ are defined according to the statistical distribution of the Mean curvature descriptor, normalized for each analyzed cornea. This means that the resulting OZ is an area where the Mean curvature has relatively homogeneous values, and the same applies to TZ and PZ.

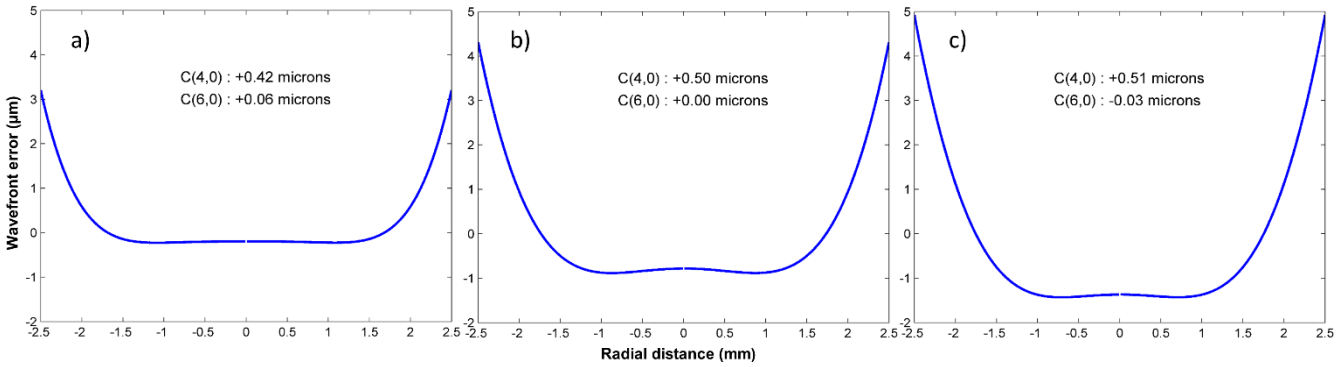

Figure 4.3. Mean radial wavefront error profiles, representative of the optical path difference inside a 5 mm pupil after ortho-k, and their impact in C_4^0 and C_6^0, for the three eyes of figure 1 (patients a, b and c).

Larger OZ's tend to have more homogeneous central zones with less positive Q values ($r=-0.55$, $p<0.01$). The central flattening creates a wider area of uniform power surrounded by a more peripheral steepening zone, as in example (a) of figure 4.3, which increases the positive contribution of 6th order SA ($C_6^0>0$) needed to fit the wavefront error profile. On the other hand, smaller OZ's, as in example (c) of figure 4.3, tend to have smoother dioptric power changes from the center to the margin of the pupil with narrow and irregular zones of flattening, which decreases the positive contribution of 6th order SA ($C_6^0\leq 0$) needed to fit the wavefront error profile. The correlation found between C_4^0 and C_6^0 ($r = -0.44$; $p<0.05$) results from the nature of Zernike polynomials, were higher-order polynomials include lower-order terms for balancing. Thus, considering the example of Figure 4.3 a) the amount of C_4^0 needed to balanced 0.06 microns of C_6^0 would be about 0.36 microns ($C_6^0 \times \sqrt{7/5} \times 5$), which indicates similar levels of Seidel primary and secondary SA. When considering the example of patient c), the contrary is seen. The amount of C_4^0 needed to balanced -0.03 microns of C_6^0 would be about -0.18 microns, which indicates a larger amount of primary Seidel SA.[29]

This increase in the eye's positive C_4^0 is the major factor responsible for the decrease in the RIQ of the unaccommodated eye, estimated using the VSMTF metric, and might also influence its accommodative response.[30-33]

In summary, the present study provides a methodology to better understand the morphology, topography and optics of the ortho-k cornea and their influence in the optical performance of these eyes. These conclusions might be useful to better understand the

influences of ortho-k in myopia progression or to investigate future ortho-k lens designs to optimize the correction of refractive errors or presbyopia.

4.6. References

1 Koffler BH, Sears JJ. Myopia control in children through refractive therapy gas permeable contact lenses: is it for real? *Am J Ophthalmol* 2013; 156: 1076-1081.e1071.

2 Reinstein DZ, Gobbe M, Archer TJ, Couch D, Bloom B. Epithelial, stromal, and corneal pachymetry changes during orthokeratology. *Optom Vis Sci* 2009; 86: E1006-1014.

3 Mountford J, Pesudovs K. An analysis of the astigmatic changes induced by accelerated orthokeratology. *Clin Exp Optom* 2002; 85: 284-293.

4 Queirós A, Villa-Collar C, González-Méijome JM, Jorge J, Gutiérrez AR. Effect of pupil size on corneal aberrations before and after standard laser in situ keratomileusis, custom laser in situ keratomileusis, and corneal refractive therapy. *Am J Ophthalmol* 2010; 150: 97-109.e101.

5 Mao XJ, Lu F, Qu J. [Effects after orthokeratology on corneal topography and monochromic wavefront aberration]. *Zhonghua Yan Ke Za Zhi* 2004; 40: 471-473.

6 Santolaria E, Cerviño A, Queirós A, Brautaset R, González-Méijome JM. Subjective satisfaction in long-term orthokeratology patients. *Eye Contact Lens* 2013; 39: 388-393.

7 Santolaria Sanz E, Cerviño A, Queiros A, Villa-Collar C, Lopes-Ferreira D, González-Méijome JM. Short-term changes in light distortion in orthokeratology subjects. *Biomed Res Int* 2015; 2015: 278425.

8 Kobayashi Y, Yanai R, Chikamoto N, Chikama T, Ueda K, Nishida T. Reversibility of effects of orthokeratology on visual acuity, refractive error, corneal topography, and contrast sensitivity. *Eye Contact Lens* 2008; 34: 224-228.

9 Lu F, Simpson T, Sorbara L, Fonn D. The relationship between the treatment zone diameter and visual, optical and subjective performance in Corneal Refractive Therapy lens wearers. *Ophthalmic Physiol Opt* 2007; 27: 568-578.

10 Maseedupally V, Gifford P, Lum E, Swarbrick H. Central and paracentral corneal curvature changes during orthokeratology. *Optom Vis Sci* 2013; 90: 1249-1258.

11 Kang P, Gifford P, Swarbrick H. Can manipulation of orthokeratology lens parameters modify peripheral refraction? *Optom Vis Sci* 2013; 90: 1237-1248.

12 Queirós A, González-Méijome JM, Jorge J, Villa-Collar C, Gutiérrez AR. Peripheral refraction in myopic patients after orthokeratology. *Optom Vis Sci* 2010; 87: 323-329.

13 Felipe-Marquez G, Nombela-Palomo M, Cacho I, Nieto-Bona A. Accommodative changes produced in response to overnight orthokeratology. *Graefes Arch Clin Exp Ophthalmol* 2015; 253: 619-626.

14 López-López M, Pelegrín-Sánchez J, Sobrado-Calvo P, García-Ayuso D. Contact lens intolerance: refitting with dual axis lens for corneal refractive therapy. *Journal Of Optometry* 2011; 4: 4.

15 Gray A. "A Monge Patch." Modern Differential Geometry of Curves and surfaces with Mathematica, 2*nd* ed: Boca Raton, FL; CRC Press 1997.

16 Navarro R. Refractive error sensing from wavefront slopes. *J Vis* 2010; 10: 3.

17 Navarro R. Objective refraction from aberrometry: theory. *J Biomed Opt* 2009; 14: 024021.

18 González L, Hernández-Matamoros JL, Navarro R. Multizone model for postsurgical corneas: analysis of standard and custom LASIK outcomes. *J Biomed Opt* 2008; 13: 044035.

19 Navarro R, González L, Hernández JL. Optics of the average normal cornea from general and canonical representations of its surface topography. *J Opt Soc Am A Opt Image Sci Vis* 2006; 23: 219-232.

20 Navarro R, Santamaría J, Bescós J. Accommodation-dependent model of the human eye with aspherics. *J Opt Soc Am A* 1985; 2: 1273-1281.

21 Faria-Ribeiro M, López-Gil N, Navarro R, Lopes-Ferreira D, Jorge J, González-Méijome JM. Computing retinal contour from optical biometry. *Optom Vis Sci* 2014; 91: 430-436.

22 Cheng X, Bradley A, Thibos LN. Predicting subjective judgment of best focus with objective image quality metrics. *J Vis* 2004; 4: 310-321.

23 Thibos LN, Applegate RA, Schwiegerling JT, Webb R, applications VSTMVs, its. Standards for reporting the optical aberrations of eyes. *J Refract Surg* 2002; 18: S652-660.

24 Thibos LN. Unresolved issues in the prediction of subjective refraction from wavefront aberration maps. *J Refract Surg* 2004; 20: S533-536.

25 Thibos LN, Hong X, Bradley A, Applegate RA. Accuracy and precision of objective refraction from wavefront aberrations. *J Vis* 2004; 4: 329-351.

26 Campbell FW, Robson JG. Application of Fourier analysis to the visibility of gratings. *J Physiol* 1968; 197: 551-566.

27 Sachs MB, Nachmias J, Robson JG. Spatial-frequency channels in human vision. *J Opt Soc Am* 1971; 61: 1176-1186.

28 Guirao A, Williams DR. A method to predict refractive errors from wave aberration data. *Optom Vis Sci* 2003; 80: 36-42.

29 Xu R, Bradley A, López Gil N, Thibos LN. Modelling the effects of secondary spherical aberration on refractive error, image quality and depth of focus. *Ophthalmic Physiol Opt* 2015; 35: 28-38.

30 Benard Y, Lopez-Gil N, Legras R. Subjective depth of field in presence of 4th-order and 6th-order Zernike spherical aberration using adaptive optics technology. *J Cataract Refract Surg* 2010; 36: 2129-2138.

31 López-Gil N, Fernández-Sánchez V. The change of spherical aberration during accommodation and its effect on the accommodation response. *J Vis* 2010; 10: 12.

32 López-Gil N, Martin J, Liu T, Bradley A, Díaz-Muñoz D, Thibos LN. Retinal image quality during accommodation. *Ophthalmic Physiol Opt* 2013; 33: 497-507.

33 Thibos LN, Bradley A, López-Gil N. Modelling the impact of spherical aberration on accommodation. *Ophthalmic Physiol Opt* 2013; 33: 482-496.

Chapter 5: Effect of Pupil Size on Wavefront Refraction during Orthokeratology

5.1. Abstract

PURPOSE: It has been hypothesized that central and peripheral refraction, in eyes treated with myopic overnight orthokeratology, might vary with changes in pupil diameter. The aim of this work was to evaluate the axial and peripheral refraction and optical quality after orthokeratology, using ray tracing software for different pupil sizes.

METHODS: Zemax-EE was used to generate a series of 29 semi-customized model eyes based on the corneal topography changes from 29 patients who had undergone myopic orthokeratology. Wavefront refraction in the central 80º of the visual field was calculated using three different quality metrics criteria: Paraxial curvature matching, minimum Root Mean Square error (minRMS) and the Through Focus Visual Strehl of the Modulation Transfer Function (VSMTF), for 3 and 6 mm pupil diameters.

RESULTS: The three metrics predicted significant different values for foveal and peripheral refractions. Compared with the Paraxial criteria, the other two metrics predicted more myopic refractions on- and off-axis. Interestingly, the VSMTF predicts only a marginal myopic shift in the axial refraction as the pupil changes from 3 to 6 mm. For peripheral refraction, minRMS and VSMTF metric criteria predicted a higher exposure to peripheral defocus as the pupil increases from 3 to 6 mm.

CONCLUSIONS: The results suggest that the supposed effect of myopic control produced by ortho-k treatments might be dependent on pupil size. Although the foveal refractive error does not seem to change appreciably with the increase in pupil diameter (*VSMTF* criteria), the high levels of positive spherical aberration will lead to a degradation of lower spatial frequencies, more significant under low illumination levels.

KEYWORDS: Pupil Size, Peripheral Refraction, Wavefront Refraction, Orthokeratology Visual metrics

5.2. Introduction

Orthokeratology (ortho-k) changes the ocular refraction by the programmed application of reverse geometry rigid gas permeable contact lenses. To correct myopia, the central cornea is flattened to induce a reversible change on the epithelial thickness profile. The central epithelial layer thins and the front surface corneal power decreases over the central 4 to 5 mm central zone. The paracentral zone (transition zone) of 1.5 to 2.0 mm surrounding the central zone increases in curvature, in a direct relationship with the amount of central flattening needed to correct the myopic refractive error.[1]

With the advent of highly permeable materials, overnight ortho-k has become an effective and safe mode of vision correction for moderate and low myopia and was approved by the United Sates Food and Drug Administration in 2002.[2] Over the last decade, systematic research reports, including randomized and controlled clinical trials, confirmed that ortho-k reduces the rate of axial length increase by 40% to 60% in children when compared with single vision spectacles or contact lenses.[3] Ortho-k is currently one of the most effective optical strategies of myopia control, and is at present the modality with the largest volume of accumulated evidence relating to the efficacy to regulate myopia progression in children.[3,4]

Previous research has explored potential predictors of the myopia regulation effect with ortho-k. Cho et al.,[5] found a moderate correlation between the treatment target and the regulation effect. In their cohort of ortho-k lens wearers aged from 6 to 10 years, higher myopes had a lower axial elongation over a 2 years' period, while the opposite was found in a spectacle control group. This result raises the hypothesis that the greater the corneal reshaping effect the higher the regulation efficacy, probably as a result of greater peripheral myopic defocus.[6,7] However, these trends have not been confirmed in other similar studies after 2 and 5 years,[8,9] including a controlled and randomized study.[10] Despite the correlation between treated myopia and peripheral myopic shift of about 1:1 seen in ortho-k eyes[11] this relationship gets complicated by the significantly different eye shapes and meridional asymmetries seen in myopic eyes.[12,13]

Recently an association was found[14] between pupil size and myopia control effect, in eyes treated with orthokeratology. Larger pupil diameters were associated with higher control effect, hypothetically as a result of a larger retinal area being exposed to the peripheral myopic defocus. This effect might come as a consequence of the peripheral increase in corneal curvature induced by these treatments, and it is expected to vary depending on the area of the cornea flattened by the lens treatment zone. However, larger pupil size might also change the pattern of relative peripheral refraction, either sphere or cylinder and contribute to the difference in regulation effects found. Thus, the theoretical evaluation of the effect of the pupil size on the effective optical focusing properties of the eye seems to be relevant to improve our understanding of the working principles and efficacy of such treatments.

Most autorefractors used to assess the effect of ortho-k treatment are limited to a measured annular zone of approximately 2.0 to 3.0 mm[15-17] irrespective of the actual pupil size of the patient. Modern aberrometers normally use two different criteria to estimate refraction from wavefront data. One approach, called Zernike refraction, specifies the vergence of a point source that focuses a ‘‘disk of least confusion’’ into the image plane, defined by the retinal layer where the aberrometer’s probe beam reflects. The second approach, Paraxial refraction, specifies the vergence of a point source that focuses paraxial rays into the plane of reflection of the aberrometer’s probe beam.[18] In the absence of higher-order aberrations, Zernike and Paraxial refractions are identical, but in eyes such as the ones treated with ortho-k the high levels of positive 4th order spherical aberration, and other higher orders,[19,20] may bias these metrics in different ways.[21] Zernike defocus will tend to yield more myopic refractions as the pupil becomes larger, due to increased contribution of positive spherical aberration. Paraxial refraction, by definition, will not change with pupil diameter if sufficient higher-orders terms are used in the calculation. Thus, none of these methods may be robust enough to obtain an unbiased estimation of refraction,[22] especially for large field angles. Considering that all the information regarding refraction and quality of vision in the periphery is derived from instruments optimized to measure axial refraction, we hypothesize that ray-tracing could be used to isolate the contribution of the different optical elements of the eye and bypass some of the encountered limitations in peripheral aberrometry.[23]

The present study aims to test the hypothesis that changes in pupil size induce changes in the pattern of axial and peripheral refraction and peripheral optical quality using ray tracing software. To this end, a fundamental aspect is to find the most appropriate metric for estimating the refractive errors from the wavefronts computed in our partially customized eye models.

5.3. Methods

Ortho-K patients and measurements

Twenty-nine patients (age 24±5 years) were fitted with Corneal Refractive Therapy® (paflufocon D, Paragon CRT®) contact lenses (CL) for 9 to 12 months to correct myopia between -1.00 and -5.75 D (mean±SD = -3.62±1.11 Diopters) with refractive astigmatism below 1.50 D.[24] Paragon CRT® Dual Axis was used in subjects with limbus-to-limbus corneal astigmatism. The initial CLs were fitted following the monograms of adaptation of the CRT® manufacturer. If needed, some CL parameters were changed to obtain a full correction of the myopic refraction and, at the same time, a well centered treatment. Trial lenses were derived from sliding table nomograms provided by the manufacturer, which have shown high levels of predictability in terms of first trial success.[25] Fitting was evaluated according to the recommendations of the manufacturer regarding fluorescein pattern, topographical evaluation, and refractive and visual outcomes. Parameters of the CRT lenses were as follows: base curve radius (mean±SD [minimum, maximum]) = 8.22±0.49 mm [7.80, 8.80 mm], return zone depth (RZD) = 530.80±19.32 µm [500, 575 µm], and landing zone angle (LZA) = 31.45°±0.88° [31.00°, 34.00°]. These refer to the final parameters of lenses worn by patients, not necessarily the first trial lenses.

All the enrolled subjects were able to achieve logMAR 0.0 visual acuity without any further compensation. Individual data from anterior elevation topography of each patient left eye, was obtained using Medmont E300 corneal topographer (Medmont, Victoria, Australia), with pupil center determined by the topographer as reference. All patients attending the measurement visit were wearing the lenses overnight for at least three consecutive days. Changes in morphology, topography and optics after ortho-k can be found in chapter 4 of this thesis.

Semicustomized eye models

Zemax-EE numerical ray tracing software was used to create a series of 29 semi-customized eyes models based on the Navarro eye model.[26] The front surface of the cornea of that initial generic eye model was replaced by the Zernike Standard Sag surface[27] computed from the elevation data of each patient. This surface includes a regular revolution conic surface plus a Zernike polynomial expansion, which accounts for departures of the real surface from the regular basis.[28] The individual data were fitted to a Zernike Standard Surface equation by a least-squares method implemented in Matlab (The MathWorks, Natick MA). The same internal optics were used in all the semi-customized eye models to isolate the contribution of the ortho-k treatments. The vitreous length of each model eye was optimized for central vision according to the Paraxial focus metric criteria. This was accomplished by minimizing the Root Mean Square (RMS) wavefront error with respect to the centroid, at a visual field of 0 degrees, of Zemax's default merit function, using a small entrance pupil diameter of 0.1 mm.

Wavefront Error

Into-the-eye ray trace was performed across the central 80º of the horizontal field, sampled in 10º steps, at a reference wavelength of 555 nm with entrance pupil diameters of 3 and 6 mm. Zemax software can provide wavefront *W(x,y)* from the optical path differences (OPDs). OPD is calculated by tracing a bundle of rays passing through a grid of points (*x,y*) on the exit pupil plane. The effective pupil is a circle on-axis and approximately elliptical off-axis. Zemax also provides a modal representation of the wavefront expressed in terms of standard Zernike polynomials.[27] However, since Zernike aberrations can be derived only for circular pupils, the software stretches the off-axis elliptical pupil along its minor axis into a circular form, by a factor equal to its aspect ratio (minor diameter/major diameter). Using this method, Zernike coefficients were calculated up to 6th order and reported using the Optical Society of America standard.[29] Both representations of the wavefront, raw data (values on a 512x512 samples grid) and modal (Zernike coefficients), were exported to Matlab for further processing.

On- and Off-Axis Refraction from Wavefront Data

The refractive state of the eye can be measured by subjective or objective methods. Although it is unknown which criteria the human eye actually uses for focusing, and as such the ideal optimization method is yet to be determined, several metrics have been used to estimate refraction from wavefront data.[18,30,31] When higher-order aberrations are significant, image plane quality metrics such as the Visual Strehl ratio computed in frequency domain (MTF method) (VSMTF) seem to be less biased by the high levels of spherical aberration.[31,32] This metric takes into account that different frequencies respond differently to defocus and neural sensitivity varies with frequency[33] in accordance to visual channel theory, which establishes that the visual pathway decomposes light in frequency bands.[34]

In this work we calculated foveal and peripheral refraction from wavefront data, obtained by ray tracing, using the following metrics:

Zernike and Paraxial Refraction

For eccentric fields, i.e. elliptical pupils, Zemax stretches the wavefront along the minor axis into a circular pupil in order to fit the wavefront OPDs with circular Zernike polynomial. Such stretching affects all the Zernike coefficients.[35] Recently, Zernike-like orthogonal polynomials were proposed for elliptical pupils.[36,37] Nevertheless, here we were mainly interested in computing the refractive error, so we used the equations provided by Atchison et al.[38] truncated at 2nd order for Zernike refraction and up to 6th order for Paraxial refraction. Since Zemax calculates the approximate shape of the wavefront at the exit pupil as seen from the on-axis chief ray image point,[27] we implemented an improvement which may be important for large field angles due to pupil aberrations: Instead of assuming that the minor axis of the off-axis pupil shortens by a factor equal to the cosine of the field angle (θ), we calculated the actual aspect ratio of the wavefront at the exit pupil. For the sake of simplicity there is no need to alter the original equations. The proper correction can be accomplished by substituting θ in the original equations by the inverse cosine of the aspect ratio of the exit pupil. Validation of this approach was performed with a Matlab script written to stretch the wavefronts imported from Zemax along their minor axis into a circular form, fit the optical path

differences with Zernike circular polynomials and compare the obtained coefficients with the ones computed in Zemax. All differences between coefficients were below 0.005 microns, justifying the validity of the approach.

VSMTF Trough Focus Refraction

The other approach used to calculate wavefront refraction was similar to the one previously described by Guirao and Williams.[39] Detailed methodology can be found in the cited paper. The procedure executes a search in a three-dimensional space, finding the values of sphere, cylinder and axis of the correcting lens that yields the maximum value of a visual quality metric. This was achieved computationally by adding to the computed wavefronts a series of defocused spherical and cylindrical wavefronts that simulate the trial lenses employed during a subjective refraction examination. In summary, this procedure finds the spherical-cylindrical wavefront which, when added to the ocular wavefront obtained by ray tracing, optimizes the eye model retinal image quality according to the *VSMTF* objective metric criteria:

$$VSMTF = \frac{\int_{-\infty}^{\infty}\int_{-\infty}^{\infty} \mathrm{CSFN(fx,fy)\cdot MTF(fx,fy)dfxdfy}}{\int_{-\infty}^{\infty}\int_{-\infty}^{\infty} \mathrm{CSFN(fx,fy)\cdot MTFDL(fx,fy)dfxdfy}} \qquad \text{Eq.(5.1)}$$

The quick contrast sensitivity functions (*qCSF*) curves measured by Rosén et al.[40] at 20 degrees of the nasal and temporal visual fields, were used (courtesy of Linda Lundström) to derive the Neural Contrast Sensitivity Functions (CSF_N) for each peripheral location. The qCSFs for 20 degrees nasal and temporal visual fields were M-scaled for the other peripheral locations according to the cortical magnification factor (*M*) equations provided by Rovamo and Virsu,[41] and applied in eq. 5.1 as general population models of the peripheral CSF_N.

Astigmatic Off-Axis Refraction

Sphero-cylindrical refractions were converted to spherical equivalent (M), with or against-the-rule astigmatism (J_0) and oblique astigmatism (J_{45}),[42] and applied in the following equations to calculate the off-axis tangential (F_T) and sagittal (F_S) power errors, considering clinical refractive notation with negative cylinder:

$$F_T = M + J_0$$
$$F_S = M - J_0 \qquad \text{Eq.(5.2)}$$

F_S and F_T components represent, in this case, the dioptric vergence required to correct the power error in the radial and sagittal meridians along the horizontal visual field (J_{45}=0). It is worth mentioning that all subjects were treated as stigmatic by removing the on-axis J_0 and J_{45} values for all field positions. This way we isolated the effect of off-axis oblique astigmatism from foveal astigmatism.

All the procedures were repeated for entrance pupils' diameters of 3 and 6 mm. The entrance pupil position and center was interactively calculated by Zemax's robust ray-aiming algorithm. Matlab scripts and a Zemax macro were written to automatize all the procedures and export the values into data sheets.

Best Metric Criteria

In order to establish which metric predicts the best foveal refraction we computed the image quality for each eye model, with 3 and 6 mm pupils. The wavefront error maps of each patient, at 9 different visual field angles, and 2 pupil diameters, were exported from Zemax to Matlab as 512x512 matrices. Each wavefront matrix was used to compute the point-spread function (PSF), and the optical transfer function (OTF), using standard Fourier optics methods. The PSFs for 0 degrees of visual field were convolved with an eye chart template to simulate the retinal image.

Two random sub sets of 29 images, correspondent to these simulated images optimized according to each of the three quality metrics described above, for 3 and 6 mm pupil diameters, were subjectively evaluated by three well corrected, experienced observers. The observers were blinded to the metric criteria used and asked to grade with a score between 5 and 0 with terms for general guidance (Excellent, Good, Fair, Poor, Bad) each of the images, presented in a 13-inch computer screen at a 50 cm distance. Measures were conducted under good levels of illumination (~300 Lux) to keep the observes pupillary diameters smaller, and thus diminishing the effect of higher-order aberrations. Each of the computed images was presented together with a second image of a perfect non-aberrated model eye for reference. A similar procedure has been used recently to grade the image quality generated by multifocal lenses by Rio and Legras.[43]

Statistical Analysis

Statistical analysis was conducted using SPSS v21.0 program (IBM Inc. IL). All data are reported as mean and standard deviation unless otherwise stated. Paired t-tests were used to compare the differences between the three metrics *(F_S, F_T* and *M* refraction components, as well as the aberration Zernike coefficients for primary horizontal coma and spherical aberration), for 3 and 6 mm pupils, at all field angles. A *p*-value < 0.05 was considered statistically significant.

5.4. Results

Figure 5.1 shows the refraction profiles across 80º of visual field along the horizontal meridian for 3 mm and 6 mm pupil diameters, calculated using three different metric criteria. The vitreous length of each eye model was adjusted for emmetropia using the Paraxial metric criteria. As a consequence, the eye models present an ametropic condition for the other two metric criteria, with more myopic axial refractions (-0.47±0.28D and -0.69±0.42D for the VSMTF and minRMS, respectively, for a 3 mm pupil). As the pupil dilates from 3 mm to 6 mm, Paraxial metric criteria predicts a hyperopic shift in axial refraction (difference = +0.25±0.17D; p<0.01). The other two metrics predicted myopic shifts in axial refraction as the pupil dilates from 3 to 6 mm, but while the *minRMS* metric predicts a significant myopic shift in axial refraction (difference = -2.66D±0.68D; p<0.001), interestingly, the *VSMTF* predicts only a marginal myopic shift (difference = -0.03D; p=0.043), which is consistent with experimental findings.[44]

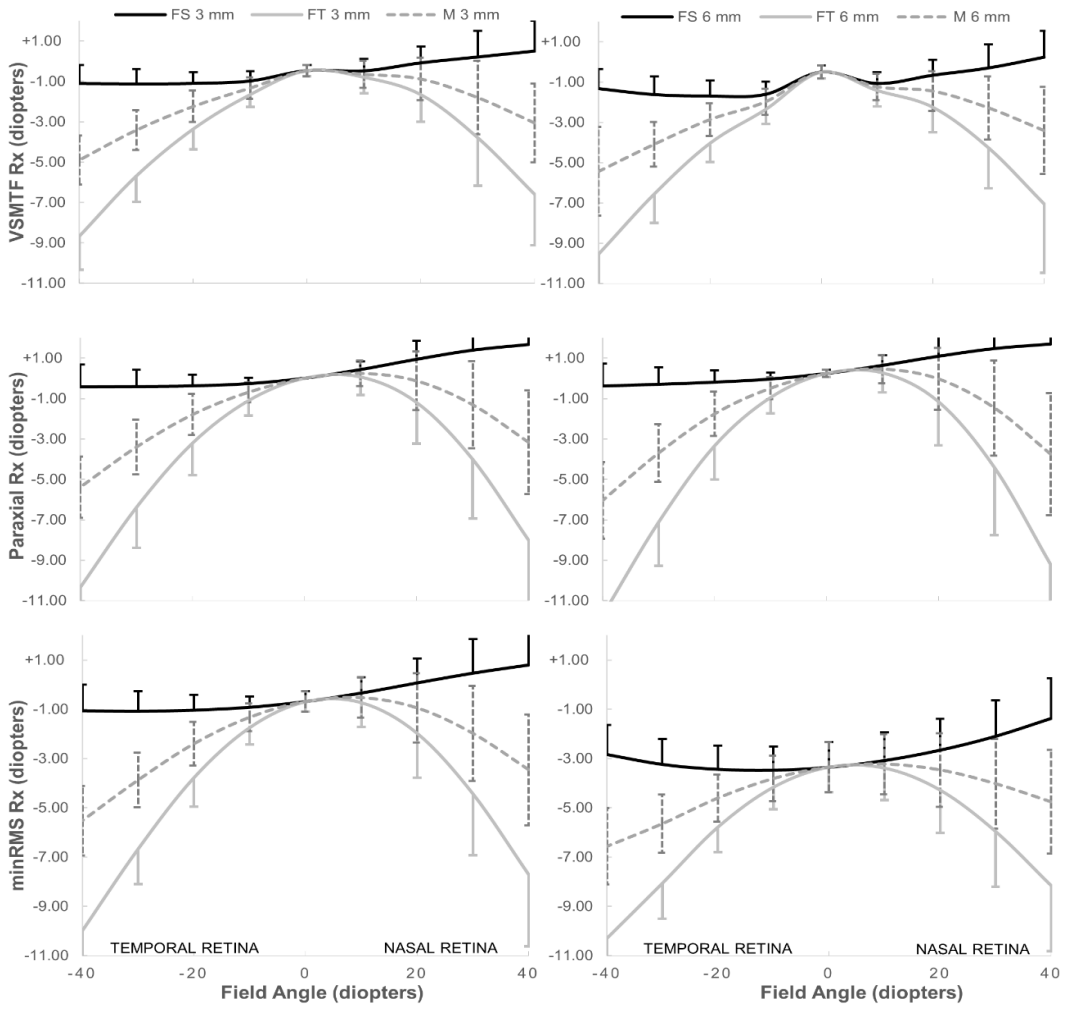

Figure 5.1. Axial and peripheral refraction for 3 mm (left column) and 6 mm (right column) pupil diameters, across 80º degrees of visual field along the horizontal meridian calculated using the *VSMTF* (top), Paraxial (middle) and *minRMS* (bottom) metrics. Negative values of eccentricity represent the temporal retina (nasal visual field) and positive values represent the nasal retina (temporal visual field). Error bars represent one standard deviation.

As for peripheral refraction, the three metrics refractive components F_S, F_T and M present statistically significant differences between pupil sizes for almost all field angles except for the VSMTF metric F_T component at -40º and 40º ($p = 0.18$ and $p = 0.09$, respectively), for the Paraxial metric F_T component at 20º ($p = 0.41$) and M component at -20º ($p = 0.08$). F_S, F_T and M refractive components also show a strong significant correlation between 3 and 6 mm pupil diameters ($r \geq 0.7$; $p < 0.05$ except for the

locations mentioned above), for all of the three metrics, with the 6 mm pupil refractive components always being more negative when calculated using the *VSMTF* and *minRMS* metric criteria. As expected the correlation between the refractive components calculated for 3 and 6 mm pupil diameter were higher (r>=0.97; p<0.01), except for F_S at 10º (r=0.86; p<0.01), when the Paraxial criteria was used. In theory, Paraxial refraction should be independent of pupil size. This lack of a perfect correlation, along with a small but significant difference (p<0.01 for all angles except for M at -20º and F_T at 20º) in the peripheral refractive pattern between the two pupil sizes, may be due to the non-inclusion of higher (than 6th) order terms, such as 8th order spherical aberration, in the calculations.

The change in the peripheral refraction pattern, associated to the increase in pupil diameter, is most substantial when using the *minRMS* than with the *VSMTF* and Paraxial metrics. The peripheral refractive profile of the *minRMS* metric seems to reflect the refractive contribution of the more peripheral zones of the cornea as the visual angle increases. With the increase in pupil diameter, there is a clear myopic shift in the most central visual fields (more light is refracted by the more curved transition zone), that decreases for more peripheral angles as the contribution of the flatter peripheral zone of the cornea increases. Curiously, this is the only metric of the three that predicts a decrease in oblique (off-axis) astigmatism as the pupil increases (the shift in F_S is greater than the shift in F_T, decreasing the interval of Sturm). The previous pattern is less evident when the *VSMTF* metric is used. This is due to the nature of the peripheral *CSF*. As the visual field increases the peripheral *CSF* gives more emphasis to the lower spatial frequencies of the *MTF*, which are optimized by a more negative lens.[21]

Peripheral refraction M component presents a strong correlation with baseline axial refraction ($M_{baseline}$) (0.79> r >0.60; p<0.001 at ±40º, for the 3 metric criteria and both pupil sizes). Despite these strong correlations, higher myopes will experience more peripheral defocus for both pupil sizes, thus the shift in peripheral refraction with the increase in pupil diameter will not be dependent of baseline axial refraction (0.05> r >0.003; p>0.5 at ±40º, for the 3 metric criteria and both pupil sizes).

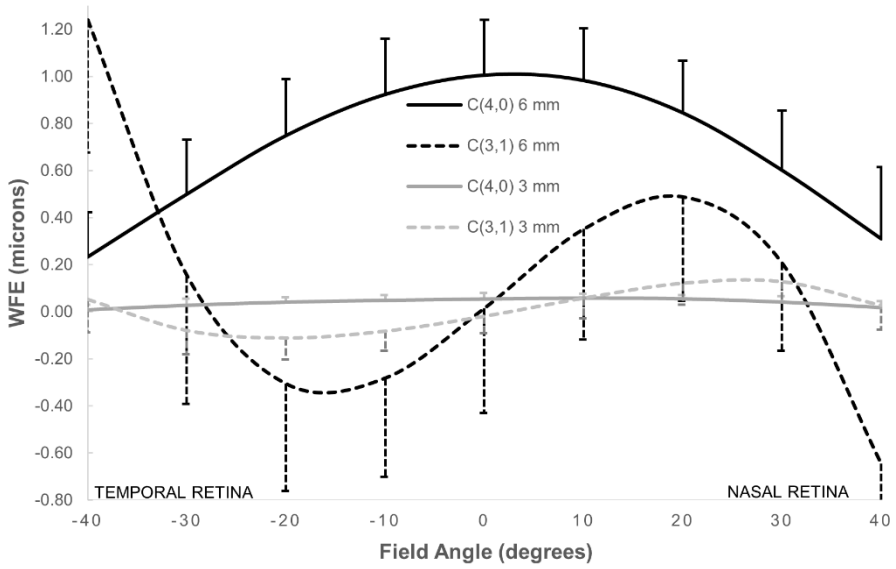

Figure 5.2. Primary Zernike spherical aberration (C_4^0) and horizontal coma (C_3^1) for the 80º degrees of visual field along the horizontal meridian, for both pupil sizes. Negative values of eccentricity represent the temporal retina (nasal visual field) and positive values represent the nasal retina (temporal visual field). Error bars represent one standard deviation.

Figure 5.2 shows the pattern of primary horizontal coma and spherical aberration coefficients for both pupil sizes. The reverse in slope seen in the primary coma near ±20º seems to be due to the sudden decrease in power, corresponding to the transition from the more curved paracentral zone to the flatter peripheral zone. It can be seen from the curve that the treatments are slightly asymmetric, and slightly decentered to the temporal side. Third-order horizontal coma showed significant differences between the 3 and 6 mm pupil size with the exception of values around zero-crossings. Difference was maximum at -40º of the nasal visual field (1.24 microns; $p<0.001$) and lower at the center (0.034 microns, $p>0.017$).

Fourth-order spherical aberration presented statistically significant differences between 3 and 6 mm pupil size for all locations measured ($p<0.001$). Difference was maximum at 0º (0.95 microns; $p<0.001$), and lower for the ±40º locations (0.29 and 0.20 microns, respectively; $p<0.001$). Spherical aberration for a 6 mm pupil diameter presents values almost 4 times higher than the ones encountered in untreated eyes.

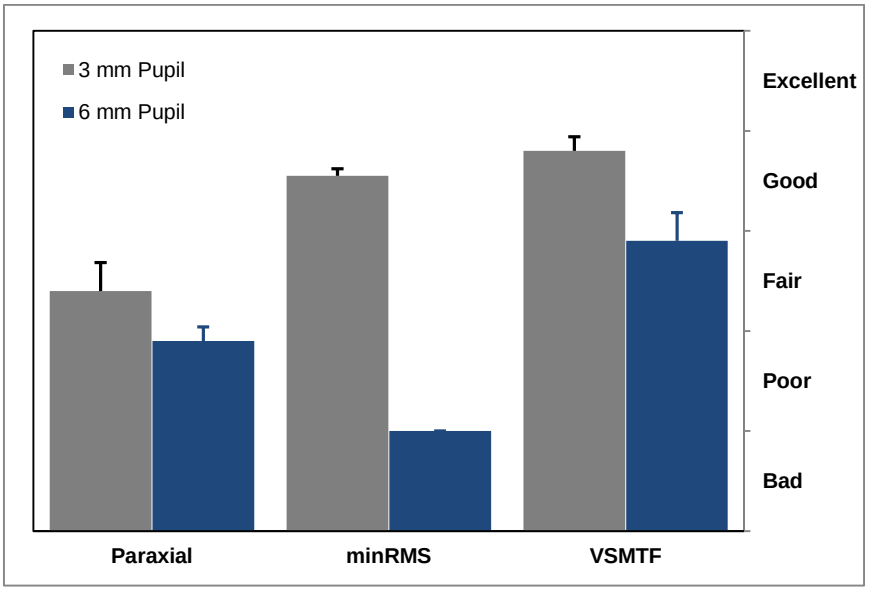

Figure 5.3. Subjective rating of the 2 sets of simulated retinal images using each of the three metrics presented to 3 trained observers to rank image quality.

Figure 5.3 shows the average rating of the two sets of images graded by the observers to derive a quantitative (though subjective) information on which metric would perform better for foveal vision. According to our observers, there are only small differences in the perceived image quality for a 3 mm pupil, between the minRMS and the *VSMFT*. The Paraxial metric clearly shows the worst performance. As for a 6 mm pupil the *VSMTF* is clearly superior to both Paraxial and *minRMS* quality metrics. For the larger pupil size Paraxial metric was graded higher than the *minRMS* metric, as opposed to the result found with the smaller pupil.

The visual quality degradation (foveal vision) as a result of the increase in higher order aberrations as a consequence of the increased pupil diameter can be seen in the convolved images of Figure 5.4.

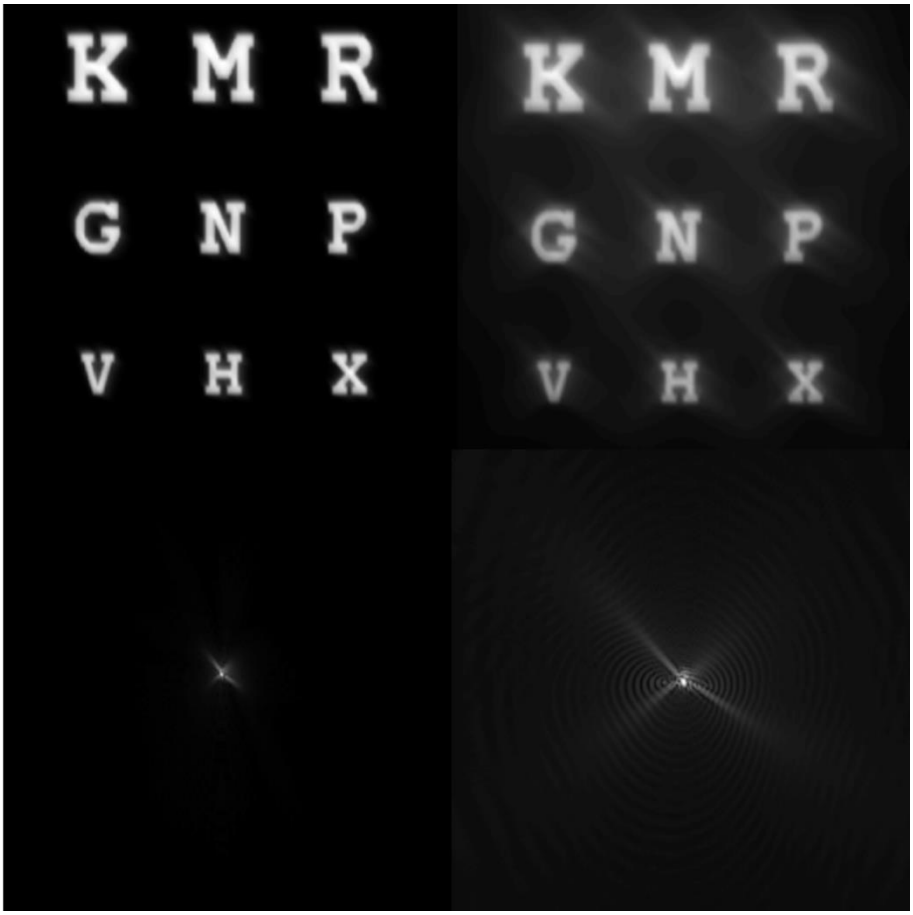

Figure 5.4. Comparison of the foveal images simulated for a patient with 3 mm (left) and 6 mm pupil diameter (right) and their respective PSFs (bottom).

5.5. Discussion

With this study we aimed to verify the hypothesis that central and peripheral refraction, in eyes treated with myopic overnight orthokeratology, might suffer variations with changes in pupil diameter. It has been suggested that, in the presence of primary spherical aberration, conventional measurements of subjective refraction closely match the ones predicted by the Paraxial refraction metric, largely because this is optimal for objects whose spatial frequency spectrum is dominated by high frequencies, such as small letters.[44] Subjective grading of simulated retinal images revealed that, although central refraction does not seem to change appreciably despite the increase in pupil diameter from 3 to 6 mm, refractive errors estimated using the observers preferred metric (*VSMTF*) tend to be more myopic than the ones predicted by

the Paraxial metric for both pupil sizes, and closer to the ones predicted by the minRMS metric for a 3 mm pupil, in concordance with the results of Xu et al.[21] This result seems to be inverted with the increase in pupil size. For a 6 mm pupil, minRMS predicts a large myopic shift that does not seem to correspond to the best image, according to our observer's evaluation. From the example of Figure 5.4 it is also clear that the quality of the image perceived by these patients is highly dependent of pupil size and probably of the spatial content of the visual task as well.[45] Although the foveal refractive error does not seem to change appreciably with the increase in pupil diameter (*VSMTF* criteria), the high levels of positive spherical aberration will lead to a degradation of lower spatial frequencies, more significant under low illumination levels, in agreement with subjective complains.[46,47] It is expected that in those scenarios patients will benefit of a more negative refraction in order to enhance lower spatial frequencies.[21,48] As the field angle increases, the on-axis spherical aberration becomes coma aberration, contributing to the peripheral image degradation. This and other high-order aberrations might interact to decrease image contrast in the periphery.

The three metrics predict significantly different peripheral refraction profiles as the pupil diameter increases from 3 to 6 mm. The subjective process used to grade the quality of the simulated foveal images corrected by each metric cannot be used for peripheral vision but, it is clear that in the presence of higher order aberrations the *VSMTF* is clearly superior to the *minRMS* and Paraxial metric criteria, for estimating the refractive correction that maximizes visual acuity based on wavefront aberration measurements. It is then reasonably to expect that for peripheral imagery, where the pupils are nearly elliptical and higher order terms are far more significant than in fovea, visual metrics that take neural factors into account should also yield less biased results than metrics calculated solely based on the Zernike coefficients. That said, the hypothesis suggested by Chen[14] that large pupil diameters could facilitate the effect of ortho-k to slow axial growth because of enhancement of the myopic shift in the peripheral retina, seems to agree with the myopic shift observed in the *VSMTF* peripheral refraction profile when the pupil diameter increases from 3 to 6 mm.

Our previous studies showed that the peripheral eye length for the average myope is shorter in the temporal retina.[13] The ortho-k treatments of our sample have

shown a displacement towards the temporal side of the cornea, which is in agreement with previous reports.[49,50] Thus, for a light beam passing at the same distance from the center of the pupil, incident light from the nasal visual field will follow a shorter optical path towards the temporal retina, compared with the incident light from the temporal visual field. Overall, the more curved cornea and shorter eye length, and the flatter cornea and longer eye length will tend to compensate each other to render a more symmetric peripheral refraction as seen in Figure 5.5.

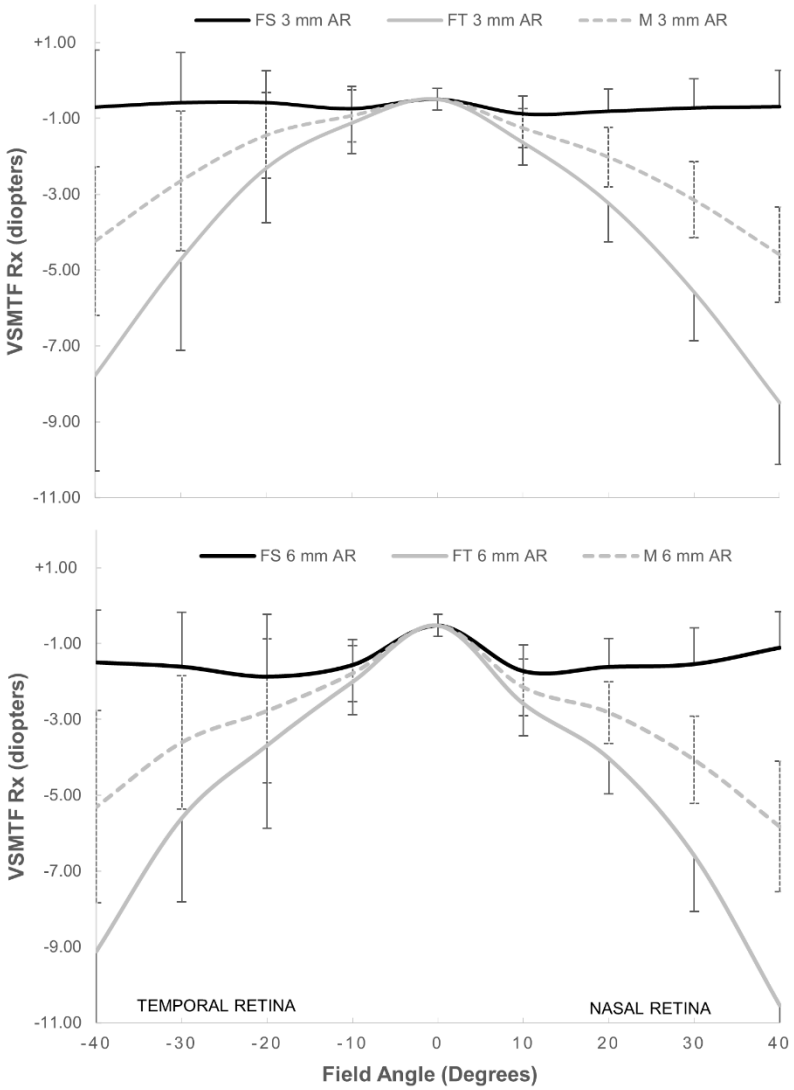

Figure 5.5. *VSMTF* refraction calculated by substituting the symmetric retina of the Navarro eye model by the average myopic asymmetric retina (AR). Error bars represent one standard deviation.

In this case, the *VSMTF* metric for a 3 mm pupil diameter predicts a relative peripheral refraction profile similar to the profiles derived from measurements with the Grand Seiko open field autorefractor after ortho-k in treatments of the same degree.[11,51-53] As the pupil diameter increases from 3 to 6 mm the average peripheral refraction profile calculated from the *VSMTF* suffers a myopic shift that can be mainly explained by the greater contribution of the paracentral zone of the treated corneas[11] and the lower sensitivity to high frequencies encountered in the peripheral retina. In turn, peripheral refraction measured by the autorefractor will not take any of this changes into account. The working principle of the Grand Seiko autorefractor uses a near infrared 2.3 mm ring-like target to illuminate the test eye and calculates second order refraction based on the size and shape of the rings' reflected image,[54] making this equipment basically insensitive to the increased higher order aberrations contribution from larger pupil diameters as well to irregularities in the wavefront that lie inside the rings' area.[16]

In the present work, refraction obtained from the *VSMTF* criterion is adapted by M-scaling to the continuously decreasing range of frequencies that are relevant with increase visual field angle compared to foveal vision. While the metrics that would best predict peripheral refraction are not well established yet, we consider that the present approach is the more reliable and robust one as it changes the spectrum of frequencies that should be more relevant to refract the eye, as we depart from the foveal region. A limitation of this study is that our eye models are only partially customized as we do not consider the actual internal optics of each eye. A more complete personalization of the eye models[55] would require more biometric and aberrometric measurements. However, for the purpose of our study, the present approach provides a good comparison framework to evaluate the changes in axial and peripheral refraction induced by corneal reshaping with overnight ortho-k contact lenses. As the ortho-k treatment acts on the anterior corneal surface of the cornea our results show a clearly myopic peripheral refraction that can be interpreted as the change that the treatment will induce on the whole optics of the eye.

5.6. References

1 Lu F, Simpson T, Sorbara L, Fonn D. The relationship between the treatment zone diameter and visual, optical and subjective performance in Corneal Refractive Therapy lens wearers. *Ophthalmic Physiol Opt* 2007; 27: 568-578.

2 Queirós A, Villa-Collar C, Gutiérrez AR, Jorge J, González-Méijome JM. Quality of life of myopic subjects with different methods of visual correction using the NEI RQL-42 questionnaire. *Eye Contact Lens* 2012; 38: 116-121.

3 González-Méijome JM, Peixoto-de-Matos SC, Faria-Ribeiro M, Lopes-Ferreira DP, Jorge J, Legerton J, Queiros A. Strategies to Regulate Myopia Progression With Contact Lenses: A Review. *Eye Contact Lens* 2015.

4 Zhou J, Xie P, Wang D, Guo X, Yang L. [The long-term clinical effects of orthokeratology in high myopia children]. *Zhonghua Yan Ke Za Zhi* 2015; 51: 515-519.

5 Cho P, Cheung SW, Edwards M. The longitudinal orthokeratology research in children (LORIC) in Hong Kong: a pilot study on refractive changes and myopic control. *Curr Eye Res* 2005; 30: 71-80.

6 Charman WN. Myopia, posture and the visual environment. *Ophthalmic Physiol Opt* 2011; 31: 494-501.

7 Flitcroft DI. The complex interactions of retinal, optical and environmental factors in myopia aetiology. *Prog Retin Eye Res* 2012; 31: 622-660.

8 Kakita T, Hiraoka T, Oshika T. Influence of overnight orthokeratology on axial elongation in childhood myopia. *Invest Ophthalmol Vis Sci* 2011; 52: 2170-2174.

9 Hiraoka T, Kakita T, Okamoto F, Takahashi H, Oshika T. Long-term effect of overnight orthokeratology on axial length elongation in childhood myopia: a 5-year follow-up study. *Invest Ophthalmol Vis Sci* 2012; 53: 3913-3919.

10 Cho P, Cheung SW. Retardation of myopia in Orthokeratology (ROMIO) study: a 2-year randomized clinical trial. *Invest Ophthalmol Vis Sci* 2012; 53: 7077-7085.

11 Queirós A, González-Méijome JM, Jorge J, Villa-Collar C, Gutiérrez AR. Peripheral refraction in myopic patients after orthokeratology. *Optom Vis Sci* 2010; 87: 323-329.

12 Faria-Ribeiro M, Queirós A, Lopes-Ferreira D, Jorge J, González-Méijome JM. Peripheral refraction and retinal contour in stable and progressive myopia. *Optom Vis Sci* 2013; 90: 9-15.

13 Faria-Ribeiro M, López-Gil N, Navarro R, Lopes-Ferreira D, Jorge J, González-Méijome JM. Computing retinal contour from optical biometry. *Optom Vis Sci* 2014; 91: 430-436.

14 Chen Z, Niu L, Xue F, Qu X, Zhou Z, Zhou X, Chu R. Impact of pupil diameter on axial growth in orthokeratology. *Optom Vis Sci* 2012; 89: 1636-1640.

15 Bennett JR, Stalboerger GM, Hodge DO, Schornack MM. Comparison of refractive assessment by wavefront aberrometry, autorefraction, and subjective refraction. *J Optom* 2015; 8: 109-115.

16 Bakaraju RC, Fedtke C, Ehrmann K, Ho A. Comparing the relative peripheral refraction effect of single vision and multifocal contact lenses measured using an autorefractor and an aberrometer: A pilot study. *J Optom* 2015; 8: 206-218.

17 Lebow KA, Campbell CE. A comparison of a traditional and wavefront autorefraction. *Optom Vis Sci* 2014; 91: 1191-1198.

18 Thibos LN, Hong X, Bradley A, Applegate RA. Accuracy and precision of objective refraction from wavefront aberrations. *J Vis* 2004; 4: 329-351.

19 Queirós A, Villa-Collar C, González-Méijome JM, Jorge J, Gutiérrez AR. Effect of pupil size on corneal aberrations before and after standard laser in situ keratomileusis, custom laser in situ keratomileusis, and corneal refractive therapy. *Am J Ophthalmol* 2010; 150: 97-109.e101.

20 Mathur A, Atchison DA. Effect of orthokeratology on peripheral aberrations of the eye. *Optom Vis Sci* 2009; 86: E476-484.

21 Xu R, Bradley A, Thibos LN. Impact of primary spherical aberration, spatial frequency and Stiles Crawford apodization on wavefront determined refractive error: a computational study. *Ophthalmic Physiol Opt* 2013; 33: 444-455.

22 Martin J, Vasudevan B, Himebaugh N, Bradley A, Thibos L. Unbiased estimation of refractive state of aberrated eyes. *Vision Res* 2011; 51: 1932-1940.

23 Shen J, Thibos LN. Measuring ocular aberrations and image quality in peripheral vision with a clinical wavefront aberrometer. *Clin Exp Optom* 2009; 92: 212-222.

24 López-López M, Pelegrín-Sánchez J, Sobrado-Calvo P, García-Ayuso D. Contact lens intolerance: refitting with dual axis lens for corneal refractive therapy. *Journal Of Optometry* 2011; 4: 4.

25 González-Méijome JM, Villa-Collar C. Nomogram, corneal topography, and final prescription relations for corneal refractive therapy. *Optom Vis Sci* 2007; 84: 59-64.

26 Navarro R, Santamaría J, Bescós J. Accommodation-dependent model of the human eye with aspherics. *J Opt Soc Am A* 1985; 2: 1273-1281.

27 Zemax. *User's Guide*. In, 2005.

28 Navarro R, González L, Hernández JL. Optics of the average normal cornea from general and canonical representations of its surface topography. *J Opt Soc Am A Opt Image Sci Vis* 2006; 23: 219-232.

29 Thibos LN, Applegate RA, Schwiegerling JT, Webb R, applications VSTMVsai. Standards for reporting the optical aberrations of eyes. *J Refract Surg* 2002; 18: S652-660.

30 Thibos LN. Unresolved issues in the prediction of subjective refraction from wavefront aberration maps. *J Refract Surg* 2004; 20: S533-536.

31 Cheng X, Bradley A, Thibos LN. Predicting subjective judgment of best focus with objective image quality metrics. *J Vis* 2004; 4: 310-321.

32 Howarth PA, Zhang XX, Bradley A, Still DL, Thibos LN. Does the chromatic aberration of the eye vary with age? *J Opt Soc Am A* 1988; 5: 2087-2092.

33 Campbell FW, Robson JG. Application of Fourier analysis to the visibility of gratings. *J Physiol* 1968; 197: 551-566.

34 Sachs MB, Nachmias J, Robson JG. Spatial-frequency channels in human vision. *J Opt Soc Am* 1971; 61: 1176-1186.

35 Charman WN, Mathur A, Scott DH, Hartwig A, Atchison DA. Specifying peripheral aberrations in visual science. *J Biomed Opt* 2012; 17: 025004.

36 Navarro R, López JL, Díaz JA, Sinusía EP. Generalization of Zernike polynomials for regular portions of circles and ellipses. *Opt Express* 2014; 22: 21263-21279.

37 Díaz JA, Navarro R. Orthonormal polynomials for elliptical wavefronts with an arbitrary orientation. *Appl Opt* 2014; 53: 2051-2057.

38 Atchison DA, Scott DH, Charman WN. Measuring ocular aberrations in the peripheral visual field using Hartmann-Shack aberrometry. *J Opt Soc Am A Opt Image Sci Vis* 2007; 24: 2963-2973.

39 Guirao A, Williams DR. A method to predict refractive errors from wave aberration data. *Optom Vis Sci* 2003; 80: 36-42.

40 Rosén R, Lundström L, Venkataraman AP, Winter S, Unsbo P. Quick contrast sensitivity measurements in the periphery. *J Vis* 2014; 14: 3.

41 Rovamo J, Virsu V. An estimation and application of the human cortical magnification factor. *Exp Brain Res* 1979; 37: 495-510.

42 Thibos LN, Wheeler W, Horner D. Power vectors: an application of Fourier analysis to the description and statistical analysis of refractive error. *Optom Vis Sci* 1997; 74: 367-375.

43 Rio D, Legras R. Which ratio of areas improves vision quality in simultaneous focus optics? *Optom Vis Sci* 2015; 92: 429-436.

44 Charman WN, Jennings JA, Whitefoot H. The refraction of the eye in the relation to spherical aberration and pupil size. *Br J Physiol Opt* 1978; 32: 78-93.

45 Liang J, Williams DR. Aberrations and retinal image quality of the normal human eye. *J Opt Soc Am A Opt Image Sci Vis* 1997; 14: 2873-2883.

46 Santolaria E, Cerviño A, Queirós A, Brautaset R, González-Méijome JM. Subjective satisfaction in long-term orthokeratology patients. *Eye Contact Lens* 2013; 39: 388-393.

47 Santolaria Sanz E, Cerviño A, Queiros A, Villa-Collar C, Lopes-Ferreira D, González-Méijome JM. Short-term changes in light distortion in orthokeratology subjects. *Biomed Res Int* 2015; 2015: 278425.

48 de Gracia P, Dorronsoro C, Marin G, Hernández M, Marcos S. Visual acuity under combined astigmatism and coma: optical and neural adaptation effects. *J Vis* 2011; 11.

49 Yang X, Gong XM, Dai ZY, Wei L, Li SX. [Topographical evaluation on decentration of orthokeratology lenses]. *Zhonghua Yan Ke Za Zhi* 2003; 39: 335-338.

50 Hiraoka T, Matsumoto Y, Okamoto F, Yamaguchi T, Hirohara Y, Mihashi T, Oshika T. Corneal higher-order aberrations induced by overnight orthokeratology. *Am J Ophthalmol* 2005; 139: 429-436.

51 Charman WN, Mountford J, Atchison DA, Markwell EL. Peripheral refraction in orthokeratology patients. *Optom Vis Sci* 2006; 83: 641-648.

52 Kang P, Swarbrick H. Peripheral refraction in myopic children wearing orthokeratology and gas-permeable lenses. *Optom Vis Sci* 2011; 88: 476-482.

53 González-Méijome JM, Faria-Ribeiro MA, Lopes-Ferreira DP, Fernandes P, Carracedo G, Queiros A. Changes in Peripheral Refractive Profile after Orthokeratology for Different Degrees of Myopia. *Curr Eye Res* 2015: 1-9.

54 Davies LN, Mallen EA, Wolffsohn JS, Gilmartin B. Clinical evaluation of the Shin-Nippon NVision-K 5001/Grand Seiko WR-5100K autorefractor. *Optom Vis Sci* 2003; 80: 320-324.

55 Navarro R, González L, Hernández-Matamoros JL. On the prediction of optical aberrations by personalized eye models. *Optom Vis Sci* 2006; 83: 371-381.

Chapter 6: Depth-of-Field after Orthokeratology: A theoretical study

6.1. Abstract

PURPOSE: To evaluate the possible effect of orthokeratology on accommodative response. The negative half of the depth-of-field was evaluated for the range of target vergences from -1.00D to -3.00D, using optical modelization to simulate the optics of pre and post ortho-k eyes.

METHODS: Two eye models were designed in Zemax-EE, to mimic the levels of primary and secondary spherical aberration found in 24 patients before and after undergoing orthokeratology (ortho-k). Five trained observers were subjected to a resolution task to identify the negative threshold of the depth-of-field (DoFi) of these model eyes by viewing a set of computed images representative of the model eyes trough focus retinal image quality for five target vergences (TV), from -1.00 to -3.00 D, in 0.50 D steps.

RESULTS: The differences in the DoFi estimated by the five observers were maximum for a -3.00D TV (0.21D), with the post ortho-k model presenting a higher DoFi compared to the pre ortho-k model. Differences were consistent for all five observers and all TV's.

CONCLUSION: The increase in spherical aberration after ortho-k seems to contribute to a small increase in the DoFi. Although small, the benefits might be sufficient to improve retinal image quality in eyes with high accommodative lag.

KEYWORDS: Depth-of-Field, Orthokeratology, Accommodative Lag, Myopia

6.2. Introduction

The tolerance of any optical system to focusing errors can be specified by the interval of distances over which the object or image planes can be moved without producing any perceived degradation, with the former being referred to as depth-of-field (DoFi) and the latter as depth-of-focus (DoF). Either term can be used in vision sciences however, DoFi seems a more useful definition since it can be measured by changing the object's vergence rather than the retina position. Thus, DoFi can be defined as the vergence range of focusing errors that does not result in a significant deterioration in retinal image quality (RIQ). This perceive deterioration in RIQ is directly linked to final acceptance of the optics worn—e.g. ortho-k treatment— and can be determined according to different subjective and objective measures.[1]

In this work we proposed that the high increase in positive primary spherical aberration (SA) after orthokeratology (ortho-k) might improve the RIQ of eyes with accommodative lag due to an increase in the DoFi.[2-4]

6.3. Methods

Corneal aberrations from 24 patients enrolled in another study (Chapter 5) were averaged to determine the mean value of primary and secondary SA before and after undergoing ortho-k. Two model eyes based on the Navarro eye model[5] were generated with ray trace software Zemax-EE (Zemax Development Corporation, Washington, USA). The anterior cornea of the Navarro eye model was modeled with a Zernike Standard Phase surface[6] to mimic the mean amount of corneal 1st and 2nd orders SA of the 24 patients, before and after ortho-k. The vitreous length of the post ortho-k average eye model was adjusted to make it emetropic for a 5mm pupil diameter, using the Visual Strehl calculated from the MTF (VSMTF)[7] as an objective visual metric criterion. The pre ortho-k average eye model was corrected for his ametropia by adding a wavefront representative of its best sphero-cylindrical correction (VSMTF criteria). Wavefront errors were computed by ray-trace and exported to Matlab in 512x512 matrices.

Fourier optics routines were implemented in Matlab to design a trough-focus experience with the purpose of simulating the changes in RIQ as the eye accommodates for five target vergences (TV; -1.00D, -1.50D, -2.00D, -2.50D and -3.00D). For each of the

five investigated TV's a trough-focus series of computed images was generated to simulate the RIQ induced by different amounts of accommodative lag, ranging from -1.00D to +0.00D, in -0.1D steps. During this process, proximal miosis as well as the changes in primary and secondary SA due to the change in the hyperbolic shape of the lens' surfaces as the eye accommodates were adjusted as a function of TV.[8]

Five well corrected trained observers viewed the set of images in a TFT 13'' screen. The size of the computed Snellen letters as well as the distance to the screen were adjusted, so that the viewing angle corresponded to a decimal visual acuity of 0.5. Measures were conducted under good levels of illumination to keep the observes pupillary diameters smaller, and thus diminishing the effect of higher-order aberrations. The negative half of the DoFi interval, for the pre and post ortho-k eye models, was determined by asking the subjects to indicate the first legible image in the trough-focus interval. The value yielded by this resolution task simulates the change on the defocus coefficient C_2^0 produced by the lens curvatures needed to produce an acceptable RIQ for the imposed TV, according to our observer's subjective criteria. This value can also be interpreted as the minimum amount of accommodative lag that still allows to maintain acceptable levels of RIQ. For each observer, the procedure was repeated three times and averaged.

6.4. Results

Figure 6.1 illustrates a trough-focus experience similar to the one viewed by five observers, for both pre and post ortho-k eye models. From the present example it is clear the effect of the increased levels of SA. Although the RIQ decreases after ortho-k due to the loss of contrast, image resolution decreases less (left to right) with the imposed defocus, suggesting a greater DoFi in the post ortho-k condition.

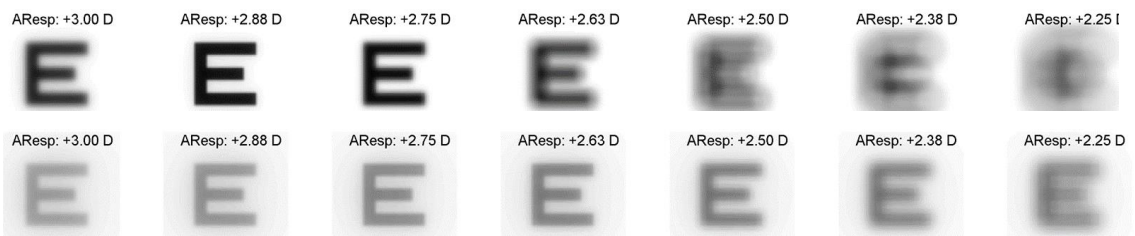

Figure 6.1. Trough-focus RIQ simulations for a 5 mm pupil, based on the Navarro accommodative eye model plus a SA phase plate to match the average SA values of the 24

subjects before (top: C_4^0 = 0.126 µm; C_6^0 = 0.001 µm) and after ortho-k (bottom: C_4^0 = 0.464 µm; C_6^0 = 0.019 µm), for a -3.00 D target vergence (TV). Pupil diameter decreases 0.35 mm/D of change in defocus with accommodation.

This hypothesis is confirmed by our observer's subjective criteria (Figure 6.2). The observed differences are not constant trough the TV range, but the variation tendency is similar in both conditions, indicating an increased DoFi for higher TV's probably due to the effect of proximal miosis.[9]

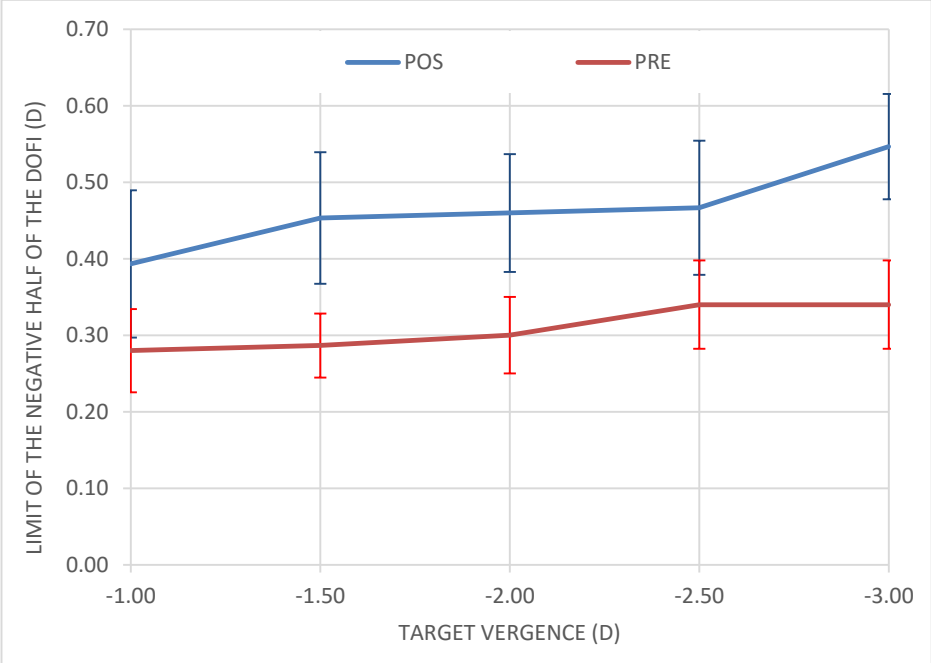

Figure 6.2. Limit of the negative half of the DoFi interval as a function of TV. These values also represent the highest amount of lag as a function of TV that still allows to maintain an acceptable RIQ, according to the observer's subjective threshold.

6.5. Discussion

It has been hypothesized that the increase in positive SA could provide an additional explanation for the myopia control effects obtained by different treatments in progressing myopes, due to a change in behavior of the accommodative system.[3,10,11] However, there is controversy in the results from different studies aiming to evaluate the actual changes in the accommodative system after corneal reshaping with refractive surgery or ortho-k. Karimian[12] et al reported an improvement in the accommodative facility

in myopes after PRK surgery. Conversely, Felipe-Marquez and collaborators[2] did not found any significant change in the accommodative function after orthokeratology. In the context of the Cambridge Anti-Myopia Study (CAMS), Allen et al[12] reported an improvement in the accommodative function with lenses that induced negative spherical aberration, but myopic corneal reshaping induced positive, rather than negative, spherical aberration. More recently, Pauné et al[13] reported a decrease in the accommodative lag of progressing myopic subjects using soft contact lenses with a peripheral gradient of positive power (positive SA) to generate relative peripheral myopia, with the primary aim of myopia control. Gambra et al.[4] showed that adding negative 4th order SA to an aberration-free eye produced a decrease in the accommodative lag, while adding positive 4th order SA produced an increase in the accommodative lag (less accurate accommodative response). Although the authors do not refer it in their paper, there could be some other effect unaccounted for in their conclusions. Adding negative Zernike SA introduces positive Seidel defocus —due to the low-order terms balance in Zernike polynomials— which would help the eye to compensate for the negative defocus produced by the accommodative lag.

Even so, from our results illustrated in Figures 6.1 and 6.2, it appears that with the increase in positive SA the eye will not need to accommodate as much, at least for high contrast resolution tasks such as reading. But judging from the trough focus simulated retinal images, this increase in positive SA provides only a marginal extension of the DoFi in the ortho-k eye model compared to the pre ortho-k results (mean difference = 0.21D for a -3.00D TV). Although clinically small, this results seems to agree with experimental findings which showed that the presence of C_4^0 increases the DoFi.[14-16] This observed causal relation might lead to two different results: on one hand, on a patient without accommodative lag it is expected to decrease RIQ due to the loss of contrast induced by the high levels of positive SA; on the other hand, on a patient with accommodative lag—where acuity is compromised during near vision—the extended DoFi might increase retinal image resolution and therefore acuity for high contrast tasks. Taking into account that the increment in positive C_4^0 after ortho-k is strongly negative correlated to baseline myopia (Chapter 5) and the treatment zone area, it is expected that this effect will be more beneficial in moderate myopes with decreased visual acuity at near due to accommodative lag and small treatment zones.

6.6. References

1 Thibos LN, Hong X, Bradley A, Applegate RA. Accuracy and precision of objective refraction from wavefront aberrations. *J Vis* 2004; 4: 329-351.

2 Felipe-Marquez G, Nombela-Palomo M, Cacho I, Nieto-Bona A. Accommodative changes produced in response to overnight orthokeratology. *Graefes Arch Clin Exp Ophthalmol* 2015; 253: 619-626.

3 Walline JJ, Greiner KL, McVey ME, Jones-Jordan LA. Multifocal contact lens myopia control. *Optom Vis Sci* 2013; 90: 1207-1214.

4 Gambra E, Sawides L, Dorronsoro C, Marcos S. Accommodative lag and fluctuations when optical aberrations are manipulated. *J Vis* 2009; 9: 4.1-15.

5 Navarro R, Santamaría J, Bescós J. Accommodation-dependent model of the human eye with aspherics. *J Opt Soc Am A* 1985; 2: 1273-1281.

6 Zemax Corporation. User's Guide 2005; 284-287.

7 Cheng X, Bradley A, Thibos LN. Predicting subjective judgment of best focus with objective image quality metrics. *J Vis* 2004; 4: 310-321.

8 López-Gil N, Fernández-Sánchez V. The change of spherical aberration during accommodation and its effect on the accommodation response. *J Vis* 2010; 10: 12.

9 López-Gil N, Martin J, Liu T, Bradley A, Díaz-Muñoz D, Thibos LN. Retinal image quality during accommodation. *Ophthalmic Physiol Opt* 2013; 33: 497-507.

10 Anstice NS, Phillips JR. Effect of dual-focus soft contact lens wear on axial myopia progression in children. *Ophthalmology* 2011; 118: 1152-1161.

11 Thibos LN, Bradley A, Liu T, López-Gil N. Spherical aberration and the sign of defocus. *Optom Vis Sci* 2013; 90: 1284-1291.

12 Allen PM, Radhakrishnan H, Rae S, Calver RI, Theagarayan BP, Nelson P, Osuobeni E, Sailoganathan A, Price H, O'Leary DJ. Aberration control and vision training as an

effective means of improving accommodation in individuals with myopia. *Invest Ophthalmol Vis Sci* 2009; 50: 5120-5129.

13 Pauné J, Thivent S, Armengol J, Quevedo L, Faria-Ribeiro M, González-Méijome JM. Changes in Peripheral Refraction, Higher-Order Aberrations, and Accommodative Lag With a Radial Refractive Gradient Contact Lens in Young Myopes. *Eye Contact Lens* 2016.

14 Benard Y, Lopez-Gil N, Legras R. Subjective depth of field in presence of 4th-order and 6th-order Zernike spherical aberration using adaptive optics technology. *J Cataract Refract Surg* 2010; 36: 2129-2138.

15 Legras R, Benard Y, Lopez-Gil N. Effect of coma and spherical aberration on depth-of-focus measured using adaptive optics and computationally blurred images. *J Cataract Refract Surg* 2012; 38: 458-469.

16 Rocha KM, Vabre L, Chateau N, Krueger RR. Expanding depth of focus by modifying higher-order aberrations induced by an adaptive optics visual simulator. *J Cataract Refract Surg* 2009; 35: 1885-1892.

Chapter 7: Main Conclusions

As main conclusions resulting from the work developed during this thesis, it should be highlighted that the use of a semi-customized eye model together with OPL measured by PCIB for different angles can be used to predict the retinal contour within tenths of microns. In general, a nasal-temporal asymmetry in the retina contour was found, showing mean larger values of vitreous chamber depth in the nasal side of the eye. Retinal shape can vary considerably for different eyes, particularly beyond 4 mm (about 15º of visual field) from the fovea. Differences in retinal sagitta between subjects can be as large as 2 mm, at a field angle of 30º, which corresponds to a refraction error of about 3D if an average contour was used. These results strength the need for a customized wide angle approach when developing optical treatments to alter the eye's field curvature.

After ortho-k, the conic model fails to describe with sufficient accuracy the elevation of the anterior cornea if a monozone approach is used. Instead better fits are obtained if the elevation data from each zone are fitted individually. Although the increase in positive SA was the major factor responsible for the decrease in the RIQ of the unaccommodated eye, it seems to contribute to an extension of the DoFi which might increase RIQ during high contrast near vision tasks, in myopic subjects with accommodative lag. Central refractive error does not seem to change appreciably with the increase in pupil diameter, but Large pupil diameters could facilitate the effect of ortho-k to slow axial growth because of enhancement of the myopic shift in the peripheral retina. This effect would not be accounted if an open field AR, such as the Grand Seiko, was used to measure peripheral refraction.

The obtained results seem to show that optical modeling can be a powerful tool in myopia research, as it enables the possibility of controlling and isolating some of the variables involved in the process, and thus contributing to a better understanding of the optical singularities of each individual.

Chapter 8: Future Work

Although this thesis tries to answer some of the questions regarding the optical singularities related to myopia progression, it only scratches the surface of this problem. It is currently accepted that myopia has multifactorial causes and involves several variables, some of them still unknown to us. It seems plausible to affirm that the mechanism responsible for the regulation of eye growth, and thus emmetropization, is visually guided and therefore the manipulation of its feedback system might allow us to interfere with the process. To do so, future work should be focused in identifying biological markers in the retinal cells response to different visual signals and formerly identify which of those signals might be used to interfere with eye growth. In this field, objective means of characterization of the retinal electrical activity such as multifocal electroretinography will be of great use to measure and differentiate the retinal response to different visual stimuli. Open and crucial questions such as: "*How the eye senses the sign of defocus?"* and "*Why does myopia eventually stops?*", might only be answered if an approach based on retinal electrical activity characterization along with heuristic modeling of its neural system is used.

Future work in this field should be directed to the development of a unified model of the optical and neural functionality of the myopic eye in order to predict the result of optical treatments targeted to interfere with myopia progression.